ISOTOPIC YIELD DISTRIBUTIONS OF PRODUCTS FORMED FROM THE FISSION OF ^{233}U AND ^{235}U BY PROTONS OF ENERGY 40-100 MeV

by

© Philip A. Beeley

A thesis submitted to the
Faculty of Graduate Studies and Research
in partial fulfilment of the
requirements for the degree of
Doctor of Philosophy

Department of Chemistry and
Foster Radiation Laboratory
McGill University
Montreal, Quebec
Canada

October 1981

ISOTOPIC DISTRIBUTIONS FROM $^{233}U(p,f)$ AND $^{235}U(p,f)$

ABSTRACT

Ph.D. Philip A. Beeley Chemistry

Isotopic Yield Distributions of Products Formed from the Fission of ^{233}U and ^{235}U by Protons of Energy 40-100 MeV

The independent formation cross-sections of $^{84,86}Rb$, $^{116m,117m,117g}In$, and $^{132,134m,134m+g,136}Cs$ from $^{233}U(p,f)$ and $^{235}U(p,f)$ reactions, and the independent formation cross-sections of ^{72}Ga from $^{233}U(p,f)$ reactions were measured radiochemically in the energy range 35 to 90 MeV. The isotopic distributions of Rb, In, and Cs from $^{233}U(p,f)$ and $^{235}U(p,f)$, and the isotopic distributions of Ga from $^{233}U(p,f)$ were measured in the energy range 40 to 100 MeV using the on-line mass spectrometric technique; their relative yields were normalized to the independent formation cross-sections measured radiochemically.

The variations of the FWHM, mean mass numbers, and mean neutron-to-proton ratios of the isotopic distributions were studied. The experimental results indicate that the mean masses of the distributions vary linearly with their atomic numbers. In conjunction with the fission option of the pre-equilibrium/exciton model, the experimental data were used to estimate average total neutron yields. The results show that there are more neutrons emitted for near-symmetric fissions than for asymmetric fissions. The charge distribution

postulates, ECD, MPE, and UCD, were examined. In the energy range studied the results indicate that the MPE postulate accounts for asymmetric fissions, and the UCD postulate accounts for near-symmetric fissions.

Résumé

Ph.D. Philip A. Beeley Chimie

Distributions de rendement isotopique des produits formés lors de la fission de ^{233}U et ^{235}U induite par des protons d'énergie allant de 40 à 100 MeV

Nous avons mesuré, par des méthodes radiochimiques, les sections efficaces de formation indépendantes de $^{84,86}Rb$, $^{116m,117m,117g}In$ et $^{132,134m,134m+g,136}Cs$ provenant des réactions $^{233}U(p,f)$ et $^{235}U(p,f)$ ainsi que les sections efficaces de formation indépendantes de ^{72}Ga provenant des réactions $^{233}U(p,f)$ dans l'intervalle d'énergie de 35 à 90 MeV. Nous avons mesuré, à l'aide de la technique de spectromètre de masse en ligne, les distributions isotopiques de Rb,In et Cs provenant de $^{233}U(p,f)$ et $^{235}U(p,f)$ ainsi que les distributions isotopiques de Ga provenant de $^{233}U(p,f)$ dans l'intervalle d'énergie entre 40 et 100 MeV; leurs rendements relatifs ont été normalisés aux sections efficaces de formation indépendantes déterminées par les mesures radiochimiques.

Nous avons étudié les variations de largeur à mi-hauteur, de nombres de masse moyens et de rapports neutron à proton moyens des distributions isotopiques. Les résultats expérimentaux indiquent que les masses moyennes des distributions varient linéairement avec leurs numéros atomiques. Nous avons utilisé à la fois les résultats expérimentaux et l'option de fission du modèle "pré-équilibre/exciton" à fin d'estimer le nombre total

moyen de neutrons émis. Les résultats montrent que plus de neutrons sont émis lors de fissions presque symétriques que pour des fissions assymétriques. Nous avons testé les postulats de distribution de charge ECD, MPE et UCD. Dans l'intervalle d'énergie utilisé, les résultats indiquent que le postulat MPE rend compte des fissions assymétriques tandis que le postulat UCD rend compte des fissions presque symétriques.

ACKNOWLEDGEMENTS

I wish to express my sincere appreciation and thanks to Professor L. Yaffe and Dr. J.K.P. Lee for their constant encouragement, guidance, and interest throughout the course of this work.

Special thanks also go to Dr. J.J. Hogan and Dr. C. Chung for supplying me with, and educating me in the use of, the computer code of the Pre-equilibrium/Exciton Model calculations obtained from Dr. E. Gadioli. Helpful discussions with Dr. J.J. Hogan and Dr. M. Dikšić are also appreciated.

I am indebted to Dr. Heather Marshall for her help during the early stages of this work and for her continued interest. I would also like to acknowledge the co-operation of my friends and colleagues in the Department of Chemistry and the Foster Radiation Laboratory; in particular, Dr. M.L. Chatterjee and Mr. N. Mobed for their helpful suggestions and their assistance with the mass spectrometric measurements. Technical assistance from the Foster Radiation Laboratory personnel is also gratefully acknowledged. Thanks also go to Mr. A. Froncioni for his assistance during the summer months of 1981, and to Dr. D. Dautet for translating the abstract.

I would like to record my appreciation of the Department of Chemistry for providing demonstratorships throughout the course of this work.

Finally, special mention must go to my family for their support and interest in my education, and to my wife, Irene, for her patience and reassurance, and for typing this text.

TABLE OF CONTENTS

LIST OF TABLES

LIST OF FIGURES

page

page

I. INTRODUCTION

A. General

During the past four decades a great deal of experimental and theoretical work has been done to characterize the nuclear phenomenon termed fission. Consequently, there exists an enormous literature covering the great variety of work in this area. Authoritative books by Hyde (Hy71) and Vandenbosch and Huizenga (Va73) have described the works covering the first three decades. In addition the proceedings of the IAEA Symposia on the Physics and Chemistry of Fission (Sa65, Vi69, Ro73, Ju79) provide a vast amount of information on the subject. Specialized reviews, such as (Ho74) and (Gr76) continue to convey the present understanding.

Over the past fifteen years a better understanding of the dynamics of fission has resulted from advances in the technologies of detectors, fast electronics and computers. In part stimulated by new experimental results, fission theory has received new emphasis resulting in numerous corrections to the liquid-drop model of the nucleus first formulated by Bohr and Wheeler (Bo39). The initial theoretical impetus was provided by Strutinsky (St67,68) who developed a method of correcting liquid-drop potentials, with contributions to the nuclear-potential surface, from shell-model theory. These corrections lead to the predictions of a double-humped fission barrier in the region of the actinide nuclei. Extensions of this idea by others (Mu73, Mo74)

have provided interpretations of phenomena which were previously difficult to explain, such as mass asymmetry in the low-energy fission of some actinide nuclei. The corrections made to the liquid-drop model to allow for the fact that nuclei contain rather fewer particles by comparison with a macroscopic liquid-drop lead to the formulation of the droplet model by Myers and Swiatecki (My70), the most recent refinement being due to Myers (My77).

Complementary advances in the complexity of experiments have resulted in correlated measurements of the mass, kinetic energies, and neutron multiplicities of fission fragments. These measurements provide the data from which a better understanding of the dynamic processes in fission is being gained. The development of on-line mass spectrometry is also providing information on isotopic-yield distributions of fission products that will hopefully supplement an understanding of the fission process. No understanding of the dynamics of fission can be complete without a knowledge of the distribution of nuclear charge. Although no theory exists which suitably explains nuclear charge distribution in fission, three hypotheses, which will be discussed later, have been used with varying degrees of success.

B. The Fission Process

The majority of heavy nuclei in their ground-state do not

undergo spontaneous fission. This is because energy is needed to deform a nucleus from its ground-state shape; there is a potential barrier to be overcome before the nucleus can reach the more stable configuration of two separate fragments. When heavy nuclei are excited by bombardment with neutrons, protons or heavier particles the nuclei go through various deviations from their ground-state shape. If during the course of these distortions a nucleus attains a deformation such that the decrease in energy of the coulomb repulsion is greater than the increase in the surface energy it will distort beyond the "saddle-point" configuration and reach the "scission-point," whence the nucleus will split into at least two fragments which are then driven apart by their mutual coulomb repulsion. Thus Bohr and Wheeler (B039) defined a "fissility parameter" as $E_c^o/2E_s^o$ where E_c^o and E_s^o are the coulomb and surface energies respectively for a spherical nucleus. This parameter is proportional to Z^2/A of the nucleus, which has in many cases been considered as the principal factor on which fissionability depends. By virtue of their nuclear bulk heavy nuclei, such as the ones used in this work, have ground-state shapes deviating from sphericity. Their coulomb barriers to fission are thus lowered making them susceptible to fission at even low excitation energies.

B1. <u>The path to fission</u>

It is impossible to discuss fission induced by charged particles without at the same time considering competing

nuclear reactions in which particles may be emitted, resulting in nuclei that do not fission. These competing reactions are collectively termed spallation reactions. Two extreme mechanisms have been formulated to explain reactions such as the interaction of energetic protons with uranium nuclei. At excitation energies of a few MeV up to about 50 MeV the chief mechanism is by compound-nucleus formation in which the projectile is absorbed into the target nucleus and the added energy is distributed amongst all the nucleons. Deexcitation then occurs by evaporation of nucleons, nuclear fission or gamma-ray emission. At energies greater than about 50 MeV the mechanism becomes that of direct interaction of the projectile and a few nucleons in the nucleus. The incoming particle enters the nucleus along a random trajectory and has a finite probability of interacting with a nucleon. If the interaction is allowed the struck nucleon will obtain some kinetic energy and momentum. The two nucleons then traverse the nucleus and may interact with other nucleons. Such a process is termed an intranuclear cascade, an outcome of which is the emission of nucleons with sufficient energy to overcome their binding energy and coulomb barrier in the case of charged particles. The final outcome of an intranuclear cascade is an excited nucleus that deexcites in a manner similar to an excited compound nucleus.

In recent years reaction models have been formulated that combine the diametrically opposed extremes of direct reactions

and compound nucleus mechanisms. These models have been collectively termed pre-equilibrium models and have been reviewed by Blann (Bl75). Among the several models formulated the pre-equilibrium/exciton model derived by Gadioli and Milazzo-Colli (Ga73) has been highly successful. The collaborative efforts of Hogan, his co-workers and Gadioli have resulted in successful fits to a variety of spallation reactions induced by protons with energies up to 100 MeV (Ho77, Ga77, Bu80). Recently this model has been successful in reproducing a broad range of experimental data in the thorium region where fission plays an important role (Ho79, Ch80).

Gadioli (Ga78) has assumed fission to be a competing reaction only during the second stage of the calculation where an equilibrium distribution of energy is attained. This is because the initial partition of projectile energy in the pre-equilibrium stage is between relatively few intrinsic degrees of freedom, whereas fission involves a major collective motion of nucleons. As mentioned previously, deexcitation from an excited nucleus in which the energy is equilibrated is by nucleon emission, fission or gamma-ray emission. Gamma-ray emission is considered to be a slow process at this stage and does not compete with the other modes of deexcitation. The deexcitation process is treated analytically by a Monte-Carlo procedure similar to the one formulated by Dostrovsky et al. (Do59). The probabilities of the various modes of deexcitation along the evaporation chain are expressed in terms

of widths (Γ), evaluated by Gadioli et al. (Ga77) as follows. The various particle emission widths (Γ_i), where i may be for neutrons, protons or alpha particles, are given by:

$$\Gamma_i = \frac{\mu_i r_{oi}^2 A_i^{2/3} (2s_i+1)}{\bar{U}_i^2 \, 2\pi\hbar^2 \, a_i \rho(E)} \cdot$$

$$\left[\frac{3}{4a_i}(x_i^2-2x_i+2) + \beta(x_i-1) - (E-B_i-C_i-\Delta_i)\right] \exp x_i \qquad \text{(I.1)}$$

and the analogous expression for the fission width, derived from Vandenbosch and Huizenga (Va73) and discussed by Gadioli (Ga78), is:

$$\Gamma_f = \frac{\left[2\sqrt{a_f(E-B_f-\Delta_s)} - 1\right] \exp\left[2\sqrt{a_f(E-B_f-\Delta_s)}\right]}{\left[\bar{U}_s^2 \, 4\pi a_f \, \rho(E)\right]} \qquad \text{(I.2)}$$

where: $\bar{U}_s$ = average excitation energy at the saddle point,

$\bar{U}_i$ = average excitation energy of the residual nucleus A_i after the emission of particle i,

Δ_s = pairing energy at the saddle point,

B_f = the fission barrier,

a_f = the level-density parameter of the nucleus when deformed to the saddle point,

μ_i = reduced mass of the excited nucleus A- emitted particle,

r_o = nuclear radius parameter,

s_i = spin of the emitted particle,

$x_i = 2\, a_i (E-B_i-C_i-\Delta_i)^{1/2}$,

$$\beta = \frac{2.12A_i^{-2/3} - 0.05}{0.76 + 2.2A_i^{-1/3}} \quad \text{for neutrons, = 0 otherwise,}$$

a_i = A/8,

B_i = binding energy of the emitted particle i,

C_i = coulomb barrier for the emission of particle i,

Δ_i = pairing energy of the residual nucleus A_i after the emission of particle i.

The term most commonly used to discuss the competition between fission and particle emission has been the fissionability, defined as Γ_f/Γ_n. This was because most of the early investigations were at relatively low energies, where the probability of charged-particle emission is low and the only mode of deexcitation competing with fission was neutron emission. However, for the proton bombarding energies used in this work charged-particle emission does become a competing mode of deexcitation for the target nuclei $^{233,235}U$. The fractional probability of fission is thus given by:

$$P_f = \frac{\Gamma_f}{\Gamma_n + \Gamma_p + \Gamma_\alpha + \Gamma_f} \qquad (I.3)$$

where P_f is termed the fissility and the various widths have been defined by equations (I.1) and (I.2).

The reaction model described above was made available during the course of this work and the pertinent results will be presented in the discussion. However, there are several points in the fission option of this model that should be

noted:

1. The fission barrier, from (Ga78), is single-peaked and defined only by its height. Fission is assumed to take place with unity transmission coefficient above the barrier and zero transmission coefficient below the barrier.
2. In calculating the various widths (Γ) no account is taken of angular momentum effects.
3. The ratio of the level-density parameter of the nucleus when deformed to the saddle-point configuration (a_f) to the neutron level-density parameter (a_n) is treated as the only free variable.

Although it has been mentioned previously that double-humped fission barriers do exist, this is of little consequence in the present evaluation where the fission barrier is easily surmounted. Furthermore, the present model may only be applied to proton-induced reactions and Gadioli (Ga77) has suggested that angular momentum effects do not seriously alter the results of these reactions.

B2. Post-fission phenomena

Post-fission phenomena may be described as those that occur after scission of the fissile nuclide into at least two fragments. The distribution of mass, charge and kinetic energy between these fragments, together with their neutron and photon yields, thus constitute these phenomena, a complete

description of which is beyond the scope of this introduction. Review articles by Nifenecker (Ni73) and Hoffman (Ho74) have surveyed the literature and provide comprehensive references. However, there are certain prominent features of these distributions that may be summarized.

i) Mass distributions

The highly excited fragments formed immediately after scission are often referred to as the primary fragments. These fragments deexcite predominantly by neutron emission followed by prompt gamma emission. The resultant products, referred to as independent fission products, are in most cases radioactive and decay usually along a chain of constant mass number until they reach stability. In some cases these decays lead to levels that are neutron unstable, resulting in delayed neutron emission and a decrease in mass number. All neutrons emitted after scission are termed post-fission neutrons. The cumulative yields of each mass chain give the post-neutron-emission mass distributions and have until recently been measured by radiochemical techniques. The yield of a fission product, or any product from a nuclear reaction, is expressed as a "cross-section" which is a measure of the probability of a reaction at a given energy for a given projectile and target. It has the dimensions of area and the unit is a barn ($=10^{-24}cm^2$). Advances in experimentation have allowed correlated measurements of mass, kinetic energies and neutron multiplicities of the fission fragments

so that primary fragment mass distributions may now be obtained. Such an experiment has been performed by Burnett (Bu68) who measured the time-of-flight of one fragment in coincidence with the pulse amplitude produced by both fragments for the proton-induced fission of ^{233}U. Unik et al. (Un73) have made a comprehensive study of mass distributions from fission of the actinide elements and obtained excellent agreement between the radiochemical and physical techniques. On-line mass spectrometric techniques are also being used to measure isotopic yields of fission products (Am73, Ni79, Ni80, Mo81, Sh81) and in some cases isobaric dispersions have been constructed and related to the charge distribution mechanisms.

One of the most prominent features of the mass distributions for low-energy fission of the actinide nuclei is the mass asymmetry. It has now been established that the fission path departs from mass symmetry at the second barrier and Pauli and Ledergerber (Pa73) have found good correlation between the mass asymmetry at the second barrier and experimentally determined primary fragment mass ratios. For all fissile nuclei symmetric yields become more probable as the excitation energy is increased. This is well illustrated by the measurements of Stevenson et al. (St58) for the proton-induced fission of ^{238}U in the energy region 10 to 150 MeV. At 10 MeV the peak-to-valley ratio of the mass distribution is 10 and diminishes to 1 at 150 MeV, corresponding to a

symmetric mass distribution. Similarly the mass-yield curves measured by Burnett (Bu71) for the proton-induced fission of ^{233}U at 8.5 and 13 MeV have peak-to-valley ratios of 7.1 and 2.2 respectively. The above examples also illustrate the larger relative symmetric mass yields for the lower mass, highly fissile uranium nuclei. The marked increase in the symmetric component of the mass-yield curves is expected at energies above the fission barrier as the mass distribution is determined by level densities and a symmetric distribution of nucleons has larger statistical weight. However, experimental results show that the asymmetric components are still persistent at higher energies, and although this may be attributed to fissioning nuclei with lower excitation energies due to multichance fission, a fair number of these nuclei still have excitation energies above their fission barriers. The observation of higher yields for symmetric mass division in the spontaneous fission of fermium isotopes as the mass is increased (Ho74a) suggests that the asymmetric/symmetric mass split may be correlated to the identity of the fissioning nuclide. Recently Chung (Ch80) correlated this mass split to the Z^2/A of the fissioning nuclide for fissioning charges between 80 and 105.

ii) Charge distributions

A complete description of the fission process must consider the distribution of nuclear charge between the fission products and how this is related to the identity of

the fissioning nucleus and primary fragments. Although at present there is no theory which predicts the details of charge distribution, the data are usually compared with three postulates; Equal Charge Displacement, Unchanged Charge Distribution, Minimum Potential Energy.

a. Equal Charge Displacement (ECD) postulate:

First introduced by Glendenin, Coryell and Edwards (Gl49), and formulated empirically from charge dispersion data for low-energy fission, this postulate states that the most probable charges (Z_p) of complementary primary fragments (A'_L, A'_H) are equally displaced from beta stability. This may be formulated as:

$$(Z_A - Z_p)_{A'_L} = (Z_A - Z_p)_{A'_H} \qquad (I.4)$$

where the Z_A's are the most stable charges along isobars A'_L and A'_H. The implication of this postulate is that the fissioning nucleus has time to redistribute its constituent nucleons prior to scission.

b. Unchanged Charge Distribution (UCD) postulate:

First introduced by Goeckermann and Perlman (Go48, 49), this postulate states that the neutron-to-proton ratio of the fissioning nucleus is maintained unchanged in the primary fission fragments. Thus:

$$(N'/Z_p)_{A'_L} = (N'/Z_p)_{A'_H} \qquad (I.5)$$

where the subscripts L and H denote the light and heavy fragments respectively. The assumption inherent in this

postulate is that the process from saddle to scission is too fast to allow a redistribution of nucleons.

c. Minimum Potential Energy (MPE) postulate:

Generally attributed to Way and Wigner (Wa48), this postulate suggests that the process from saddle to scission is slow and that the division will be such as to minimize the nuclear potential energy. A number of formulations of this hypothesis has been used over the years (Fo56, No66, Ch80) with varying degrees of success. This has been largely due to the calculations being strongly dependent on the mass equations and shell corrections used. This postulate was tested in this work and the formulation will be given in the discussion.

In order to correlate the measured independent fission-product yields to the charge-distribution postulates various methods of constructing charge-dispersion curves were formulated. The first attempt was made by Glendenin (Gl51) who obtained charge-dispersion curves by plotting the independent yields versus $(Z-Z_p)$ of the products, where Z_p was calculated using the ECD postulate. This required a knowledge of Z_A as shown by equation (I.4) and resulted in discontinuities near shell edges. In order to circumvent this difficulty Wahl (Wa58) proposed an empirical method based on the determination of Z_p from a plot of independent yields versus the atomic numbers (Z) of the products. Further work by this author (Wa62,69) showed that charge dispersion curves could be

represented by a Gaussian distribution of the form:

$$P(Z) = (\pi C)^{-1/2} \cdot \exp[-(Z-Z_p)^2/C] \qquad (I.6)$$

where $P(Z)$ is the probability of formation of a product of atomic number (Z) in a given mass chain and C is a constant relating to the width of the distribution.

Most of the early works on charge dispersion employed only radiochemical techniques and were thus restricted to the few cases where at least three members of the same mass chain could be measured. However, the recent on-line mass spectrometric measurements of Amiel and co-workers (Am74, 75, Sh81) have shown that this problem can be overcome by combining absolute radiochemical measurements with the relative isotopic yields, and previously unmeasured isobaric distributions can now be obtained.

In order to correlate isotopic yields to charge dispersion Friedlander et al. (Fr63) proposed that the yields be plotted as a function of the neutron-to-proton ratio (N/Z) of the product. The peak of these dispersions gives N/Z_p from which Z_p may be derived. There are, however, two implicit assumptions when one uses this approach: (i) for any value of A the total chain yield must be assumed to be the same in the mass range under consideration;(ii) N/Z_p has the same value for different mass chains. Hogan and Sugarman (Ho69) have shown that isotopic charge dispersion curves may be compared to isobaric charge dispersion curves if a correction is made for the variation of N/Z_p with A. More recently Miller and

Yaffe (Mi73) and Galinier et al. (Ga77b) have shown the variation of N/Z_p with A for the proton-induced fission of ^{238}U at various energies.

The three postulates have had varying degrees of success in predicting the experimentally determined most probable charge (Z_p) for various fissioning systems at different energies. However, in general, the evaluations indicate that the ECD postulate is successful in predicting charge distribution for low-energy fission data, the MPE postulate predicts the data in the intermediate-energy range and at high energies the charge distributions are predicted by the UCD postulate. This categorization of charge distribution as a function of energy is far from definitive; for example, Reisdorf (Re71) derived primary fragment charge distributions following spontaneous fission of ^{252}Cf and thermal-neutron-induced fission of $^{233,235}U$ and ^{239}Pu, and concluded that the most probable charges were closer to the values predicted by the MPE postulate. The same conclusion was obtained by Chung (Ch80) for these reactions.

One of the most extensive studies of charge distribution from the fission of actinide nuclei by protons in the energy range 20 to 90 MeV has been made by Yaffe and his co-workers. Studies on ^{232}Th (Mc71, Ho73, Di79), $^{233,235,238}U$ (To69, Kh70, Sa71, Ma73, Di74, Sa76, Ga77), ^{237}Np (Mc72) and ^{239}Pu (Sa70) have shown that the charge-dispersion curves broaden with an increase in the proton energy, the most probable charge (Z_p)

moves towards stability and $Z_A - Z_p$ is a function of the N/Z ratio of the target. Interpretation of the results in terms of the charge postulates has been inconclusive, largely due to the complications of multichance fission. Recently Chung (Ch80) performed ab initio calculations of charge distribution in the thorium region and compared his predictions with the experimental data of Yaffe's group. He concluded that the MPE postulate gave the best fit to the data for asymmetric fission, although reasonable fits were obtained by the ECD postulate, and the UCD postulate correlated the data for symmetric fission. These results support the two-mode-fission hypothesis suggested by Turkevich and Niday (Tu51), although Chung has assigned the asymmetric/symmetric split to the identity of the fissioning nucleus. Chung and Hogan (Ho81) have performed similar calculations for the proton-induced fission of ^{238}U and conclude the same trends as those observed for the ^{232}Th work.

iii) Kinetic-energy distributions and neutron and photon yields

The kinetic energy of fission fragments is primarily a result of the coulomb repulsion between the fragments at scission. The distribution of these kinetic energies is dependent upon the identity of the fissioning species, the excitation energy and the mass and charge of the fragments, and has been reviewed by Hoffman and Hoffman (Ho74). One of the most prominent features of the average total kinetic-energy distribution as a function of the primary-fragment

mass, for the proton-induced fission of ^{233}U (Bu68), is the double humped shape of the distribution with the valley occurring in the region of near-symmetric mass splits. Furthermore, the average total kinetic energy decreases slightly as the bombarding energy increases. These features have been correlated to the observed higher total neutron yields for complementary near-symmetric fragments as compared to complementary asymmetric fragments, and also to an increase in the average total neutron yields with increased bombarding energy.

The discussion of charge distribution in the previous section illustrates the need for detailed knowledge of neutron emission as a function of fragment mass and charge in order to obtain the identity of the primary fragments. The total number of neutrons emitted when a nucleus such as ^{233}U is bombarded with energetic protons consists of pre and post-fission neutrons. The pre-fission neutrons include those emitted during the fast pre-equilibrium stage of the reaction and the slower evaporation stage prior to fission. As previously mentioned the post-fission neutrons include all those emitted after scission, the majority of which are prompt neutrons emitted from the fully accelerated primary fragments. The variation of neutron yields as a function of fragment mass was first shown by Fraser and Milton (Fr54) for the neutron-induced fission of ^{233}U. Their study showed that the number of neutrons emitted by complementary fragments was unequal, most of the neutrons being emitted by the heavier light and

heavier heavy fragments. This was also observed by Terrell (Te62) for the fission of $^{233,235}U$, ^{239}Pu and ^{252}Cf, and the enhanced yields at certain fragment mass numbers were attributed to nuclear structure effects in these fragments. The saw-toothed variation of neutron yields as a function of fragment mass diminishes considerably with increasing excitation energy as shown by Burnett (Bu68) for the proton-induced fission of ^{233}U at 8.5 and 13 MeV and Bishop et al. (Bi70) for the 11.5 and 22 MeV proton-induced fission of ^{238}U. This trend is consistent with other observations that shell effects tend to disappear with increasing excitation energy. Furthermore, an increase in excitation energy manifests itself in the heavy fragment and in general there are more neutrons emitted from the heavy fragment than from the light fragment.

Photon (or gamma-ray) emission from fragment nuclei has received less study than most other aspects of fission, largely due to their supposedly limited relevance to the details of fission. Despite the experimental difficulties a number of measurements has been made and reviewed by Nifenecker et al. (Ni73). In summary, it may be said that the total gamma-ray energy emitted in fission lies around 7.5 MeV with an absolute uncertainty of 0.5 MeV for most of the known cases; the gamma-ray yield per fragment versus fragment mass for low-energy neutron-induced fission exhibits the same saw-toothed variation as the neutron yield; and there exists a linear relation between the total gamma-ray energy and number of neutrons emitted.

C. Previous Work of Interest

In 1967 Klapisch et al. (Kl67) reported the successful use of an on-line mass spectrometer for measuring relative isotopic yields of elements produced in nuclear reactions. The utilization of the spectrometer for the measurement of isotopic fission yields was reported by Tracy et al. (Tr72). They measured the isotopic yields of rubidium (Rb) and cesium (Cs) formed in the fission of ^{232}Th and ^{235,238}U by protons of energies 40 to 60 MeV, and observed that the distributions were Gaussian in shape, although the Cs distributions were asymmetric. As the proton bombarding energy was increased the neutron-rich sides of the distributions remained fairly constant, whereas the neutron-deficient sides moved to lower mass numbers, resulting in a decrease in the mean mass numbers and an increase in the widths of the distributions. Furthermore, as Rb and Cs were complementary, or nearly complementary fragments for the reactions studied, average total neutron yields were obtained and charge-distribution mechanisms were studied. They concluded that the ECD postulate was better than the UCD postulate in predicting the data in the energy range studied. Since then the McGill group has made a number of on-line mass spectrometric studies of proton-induced fission of ^{232}Th (Ni80) and ^{235,238}U (Le75, Ch77, Su77), and deuteron-induced fission of ^{232}Th (Ko78) and ^{233,235,238}U (Cl78, Mo81). In a number of these studies

gallium (Ga) and indium (In) distributions have been obtained in addition to the Rb and Cs distributions. In all cases pronounced shoulders were observed on the neutron-rich side of the Cs distributions. These distortions have been attributed to contributions from lower excitation energy events by Nikkinen et al. (Ni80) and overlapping neutron stability zones around N=82, 86-88 by Mobed et al. (Mo81). All investigations showed that the centroids of the isotopic distributions move to lower mass numbers and the widths of the distributions increase as the incident particle energy is increased. The charge-division mechanism for the asymmetric components was consistently attributed to the ECD postulate. The only test of the MPE postulate was made by Mobed et al. (Mo81) and these investigators showed that charge division could also be attributed to a minimization of the potential energy, but no conclusion was drawn as to whether ECD or MPE was in better agreement with the data.

Very few nuclear-charge dispersion studies have been carried out for the fission of ^{233}U and ^{235}U in the energy range pertinent to this work. Studies on nuclear-charge dispersion of light-mass fission products have been carried out by Khan et al. (Kh70) for the proton-induced fission of ^{235}U and Marshall and Yaffe (Ma73) for the proton-induced fission of ^{233}U in the energy range 20 to 85 MeV. Studies in the heavy-mass region have been done by Tomita and Yaffe (To69) for the proton-induced fission of ^{233}U and Saha et al. (Sa71) for ^{235}U. These investigations have shown that in the

heavy-mass region the displacement of the most probable charge from stability is dependent on the neutron-to-proton ratio of the target, whereas in the light-mass region no such dependence exists. Marshall and Yaffe (Ma72) have thus concluded that the variation introduced by the targets manifests itself in the heavy fission fragments. Furthermore, the experimental results indicate that the most probable charges of the light and heavy fragments are not equidistant from beta stability when Z_A is taken for the fission products. This cannot be concluded as a failure of the ECD postulate as the postulate is related to primary fission fragments and not fission products. Khan et al.(Kh70) computed Z_p values based on the ECD and UCD postulates and concluded that ECD results were closest to their experimental values. Similar calculations by Saha et al. (Sa71) resulted in the UCD postulate giving the best fit to the experimental results, whereas Tomita and Yaffe (To69) found that their results fell between those predicted by the two postulates, and suggested this was a consequence of the two-mode fission hypothesis.

D. Purpose of the Present Study

This study was undertaken to supplement the existing data for the proton-induced fission of ^{233}U and ^{235}U in the energy range 40 to 100 MeV. The availability of an on-line mass spectrometer facilitated the accurate measurement of

isotopic distributions of Rb and Cs in fission. These distributions have not been measured for the proton-induced fission of ^{233}U and this work concludes a systematic mass spectrometric study of the proton-induced fission of the readily-obtainable uranium nuclei. Although these distributions have been measured for the proton-induced fission of ^{235}U there exists a discrepancy between the results obtained by Sutherland (Su77) and Tracy et al. (Tr72). Considering the experimental accuracy of the mass-spectrometric technique, a verification of the ^{235}U results was considered in order. We found that the measurement made by Tracy et al. at 50 MeV was in good agreement with the systematics of our measurements in the energy range 40 to 100 MeV.

Since Rb and Cs represent near-complementary products from the proton-induced fission of uranium, and assuming that their true complementary products could easily be determined, a qualitative procedure of testing the charge-distribution postulates was formulated. Although this did not require a knowledge of the number of neutrons emitted from each of the primary fragments, the total number of neutrons emitted was required, and this was estimated from the position of the centroids of the isotopic distributions and the identities of the fissioning nuclei. The calculations briefly outlined in this paragraph require a reliable reaction model to supply the identities of the fissioning nuclei and the probabilities of the various multichance fission events. The pre-equilibrium/

exciton model formulated by Gadioli was chosen for this purpose.

A modification of the surface-ionization ion source (Ni80a) used in the mass spectrometer allowed isotopic distributions of In to be obtained. These products are representative of near-symmetric mass splits from the proton-induced fission of uranium and an attempt was made to test the charge-distribution postulates in this region. Although no data exist in the complementary technetium/ruthenium region the results in this region were estimated from the systematics of the measured isotopic distributions. Isotopic yields of Ga were also obtained at 80 and 100 MeV for the fission of ^{233}U. However, these results are only tentative as the low yields prevented a measurement of the diffusion curve in order to correct for beta decay and feeding from precursors.

In all cases the relative isotopic yields were normalized to independent formation cross-sections which were measured radiochemically. Excitation functions were constructed for ^{72}Ga, $^{84,86}Rb$, $^{116m,117m+g}In$, and $^{132,134m+g}$, ^{136}Cs. The Cs measurements were in excellent agreement with the previous measurements by Tomita and Yaffe (To69) and Saha et al. (Sa71). The shape of these excitation functions will be discussed and compared to previous trends.

II. EXPERIMENTAL PROCEDURES

A. On-Line Mass Spectrometry

A1. The mass spectrometer

Isotopic distributions of the fission products studied in this work were obtained using an on-line mass spectrometer located at the exit of the external beam line of the McGill Synchrocyclotron. This allowed irradiations up to a maximum proton beam energy of 100 MeV. Lower energies were obtained by placing beryllium degraders in the path of the extracted beam and the energies of the degraded beams were calculated using the range/energy tables of Williamson and Boujot (Wi62). A schematic diagram of the mass spectrometer is shown in Figure II.1. The main features shown in the diagram are, the ion source which was maintained at an operating vacuum of 10^{-6} torr, the 90° sector magnet that deflected the ions emerging from the ion source and the electron multiplier that detected these ions. The slits S_1 and S_2 are image slits through which the extracted ions were focussed.

The operating principle of a mass spectrometer is based on the fact that a particle with charge q, and mass m, moving in a uniform magnetic field B. with velocity V, will follow a circular orbit of radius ρ. This implies that:

$$qVB = \frac{mV^2}{\rho} \qquad \text{(II.1)}$$

and equating the kinetic energy (KE) to the potential energy (PE) gives:

Figure II.1

Schematic of the mass spectrometer

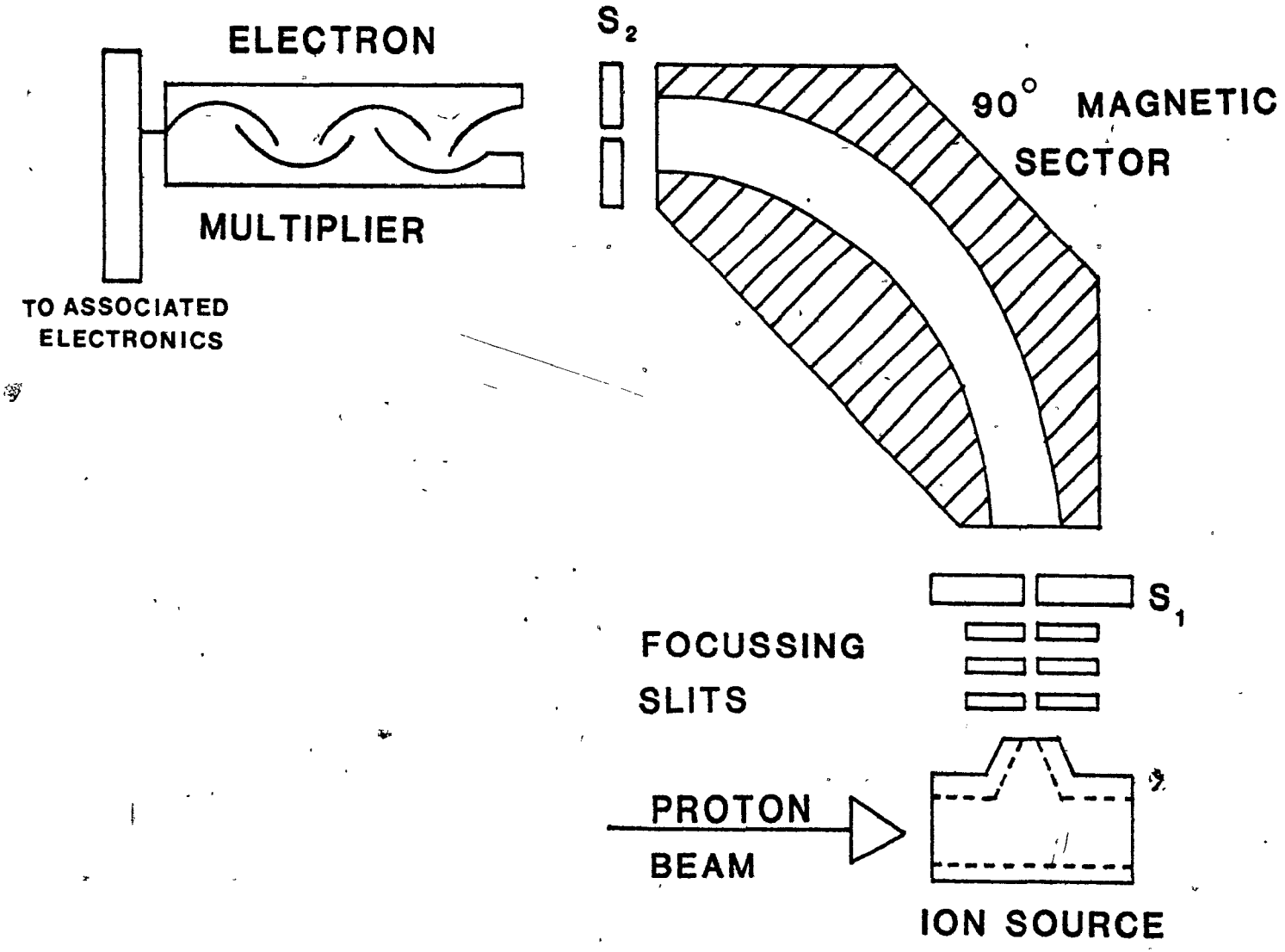
ELECTRON
MULTIPLIER
TO ASSOCIATED
ELECTRONICS
S2
90° MAGNETIC
SECTOR
S1
FOCUSSING
SLITS
PROTON
BEAM
ION SOURCE

$$KE = \frac{mV^2}{2} = \frac{qVB\rho}{2} = PE = qVo \qquad (II.2)$$

where Vo is the accelerating potential. Therefore:

$$m = \frac{qB^2\rho^2}{2Vo} \qquad (II.3)$$

The radius of curvature of the analysing magnet in the mass spectrometer used in this work was 30cm. From equation (II.3) it can be seen that by adjusting either the magnetic field (B) or the accelerating voltage (Vo) the desired mass could be selected .

During normal operation the spectrometer ion source was held above ground potential at a positive voltage of 5kV. Positive ions emerging from the ion source were accelerated through a 0.2mm wide defining slit and entered the magnetic field. After leaving the field region the ions passed through a 1.0mm image slit and entered the electron multiplier. The ability of the spectrometer to separate adjacent masses, termed the resolving power and defined as $M/\Delta M$, where M was the measured mass and ΔM was the full width at 1% maximum, was in the region 160 to 200 (Ni77), which was adequate for the mass regions under study.

An important component of a mass spectrometer used for fission product measurements is the ion source. It determines which elements can be ionized and thus establishes the selectivity and overall efficiency of the apparatus.

A2. Ion source

The ion source used in this work consisted of two major components: a cylindrical oven for heating the target disks and an ionizing surface. A diagram of the ion source is shown in Figure II.2. The oven, machined from fine grained high purity graphite was 44mm long with a 12mm central bore. The wall of the oven was 150 microns thick, the thickness being increased to 1.33mm in the central region where a 12mm hole allowed for insertion of the ionizing structure. The ends of the oven were enlarged to 22mm to allow an even current distribution, the current being supplied through tantalum electrodes screwed into the enlarged ends. Graphite disks, coated on one side with target material and separated by 0.3mm graphite spacers, were located in the central region of the oven. A 0.25mm tantalum heat shield surrounded the oven to contain the radiated heat and provide a uniform temperature distribution within the oven.

The ionizing structure, commonly called "the horn," consisted of an ionizing foil spot-welded between two tantalum posts, one terminating in the form of a plug and the other as a slit. The tantalum electrodes of the horn and oven were coupled to separate high-current electrical feedthroughs and each component was heated by the Joule effect from separate power supplies.

The operation of the ion source depended on the fast diffusion of certain elements out of hot graphite and the

Figure II.2

Ion source

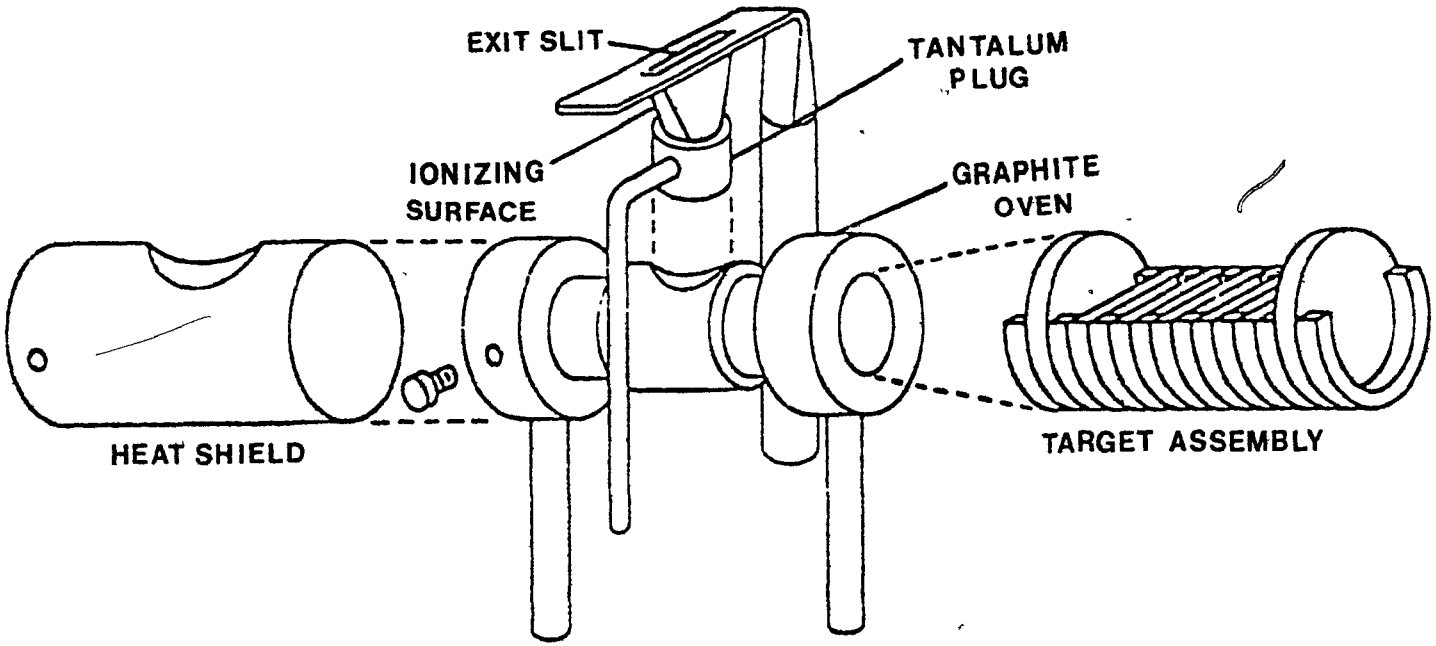
EXIT SLIT
TANTALUM PLUG
IONIZING SURFACE
GRAPHITE OVEN
HEAT SHIELD
TARGET ASSEMBLY

selective ionization of these elements. The former criterion restricted the products available for study to the alkali elements and indium and gallium. The study of the fast diffusion of these recoiling fission products out of hot graphite has been well documented by Pilar (Pi74) and Nikkinen (Ni77) and will thus not be elaborated.

The latter criterion, the ionization probability, was a major factor in determining the chemical selectivity of the ion source. The probability of surface ionization is governed by the Saha-Langmuir equation (La74):

$$\frac{n_+}{n_o} = \frac{g_+}{g_o} \exp(W-1)/kT \qquad \text{(II.4)}$$

where:

$\frac{n_+}{n_o}$ = the fraction of atoms ionized,

W = work function of ionizing surface,

I = ionization potential of an atom in contact with the surface,

$\frac{g_+}{g_o}$ = ratio of the electron spin degeneracy of the ion to the spin degeneracy of the neutral atom,

k = Boltzmann's Constant,

T = the surface temperature.

Thus a material with a high work function was required as the ionizing surface, and elements with low ionization potentials were most efficiently ionized. The probability of ionization is also dependent on the surface temperature and a judicious choice of this temperature and the material used as the

ionizing surface was necessary to obtain maximum ionization probabilities for the elements under study. The chemical selectivities of the ion source for rubidium, cesium, indium, and their neighbouring contaminants are shown in Table II.1. As indicated in the table a tantalum foil, 25 microns thick, was used as the ionizing surface for the rubidium and cesium experiments, and the normal operating temperatures of the oven and horn were 1600°C and 1000°C respectively. For the indium and gallium ($I \approx 6.0$eV) determinations the oven was operated at 1700°C and a 25 micron thick rhenium foil maintained at 1100°C was used as the ionizing surface. Anomalous ionization was observed for the indium and gallium experiments and it has been previously found (Ni77, 80a) that the ionization probabilities of indium and gallium do not agree with the Saha-Langmuir equation. However, reasonable source efficiencies were obtained by heating the ionizing surface to 1800°C for a period of 30 to 40 minutes prior to the determinations after which experiments were performed at an operating horn temperature of 1100°C for approximately five hours. This suggested that surface coating phenomena may enhance efficient ionization. Indium data were still obtained with the desired purity and a gamma-ray spectrum of an extracted ^{120}In source (Ni80a) showed no contamination from neighbouring elements. Gallium data were only obtained at the higher energies due to its low fission yield and anomalous ionization.

Table II.1: Selectivity of the Ion Source

Ionizing Surface	Surface Temperature	Element Ionized	Ionizing Potential (eV)	Fraction Ionized $n_+/n_+ + n_0$
Ta(W=4.19eV)	1000°C	Rb	4.176	0.36
		Sr	5.692	$\sim 10^{-5}$
		Cs	3.93	0.89
		Ba	5.21	$\sim 10^{-7}$
Re(W=5.1eV)	1800°C	In	5.785	0.02
		Cd	8.991	$\sim 10^{-10}$

[Data from Nikkinen (Ni 77)]

A3. Target preparation

The target disks* were prepared by the deposition of uranium oxide from a uranium oxide-acetone slurry onto graphite disks 12.5mm in diameter and 0.25mm thick. The target material was confined to a region 8.5mm in diameter in the centre of each disk and the disks were separated by graphite spacers in the target assembly.

The ^{233}U was deposited as isotopically pure $^{233}UO_2$ and each of the 20 disks in the target assembly contained 1.0mg of ^{233}U. For the ^{235}U target assembly the deposition was as enriched $^{235}U_3O_8$ and each of the 17 disks in the stack contained 1.0mg of ^{235}U. A mass spectrum of this target indicated that the ^{235}U was enriched to approximately 93%.

The beam degradation in the target stacks was determined using the range/energy tables of Williamson and Boujot (Wi62) and the bombarding energies, expressed as the average of the incident and exiting beam energies, will be given in the section on experimental results, together with the calculated energy spread.

A4. Electronics and data acquisition

A schematic diagram of the electronics incorporated with the mass spectrometer is shown in Figure II.3. In order to to obtain isotopic distributions of the fission products under

---

* We are grateful to Atomic Energy Canada Ltd., Chalk River for preparing and supplying the target disks.

Figure II.3

Schematic of the mass spectrometer electronics

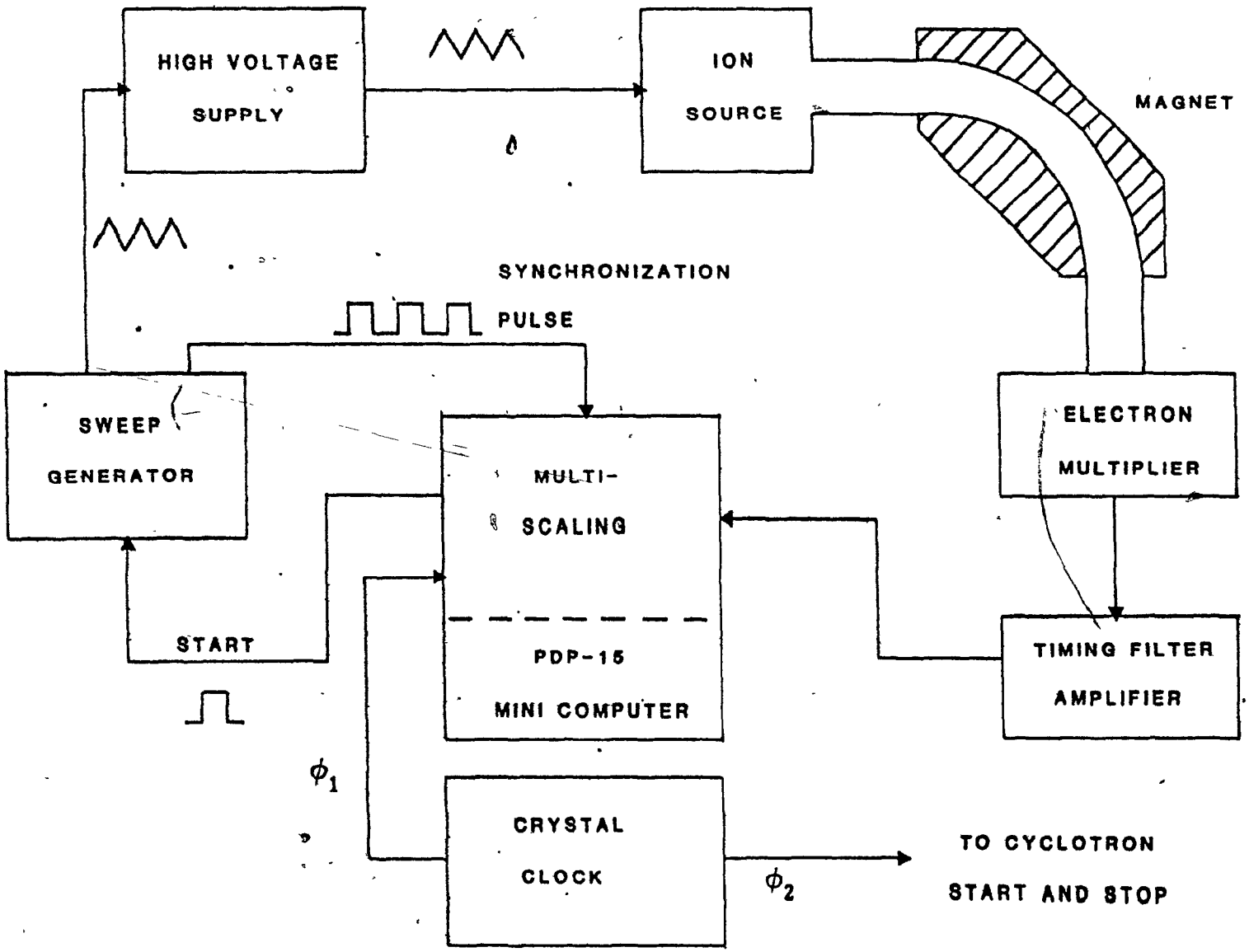
HIGH VOLTAGE
SUPPLY
ION
SOURCE
MAGNET
SYNCHRONIZATION
PULSE
SWEEP
GENERATOR
MULTI-
SCALING
ELECTRON
MULTIPLIER
START
PDP-15
MINI COMPUTER
TIMING FILTER
AMPLIFIER
ϕ_1
CRYSTAL
CLOCK
ϕ_2
TO CYCLOTRON
START AND STOP

study it was desirable to obtain yields for several isotopes under identical experimental conditions. This was accomplished by tuning the magnetic field to select one isotope in the mass region of interest, and then modulating the constant 5kV accelerating voltage on the ion source with a 48.5Hz triangular voltage wave from a sweep generator. A clock pulse ϕ_1 started the PDP-15 mini-computer in the data acquisition mode and simultaneously triggered the sweep generator. At the correct phase of the triangular modulation a synchronization pulse from the sweep generator started data accumulation in channel zero of the first data block of 1024 channels. Accumulation proceeded for a predetermined number of cycles in successive memory blocks until the specified number of blocks had been completed. The sweep generator was then disabled and the computer awaited the next clock pulse to restart the data accumulation cycle. A second clock pulse ϕ_2 started a timer that switched on the cyclotron beam for a fixed period of time during the data acquisition cycle. The pulse ϕ_2 was delayed from the data acquisition pulse ϕ_1 such that the cyclotron beam was on while the computer was accumulating data in the second memory block. Data were collected in either three or four memory blocks so that spectra before, during, and after each beam burst could be obtained.

This accumulation mode constitutes a timing sequence that was repeated until data were accumulated to the desired statistical accuracy. Mass spectra obtained in the manner

just described are shown in Figure II.4. The "mirror image" nature of the spectra was due to the triangular shape of the modulated high voltage, such that the spectra on the left were obtained during the down-ramp of the triangular sweep and the spectra on the right were obtained during the up-ramp. Subtraction of the background spectrum (a) from the "beam-on" spectrum (b) gave the relative isotopic distribution of the element under study.

The duration of the timing sequence mentioned in the preceding paragraph was selected according to the diffusion characteristics of the elements and the decay times of the isotopes. The diffusion characteristics were determined by selecting one mass near the peak of the distribution for each element. With the sweep generator disabled, a spectrum was collected before, during, and after each beam burst in one memory block of 1024 channels. A sample "diffusion curve" spectrum of ^{90}Rb is shown in Figure II.5. The spectrum shows the growth in the activity of the isotope while the beam was on, followed by the decay after the beam burst. The time taken for the activity to reach the background level determined the timing sequence.

Diffusion curve spectra collected before and after each experiment were also used to correct for beta decay of unstable isotopes diffusing out of the target and for added production due to precursor feeding. The spectra were fitted to the sum of two decaying exponentials.

Figure II.4

Indium Mass Spectra

a. Background spectrum

b. Fission spectrum

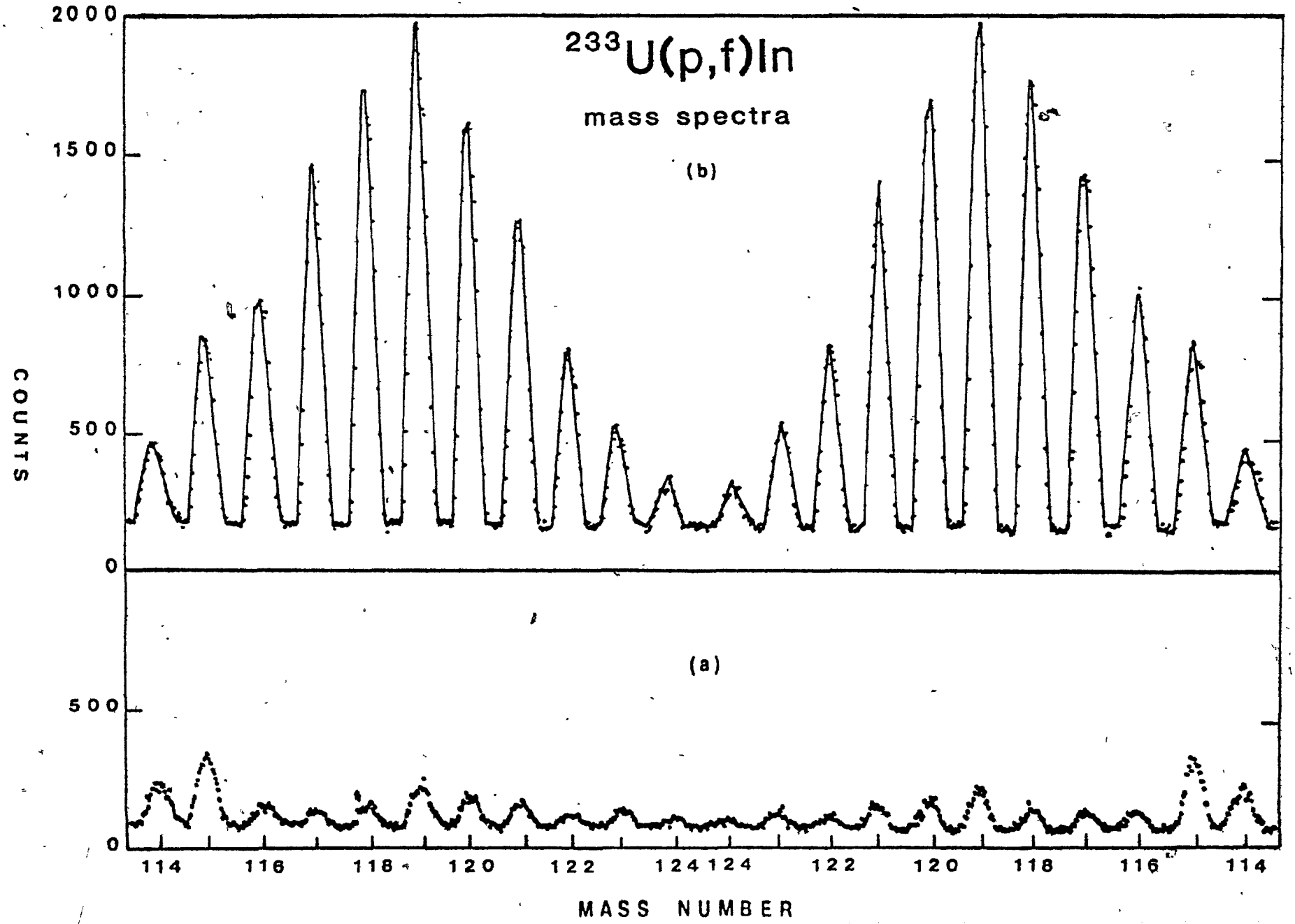
^{233}U(p,f)In
mass spectra
(b)
(a)
2000
1500
1000
500
0
500
0
COUNTS
114
116
118
120
122
124
124
122
120
118
116
114
MASS NUMBER

Figure II.5

^{90}Rb diffusion curve

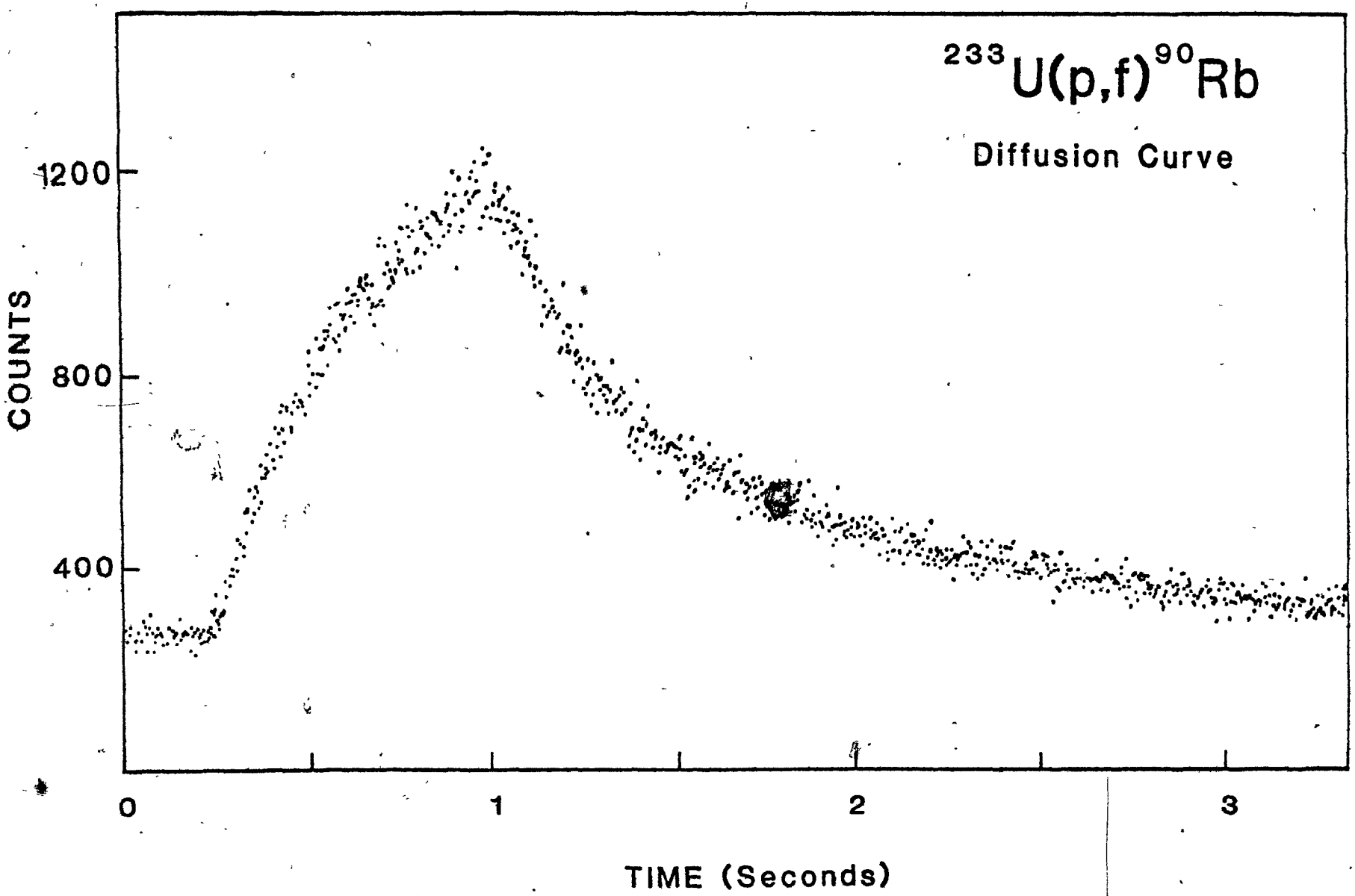
$^{233}U(p,f)^{90}Rb$
Diffusion Curve
COUNTS
1200
800
400
0
1
2
3
TIME (Seconds)

$$Y = W_1 \exp(-\lambda_1 t) + W_2 \exp(-\lambda_2 t) \qquad \text{(II.5)}$$

where λ_1 and λ_2 were the time constants and W_1 and W_2 were the relative weights of each diffusion mode. These constants, together with the irradiation time and duration of the timing sequence, were used in a computer program to calculate correction factors for the unstable isotopes of the element under study. A detailed description of the analysis and listing of the computer program is given by Clara (Cl78).

The counting system deadtime was required to make the necessary corrections to the data. This was accomplished by feeding a series of double pulses into the signal processing electronics. By reducing the time interval between pulse pairs until the count rate recorded by the computer dropped by a factor of two the system deadtime was found to be 5.6±0.1μsec.

The corrections briefly mentioned above, together with the mass discrimination corrections, will be discussed in the section on data analysis.

B. Internal Irradiations

B1. Target preparation

The target materials used for the internal irradiations were two oxides of uranium. For the ^{233}U experiment the oxide was isotopically pure $^{233}UO_2$ [1.] and for the ^{235}U experiments the oxide was $^{235}U_3O_8$ [2.] enriched to 93%, the isotopic impurity

being ^{238}U (6%) and ^{234}U (1%). The targets were prepared by mixing the weighed oxide with an approximately equal amount of accurately-weighed CuO so that the $^{65}Cu(p,pn)^{64}Cu$ reaction could be used to monitor the intensity of the proton beam. The excitation function of this reaction in the energy range pertinent to this work has been measured by Newton et al. (Ne73) and their results were used throughout.

For each irradiation a weighed amount of the mixed oxides (10-20mg) was packed into the central region of a short length of aluminium tubing.[3] The tubing was flattened, folded and clamped to a target holder that could be mounted on the end of the cyclotron probe as shown in Figure II.6.

B2. Irradiations

Each target was irradiated by inserting the cyclotron probe to a radial distance such that the leading edge of the target was irradiated by a beam of the desired energy. The variation of energy with target distance was taken from the data of Moore (Mo75) and is reproduced in Figure II.7. The energy range covered was 35 to 90 MeV and the duration of each irradiation was chosen according to the following criteria: the fission fragment under study; the internal beam

---

1. This material was supplied by Atomic Energy Canada Ltd., Chalk River.

2. This material was supplied by Oak Ridge National Laboratory, Oak Ridge, Tennessee, U.S.A.

3. The tubing was 1100 aluminium (wall thickness $\approx$ 10mg/cm^2) from Precision Tube Company Inc., North Wales, Pa., U.S.A.

Figure II.6

Target assembly at end of cyclotron probe

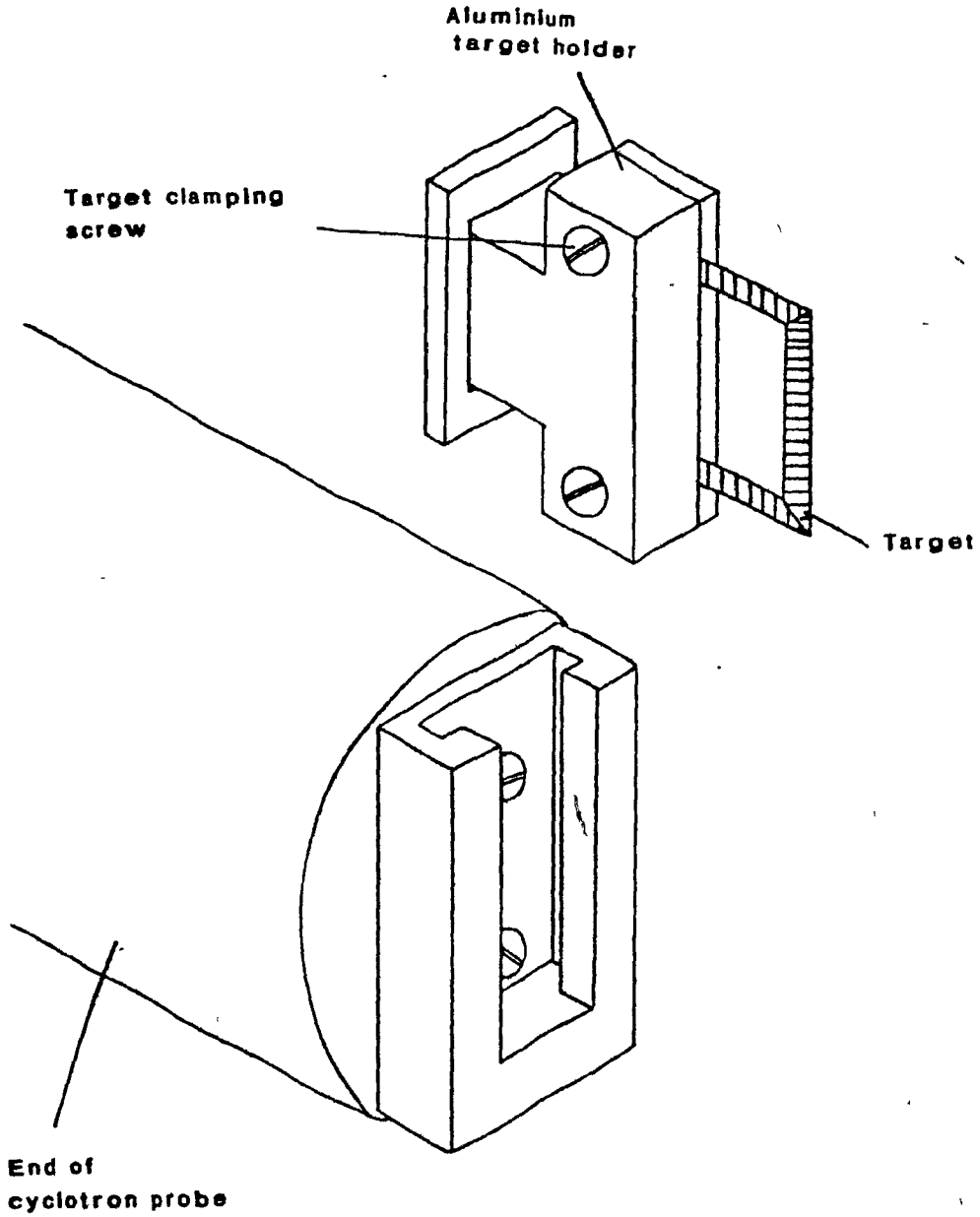
Aluminium
target holder
Target clamping
screw
Target
End of
cyclotron probe

Figure II.7

Bombarding energy vs. target radius

after Moore (Mo75)

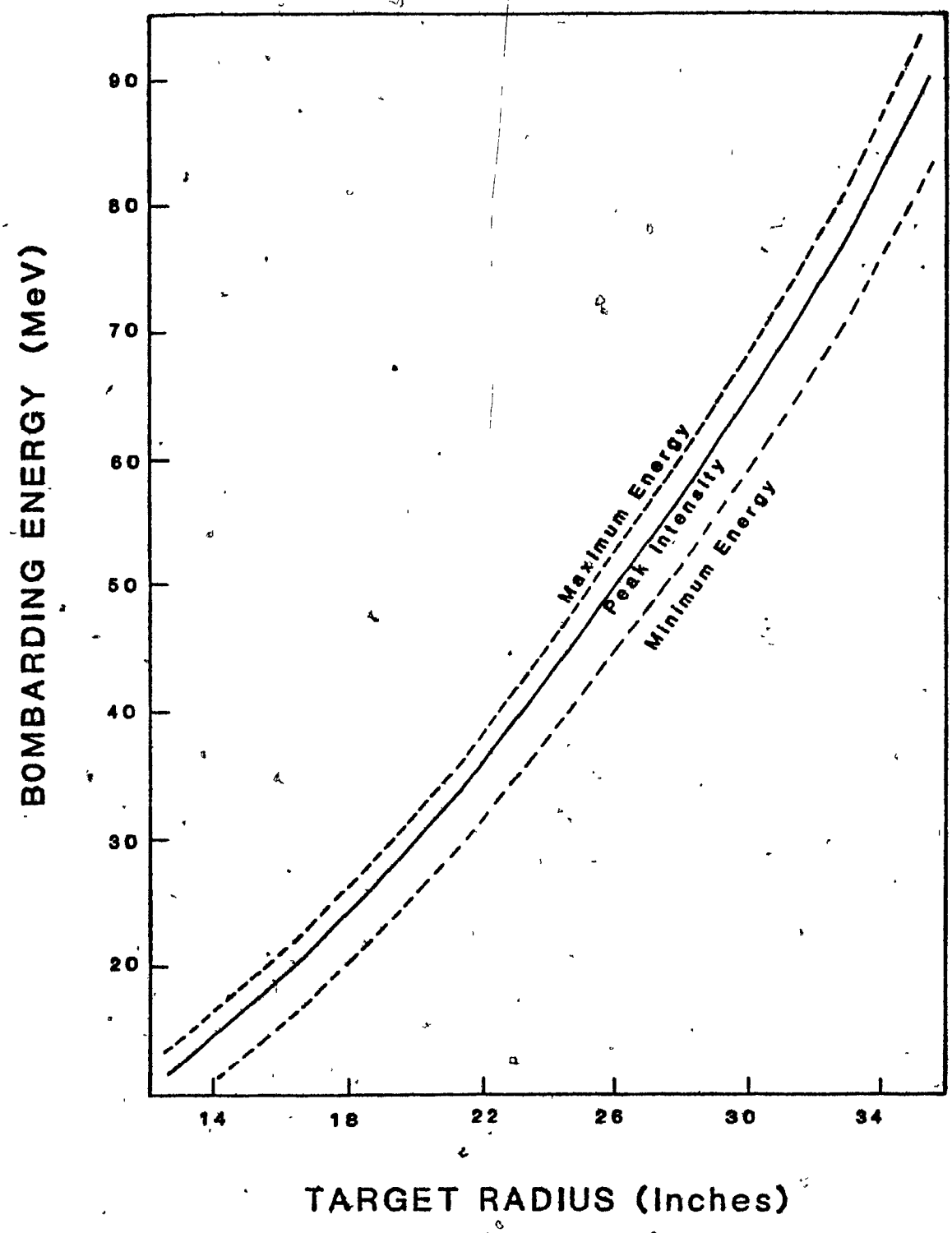
BOMBARDING ENERGY (MeV)
90
80
70
60
50
40
30
20
Maximum Energy
Peak Intensity
Minimum Energy
14
18
22
26
30
34
TARGET RADIUS (Inches)

current; and the induced radioactivity. Irradiations varied from 5 to 10 minutes and the internal beam current was between 1.0 and 2.0μA.

The beam degradation in the aluminium tubing and target was calculated for each incident energy using the tables of Williamson and Boujot (Wi62). Throughout the range covered the energy loss in the target assembly was found to be much less than the minimum beam spread of ±2 MeV.

C. Radiochemical Procedures

After each irradiation the target was dissolved in a suitable solvent to give a solution of mixed fission products. The radiochemical isolation of fission products pertinent to this work was then accomplished by adding inactive carrier solutions for the elements under study. After a series of purification steps the desired elements were precipitated according to a suitable gravimetric procedure. This required standardization of the carrier solutions in order to determine chemical yields needed for the computation of absolute cross-sections.

In order to reduce the number of irradiations, radiochemical procedures were developed so that rubidium and cesium could be isolated from the same target. Similar procedures were developed for the isolation of indium and gallium.

The procedures described in the following sections were

carried out in 40ml centrifuge tubes unless otherwise stated. All solids were precipitated onto No. 542 Whatman filter papers and the precipitates were mounted on cardboard holders and held in place with "Scotch" tape for activity measurements.

C1. Standardization of carrier solutions

Both rubidium and cesium carrier solutions were prepared by dissolving a known amount of the pure chloride, dried at 110°C, in distilled water. The solutions were then made up to a volume such that the concentration of alkali element was approximately 10mg/ml. The solutions were standardized by adding a slight excess of 0.5M chloroplatinic acid to 5ml of the carrier solutions. The resulting solutions were cooled in an ice bath and absolute ethanol (15ml) was added. The precipitates were filtered into tared sintered glass crucibles, washed with cold ethanol until the wash was colourless, dried at 110°C for ten minutes, cooled and weighed as Rb_2PtCl_6 or Cs_2PtCl_6. Three determinations were performed for each carrier.

The gallium carrier solution was prepared by dissolving a known amount of gallium (III) oxide in conc. HCl. The resulting solution was diluted to a volume such that the concentration of gallium was approximately 10mg/ml and the solution was 6M in HCl.

The indium carrier solution was prepared by dissolving indium metal (99.9% pure) in a minimum of conc. HCl and diluting with 1.5M HCl. The solution was made up to a volume such that the concentration of carrier was approximately 10mg/ml.

Both gallium and indium carrier solutions were standardized by precipitation of the oxine derivatives. The carrier solution (5ml) was pipetted into a 100ml beaker and distilled water (20ml) was added. The solution was heated to 60°C and 1% 8—hydroxyquinoline in 2M acetic acid (3ml) was added. Ammonium acetate buffer (6M) was added dropwise until a permanent precipitate formed. Five drops of a 1% aerosol solution was added and the precipitate was digested for five minutes. The precipitate was filtered into a tared sintered glass crucible, washed with warm distilled water (10ml), three washings of cold distilled water (5ml), dried at 110°C for 15 minutes and cooled. The precipitates were weighed as $Ga(C_9H_6NO)_3$ or $In(C_9H_6NO)_3$ and three determinations were performed for each carrier.

C2. Rubidium and cesium radiochemistry

The separation of rubidium and cesium from other fission products was based on the methods used by Evans (Ev51, 51a), in which the alkali ions were isolated from most other fission product cations by precipitating the latter as hydroxides or carbonates. Further radiochemical purification was accomplished by $La(OH)_3$ scavenging after which cesium was separated from rubidium by precipitating the former as $Cs_3Bi_2I_9$. The details of the procedure are as follows:

1. The target was dissolved in hot conc. HCl (2ml) and conc. HNO_3 (2 drops). Cesium carrier (20mg), rubidium

carrier (20mg), and a mixed solution of cerium [$Ce(NO_3)_3 \cdot 6H_2O$], yttrium [$Y(NO_3)_3 \cdot 4H_2O$], lanthanum [$La(NO_3)_3 \cdot 6H_2O$], zirconium [$ZrOCl_2 \cdot 8H_2O$], strontium [$SrCl_2 \cdot 6H_2O$], and barium [$Ba(NO_3)_2$] carriers containing 5mg of each cation were added to the resulting solution. The solution was made basic to phenolphthaline by the dropwise addition of 12M NaOH, and 1M Na_2CO_3 (1ml) was added. The precipitate was retained for the copper chemistry and uranium recovery.

2. The supernatant was made just acidic with conc. HCl and lanthanum carrier (10mg) was added. The solution was made basic to phenolphthaline as above and the precipitate was discarded.

3. The supernatant was made just acidic with glacial acetic acid and 1ml of HI/BiI_3 reagent [BiI_3 (10g) dissolved in 55% HI (50ml)] was added. The solution was cooled in an ice bath for ten minutes and $Cs_3Bi_2I_9$ was precipitated. Greater yield was effected by scratching the sides of the tube with a glass rod. The supernatant was retained for the rubidium purification.

4. Cesium purification: The precipitate from step 3 above was washed with cold distilled water (7ml), cold dil. HCl (3ml) and dissolved in the minimum amount of conc. HCl by heating to boiling. Rubidium hold-back carrier (10mg), distilled water (2-3ml) and HI-BiI_3 reagent (1ml) were added to the solution, and the resulting

solution was cooled in an ice bath. Cesium was precipitated as above, washed with dil. HCl (2ml) and filtered onto a tared filter paper. The precipitate was washed successively with 5ml portions of absolute ethanol and ether, dried at 110°C for ten minutes, cooled, weighed as $Cs_3Bi_2I_9$, and mounted for activity measurements. Yields were consistently 35-40%.

Rubidium purification: Three successive $Cs_3Bi_2I_9$ precipitations were made from the supernatant from step 3 above by adding cesium carrier (10mg), $HI-BiI_3$ reagent (1ml) and cooling in an ice bath. Complete precipitation of cesium was effected by scratching the sides of the tube and cooling for thirty minutes. The final supernatant was boiled with conc. HNO_3 (2ml) to remove iodine, evaporated to near dryness, and taken up in distilled water (5ml). This effected the removal of bismuth as the oxynitrate. Conc. HNO_3 (1ml) and absolute ethanol (10ml) were added to the supernatant and the solution was cooled in an ice bath. Chloroplatinic acid (0.5ml of 0.5M H_2PtCl_6 in 50% ethanol) was added to the solution to precipitate rubidium as the chloroplatinate. A further 5ml of ethanol was added and the precipitate was filtered onto a tared filter paper. The precipitate was washed with cold ethanol (2x5ml portions), ether (5ml), dried at 110°C for ten minutes, cooled, weighed as Rb_2PtCl_6, and mounted for activity measurements. Yields were in the

range 50-70%.

C3. Indium radiochemistry

The separation of indium from other fission products was based primarily on the method used by Glendenin (Gl51) in which In_2S_3 was precipitated from a slightly acidic solution. Cycles of palladium sulphide scavengings at acidities high enough to keep indium in solution removed the majority of contaminants and finally lanthanum hold-back carrier removed zirconium and silver contaminants prior to the final In_2S_3 precipitation.

Modifications to the original procedure were required for two reasons. First, the isolation of gallium from the solution of mixed fission products was required and secondly, a rapid separation of indium from cadmium was needed so that the separation time of indium from its parent activity could be known. A later separation of indium from the decaying cadmium was performed for reasons explained in section three. Gallium was isolated by solvent extraction into isopropyl ether and the separation will be explained in the outline of the gallium radiochemistry. The separation of indium from cadmium was based on the method used by Cowan (Co58) in which $In(OH)_3$ was precipitated with an excess of conc. NH_4OH, cadmium remaining in solution as the ammoniacal complex. Copper also remained in solution as the ammoniacal complex and was recovered after the second indium/cadmium separation. The details of the procedure are as follows:

1. The target was dissolved in hot conc. HCl (2ml) and conc. HNO_3 (2 drops). Gallium carrier (20mg), indium carrier (20mg) and cadmium hold-back carrier (10mg as $3CdSO_4 \cdot 8H_2O$ dissolved in distilled water) were added to the resulting solution. The cooled solution was contacted with isopropyl ether (12ml pre-equilibrated with 6M HCl) for 30 seconds and the ether layer was retained for the gallium chemistry.

2. An excess of conc. NH_4OH was added to the aqueous phase and the solution was heated to coagulate the precipitate $In(OH)_3$. After centrifugation the supernatant was decanted and the time of separation of indium from cadmium was recorded. The supernatant was retained for "milking" the indium growing from the cadmium decay and for the copper recovery.

3. The precipitate was washed with hot distilled water, dissolved in a minimum of 6M HCl and diluted to 5ml with distilled water. A further $In(OH)_3$ precipitation was performed.

4. The precipitate was washed as before and dissolved in 6M HCl (10 drops). Distilled water (5ml) and 6M ammonium acetate (10 drops) were added and In_2S_3 was precipitated by bubbling H_2S gas through the solution. This precipitate was washed with hot distilled water.

5. The In_2S_3 was dissolved in 6M HCl (1ml) and distilled water (10ml) was added. Palladium carrier (5mg, added as

$PdCl_2$ dissolved in distilled water) was added and PdS precipitated by bubbling H_2S through the solution. The precipitate was discarded.

6. An excess of conc. NH_4OH was added to the supernatant to precipitate $In(OH)_3$. The precipitate was washed as before and steps 5. and 6. were repeated.

7. The $In(OH)_3$ precipitate was dissolved in 6M HCl (10 drops) and distilled water (5ml) was added. Lanthanum hold-back carrier [5mg as $La(NO_3)_3 \cdot 6H_2O$] and 6M ammonium acetate (10 drops) were added, and H_2S gas was bubbled through the solution to precipitate In_2S_3.

8. The resulting mixture was boiled to coagulate the precipitate and In_2S_3 was filtered onto a tared filter paper. The precipitate was washed with hot distilled water and ethanol, dried at 110°C for ten minutes, cooled, weighed as In_2S_3 and mounted for activity measurements. Yields were in the range 40-60%.

C4. Gallium radiochemistry

The separation procedure for gallium was a composite of techniques outlined in a monograph by Lewis (Le61). The major steps employed in the procedure were the extraction of gallium chloride by isopropyl ether (Na49), followed by anion exchange in hydrochloric acid (Kr54). The solvent extraction separated gallium from most fission products (Si51) and provided a rapid separation of gallium from its precursor zinc, the latter

remaining in the aqueous phase. The principal contaminants partially extracted into isopropyl ether were Ge, As, Mo, Sn, Sb and Tl, and these were removed by anion exchange following the reduction of any Sb(V) to Sb(III) by stannous chloride. The details of the procedure are as follows:

1. The ether phase from the indium chemistry was washed with 6M HCl (3x5ml portions) and gallium was back extracted into distilled water (3x5ml portions).

2. The resulting solution was made 3M in HCl and 3mg of stannous ion as $SnCl_2$(aq.) was added. The solution was passed down a Dowex-1-X8 anion exchange column (100-200 mesh, 15cm x 1cm) pre-equilibrated with 3M HCl. The column was washed with three column volumes of 3M HCl and gallium was eluted with 0.2M HCl into a 100ml beaker.

3. Distilled water (30ml) was added to the effluent and the solution was heated to 60°C. One per cent 8-hydroxyquinoline (3ml) was added to the solution and 6M $NH_4C_2H_3O_2$ was added dropwise until a permanent precipitate formed. A further two drops of precipitant and five drops of 1% aerosol solution were added to the mixture.

4. The solution was digested for two minutes and filtered onto a tared filter paper. The precipitate was washed with warm distilled water (2 x 5ml portions), cold distilled water (2x5ml portions), dried at 110°C for 15 minutes, cooled, weighed as $Ga(C_9H_6NO)_3$ and mounted for activity measurements. Yields were in the range 20-30%.

C5. Copper radiochemistry

The radiochemical procedure for the recovery of copper was adapted from that of Kraus and Moore (Kr53) with modifications based on the work of Meinke (Me49). No carrier for copper was required as the CuO in the target acted as carrier. An additional step for the copper recovery was employed when the fission products separated were rubidium and cesium as copper was retained as $Cu(OH)_2$. The hydroxide was dissolved in 6M HCl (2ml) and an excess of conc. NH_4OH was added. When indium and gallium were separated copper was retained as the ammoniacal complex and the recovery from this stage was as follows:

1. Barium, iron and strontium scavengers [5mg of each cation as $Ba(NO_3)_2$, $FeCl_3$ hydrate and $SrCl_2 \cdot 6H_2O$ dissolved in hot distilled water, cooled and diluted to volume] and 1M Na_2CO_3 (1ml) were added to the ammoniacal solution, and the solution was heated to boiling. The precipitate was discarded.

2. The solution was made just acidic with conc. HCl and Sr, La, and Y hold-back carriers [5mg of each cation added as $SrCl_2 \cdot 6H_2O$, $La(NO_3)_3 \cdot 6H_2O$ and $Y(NO_3)_3 \cdot 4H_2O$, dissolved in distilled water and diluted to volume] were added. CuS was precipitated by bubbling H_2S gas through the solution.

3. The precipitate was washed with hot distilled water and dissolved in conc. HCl (1ml) and conc. HNO (3 drops)

in a 50ml beaker. The solution was evaporated to dryness and taken up in 4.5M HCl (2ml).

4. The new solution was transferred to a Dowex-1-X8 anion exchange column (100-200 mesh, 15cm 1cm). The column was washed with five column washes of 4.5M HCl to elute Zn, Co and any remaining iron, and Cu was eluted with 1.5M HCl into a 100ml beaker.

5. The solution was diluted to 10ml with distilled water and heated to 60°C. Copper (II) was reduced to copper(I) by adding solid $NaHSO_3$, and CuSCN was precipitated by the dropwise addition of 10% NH_4SCN to a slight excess of thiocyanate.

6. The precipitate was digested for 20 minutes at 90°C and transferred to a tared filter paper. The precipitate was washed with 30% ethanol followed by acetone, dried at 110°C for ten minutes, cooled, weighed as CuSCN, and mounted for activity measurements. Yields were in the range 60-80%.

D. Activity Measurements

High resolution gamma-ray spectroscopy provided an effective means of studying the isolated fission products pertinent to this work. The excellent resolving power of lithium-drifted germanium [Ge(Li)] detectors, together with multichannel analysers, provided a means of studying several isotopes of the isolated element simultaneously. This was accomplished

by obtaining the gamma-ray energies for the decay of nuclides of interest from a standard reference (Le78) and assigning the corresponding lines in the gamma-ray spectrum. All isotopes pertinent to this work were studied by gamma-ray spectroscopy. The ^{64}Cu activity was measured by detecting the 511-keV annihilation photons following positron decays in this isotope. To ensure complete annihilation of the emitted positrons the copper samples were sandwiched between two thin aluminium disks, thick enough to absorb the positrons.

D1. Data acquisition systems

Two data acquisition systems were used in this work. In both systems the same 40cc Ge(Li) detector (Ortec model 8101-0725), high voltage power supply (Ortec model 456), and pre-amplifier (Ortec model 120-2B) were used. During the course of this work the original pre-amplifier was replaced by an Ortec model 120-2F pre-amplifier. The detector, pre-amplifier and radioactive sample were housed inside a lead shield to minimize background from local and environmental radioactivity. The interior of the lead housing was covered with a copper foil and lucite sheet to render the cavity impervious to the shielding's gamma-rays, and to reduce gamma-ray back scattering. The major difference between the data acquisition systems was the multichannel analyser used.

Canberra-8100 System:

This system consisted of a 4096 channel analyser (Canberra model 8100) connected to the detector, associated electronics

and digital recorder (HP model 5055A). A block diagram of the system is shown in Figure II.8(a). The conversion gain of the analyser was set at approximately 0.7-keV/ channel, which was sufficient to cover the energy range of interest. During the course of this work the internal amplifier of the Canberra analyser was replaced by an amplifier (Ortec model 572) and the amplified signal was routed to the external input of the analyser's analog to digital convertor (ADC).

Nuclear Data-2400 System:

This system was used for the majority of the experiments performed. The detector and associated electronics were incorporated with an amplifier (Ortec model 452), 1024 channel analyser (ND-2400), cathode ray tube (HP model 1208B) and magnetic tape drive system (Pertec). In order to maintain a conversion gain of 0.7-keV/ channel and still cover the desired energy range the output of the amplifier was routed, when necessary, through a biased amplifier (Ortec model 408) that provided a step gain to expand the energy range of the analyser. A block diagram of the system is shown in Figure II.8(b).

D2. Calibration of the detector system

In order to assign the peaks in a fission-product spectrum an energy calibration of the system was required. This was done prior to every set of experiments by measuring the following standard sources; ^{22}Na, ^{133}Ba, ^{137}Cs and ^{207}Bi, and correlating their characteristic gamma lines to the channel numbers in which they peak.

Figure II.8

Block diagrams of data acquisition systems

a. Canberra 8100 System

b. Nuclear Data 2400 System

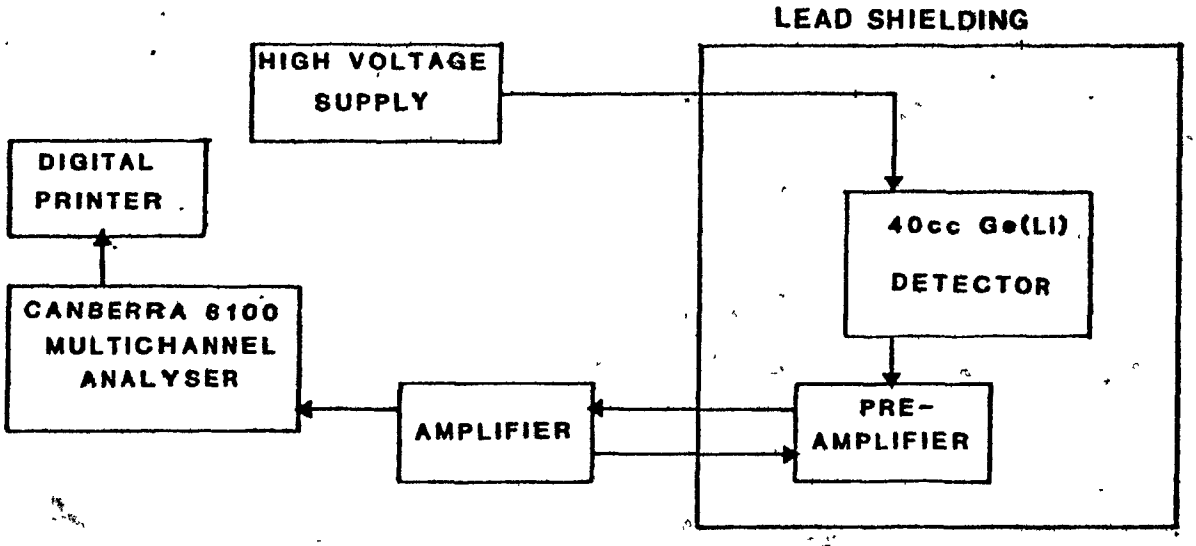

FIG. II.8(a)

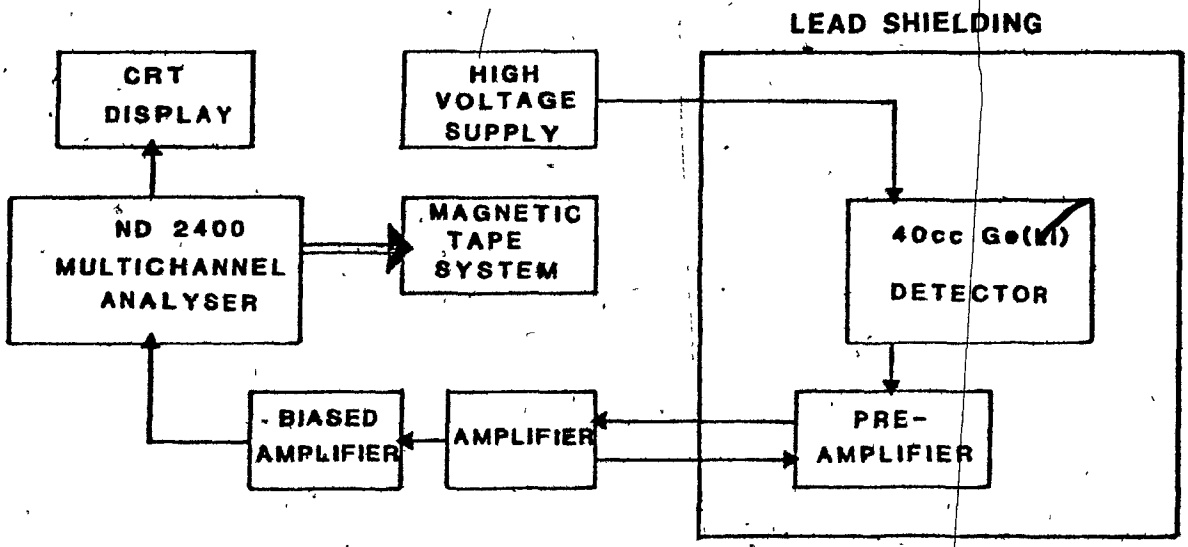

FIG. II.8(b)

An absolute efficiency calibration of the 40cc Ge(Li) detector was required for a quantitative measurement of gamma-ray intensities. This has been done for the detector used in this work by Chung (Ch78). The primary calibration was made at a source-to-detector distance of 149mm for gamma-ray energies between 80-keV and 1775-keV, using standard point sources. A 6.5mm plastic absorber was placed immediately in front of the detector to prevent coincidence events such as beta-gamma summation. Whenever possible radioactive samples were measured at 149mm from the detector. Very low activity samples were measured at 63mm from the detector and, following the recommendation of Fowler (Fo72), the estimation of the efficiency at this distance was made relative to the efficiency at 149mm. This was done by measuring a moderately active sample at 149mm and then 63mm. By accounting for the decay in the latter case the activity in the former case could be computed and compared to the measured value. The difference was used to compute efficiency ratios. This procedure was repeated ten times over a three-year period and gave results consistent to within ±7%.

The energy resolution of the detector system was found to be 1.78-keV for the 356-keV peak of ^{133}Ba, 1.99-keV for the 662-keV peak of ^{137}Cs, and 2.34-keV for the 1173-keV peak of ^{60}Co, corresponding to the full-width at half-maximum (FWHM) of the said peaks.

Both systems were used in the "live time" mode so that the analysers self-corrected for dead-time losses. The

dead-times indicated by the analysers never exceeded 10%, thus further dead-time corrections to the recorded data were not considered necessary.

III. DATA ANALYSIS

A. Analysis of Radiochemical Data

A1. Analysis of gamma-ray spectra

As mentioned in the previous section the ND-2400 analysing system was used for the majority of experiments. The data were collected on magnetic tape and analysed using the computer code GAMANAL (Gu72). Data collected with the Canberra-8100 system were recorded on paper tape and analysed manually.

The computer code GAMANAL analysed the data by first determining an average background under the spectrum. This served to locate the peak regions. The background continuum in each region was then estimated by a stepwise interpolation method, the step function being subsequently smoothed to give the final background. Summation of the data over the total number of channels defining the peak, followed by background subtraction, gave the photopeak areas. Each area represented the total activity of a given gamma-transition for a given measurement period. The standard deviation of this activity was calculated as the square root of the total peak area plus the background. This procedure was repeated for each spectrum recorded. The analysis of the data recorded on paper tape was similar to the procedure given above with the exception of the background analysis. Once a peak was defined a group of half the channels needed to span the peak was taken as background on either side of the said peak.

The photopeaks of interest were identified by the energy

of their gamma-rays. The energy calibration of the analysing system was obtained by measuring a set of standard sources that gave gamma peak positions corresponding to known gamma-ray energies. When GAMANAL was used for the analysis of the data a least-squares fit of the calibration spectra to a fifth-order polynomial was used, otherwise a simple linear regression was found adequate for locating the desired peaks.

A2. Decay-curve analysis

The activities of the chosen transition or transitions for each nuclide were in most cases measured ten to fifteen times over a period of at least three half-lives. For the majority of nuclides measured decay-curves were constructed in order to extrapolate activities at the end of irradiation or chemical separation from the parent nuclide.

The data were analysed with the Brookhaven National Laboratory computer code, CLSQ (Cu72), which used a least-squares procedure to compute the activity at some arbitrary initial time. At a given time (t), the observed activity A(t) is the sum of contributions of the components (m) such that:

$$A(t) = \sum_{j=1}^{m} [I_j \exp(-\lambda_j t) + V(t)] \qquad \text{(III.1)}$$

where I_j is the initial activity of the j^{th} component, λ_j is its decay constant, and V(t) is the residual due to experimental error and statistical fluctuations. For each observation of A(t) there is an equation of the form of (III.1), which is

linear with respect to the initial activity. By minimizing the squares of the weighted residuals a least-squares solution of the I_j's is obtained. This analysis also provided the calculated half-lives of the nuclides observed and served to verify their identities.

The initial activity (A°) of each nuclide was then corrected for detector efficiency, gamma-ray abundance, and chemical yield to give absolute disintegration rates (D°):

$$D^\circ = \frac{A^\circ}{\varepsilon \cdot S} \cdot \frac{1}{Y} \cdot \frac{1}{I_\gamma} \qquad \text{(III.2)}$$

where: ε = detector efficiency,

Y = chemical yield,

I_γ = number of gamma-rays per disintegration,

S = ratio of the detector efficiency at a given source-to-detector distance to that at a chosen standard distance.

The decay properties of the nuclides measured in this work are given in Table III.1 . It may be noted that ^{117m}In was not measured directly but observed through the decay of its daughter ^{117g}In. The decay-curve was thus resolved into two components, yielding contributions from ^{117m}In and ^{117g}In.

The activities due to ^{134g}Cs were not measured until at least 30 days after irradiation of the target nuclides to allow for decay of other fission products. The activities of ^{134g}Cs were then measured until reasonable statistics were obtained (statistical error $\lesssim 6\%$), and the activities at the end of irradiation were computed using standard decay equations. This

Table III.1: Nuclear Properties of Products Observed in the Radiochemical Measurements

Nuclide	Half-life*	Gamma Rays Observed (keV)	Gamma Ray Abundance (%)	Reference
^{64}Cu	12.70h	511.00	38.6	(Le78)
^{72}Ga	14.10h	629.90	24.4	"
		834.02	95.6	"
^{84}Rb	32.90d	881.60	74.0	"
^{86}Rb	18.82d	1077.20	8.8	"
^{116m}In	54.10m	416.86	32.4	"
^{117m}In	1.93h	552.90	99.7	"
^{117g}In	42.30m	552.90	99.7	"
^{132}Cs	6.47h	667.50	97.5	"
^{134m}Cs	2.90h	127.42	12.5	"
^{134g}Cs	2.06y	604.66	97.6	"
		795.76	85.4	"
^{136}Cs	13.10d	340.57	46.9	"
		818.50	99.7	"

* m= minutes; h= hours; d= days; y= years.

+ Followed through the daughter.

procedure was also employed for the observed activities of ^{84}Rb from $^{235}U(p,f)$ reactions and ^{86}Rb from $^{235}U(p,f)$ reactions at 40 and 50 MeV. Decay-curves were constructed for all other measurements.

A3. Cross-section calculations

1. General equations:

The disintegration rate (D_p^o) of a nuclide at the end of irradiation can be related to its formation cross-section (σ_p) according to the equation:

$$D_p^o = In_T\sigma_p [1-\exp(-\lambda_p t_b)] \qquad \text{(III.3)}$$

where: I = beam intensity of the bombarding particle, number of protons/s,

n_T = number of target atoms/cm^2,

σ_p = formation cross-section of the product, cm^2,

λ_p = decay constant of the product, s^{-1},

t_b = duration of irradiation, s.

As stated before, the beam intensity was not measured directly, but monitored using the $^{65}Cu(p,pn)^{64}Cu$ reaction cross-sections measured by Newton et al. (Ne73). The cross-sections of this reaction are listed in Table III.2. The disintegration rate of ^{64}Cu at the end of irradiation can be related to its formation cross-section by an equation similar to equation (III.3). Thus:

$$D_m^o = In_m\sigma_m [1-\exp(-\lambda_m t_b)] \qquad \text{(III.4)}$$

Table III.2: Monitor Cross-sections used in this Work

Incident Proton Energy E_p (MeV)	Cross-sections (mb)	Reference
35	249.7	(Ne73)
40	244.6	"
45	194.5	"
50	186.6	"
55	178.2*	"
60	169.7*	"
65	162.5*	"
70	155.3*	"
75	151.5*	"
80	146.2*	"
90	140.7	"

*. Interpolated values.

where the subscripts m' and m refer to the monitor and the reaction product of the monitor respectively. The formation cross-section of the desired fission product may then be determined relative to the known monitor cross-section by combining equations (III.3) and (III.4):

$$\sigma_p = \sigma_m \cdot \frac{D_p^o}{D_m^o} \cdot \frac{n_m}{n_t} \cdot \frac{[1-\exp(-\lambda_m t_b)]}{[1-\exp(-\lambda_p t_b)]} \qquad \text{(III.5)}$$

The beam intensities cancel out in the above equation as both the target and monitor nuclei were subjected to the same beam of protons for the same period of time.

The number of atoms (n) in equation (III.5) was calculated as follows:

$$n = \frac{W \cdot f}{AW} \cdot A_b \cdot N \cdot A_{eff} \qquad \text{(III.6)}$$

where: W = the weight of $^{233}UO_2$ or $^{235}U_3O_8$ for the target and the weight of CuO for the monitor, g,

f = the fraction of ^{233}U or ^{235}U in each target oxide and the fraction of Cu in CuO for the monitor,

A_b = the isotopic abundance of the target nuclide,

AW = the atomic weight of the target nuclide, g/mole,

N = Avogadro's number, atoms/mole,

A_{eff} = effective area of target or monitor, cm^2.

As mentioned in the section on target preparation the ^{233}U targets were isotopically pure, thus $A_b = 1$. The ^{235}U targets were enriched to 93%, the isotopic impurity being

$^{234}U(1\%)$ and $^{238}U(6\%)$. When computing the formation cross-sections of fission products from the $^{235}U(p,f)$ experiments the ^{234}U impurity was neglected but the following corrections were applied to account for the 6% ^{238}U present. The isotopic abundance of the target nuclei was taken as 1 and the atomic weight was computed as 93.5% of the atomic weight of ^{235}U and 6.5% of the atomic weight of ^{238}U. The total cross-section (σ_T) may thus be computed as:

$$\sigma_{T(E_i)} = (0.935\sigma^{235}_{E_i} + 0.065\sigma^{238}_{E_i}) \qquad \text{(III.7)}$$

where: $\sigma^{235}_{E_i}$ = the formation cross-section of the desired fission product from $^{235}U(p,f)$ at energy E_i,

$\sigma^{238}_{E_i}$ = the formation cross-section of the corresponding fission product from $^{238}U(p,f)$ at energy E_i.

Equation (III.7) may be rearranged to give:

$$\sigma_{T(E_i)} = (0.935 + 0.065)\sigma^{235}_{E_i} - 0.065(\sigma^{235}-\sigma^{238})_{E_i} \qquad \text{(III.8)}$$

$$\sigma^{235}_{E_i} = \sigma_{T(E_i)} + 0.065(\sigma^{235}-\sigma^{238})_{E_i}$$

One iteration of the above equation was found sufficient to obtain the desired precision for $\sigma^{235}_{E_i}$. Although the results obtained using this method do not differ markedly from those obtained assuming the isotopic abundance in equation (III.6) to be 93%, this method was considered essential for correcting the isotopic distributions, where the small contribution from ^{238}U may effect the position of the centroids. Furthermore,

as can be seen from equation (III.8), the errors in the cross-section measurements are not greatly altered by employing this method. The monitor-corrected Rb and Cs cross-sections from the $^{238}U(p,f)$ reactions used in these corrections were taken from the data of Davies and Yaffe (Da63), and the $^{238}U(p,f)In$ data were taken from Chan et al.(Ch77).

2. Calculation of disintegration rates at the end of irradiation

The decay curves of the nuclides ^{64}Cu, $^{84,86}Rb$ and ^{132}, ^{134m}, ^{136}Cs were extrapolated to the time at the end of irradiation and the ^{134g}Cs activity was computed at the end of irradiation, as these nuclides were shielded from feeding by precursors. The disintegration rates subsequently obtained were therefore applied directly to equation (III.5) to compute independent formation cross-sections. The nuclide ^{72}Ga was considered to be effectively shielded from its precursor ^{72}Zn ($t_{1/2}$=46.5 hours) as the time of chemical separation of these elements never exceeded 20 minutes after the end of irradiation. The cross-sections of ^{72}Ga were therefore calculated directly using equation (III.5).

The nuclides $^{117m,117g}In$ were not shielded from their precursors $^{117m,117g}Cd$. The decay-curves for these nuclides were thus extrapolated to the time of chemical separation of cadmium and indium. In order to compute independent formation cross-sections it was necessary to correct the disintegration rates for contributions due to decay of the precursors. The

pertinent sections of the decay chain for mass 117 are shown in Figure (III.1). The genetic relationship of the indium isomers can be illustrated as:

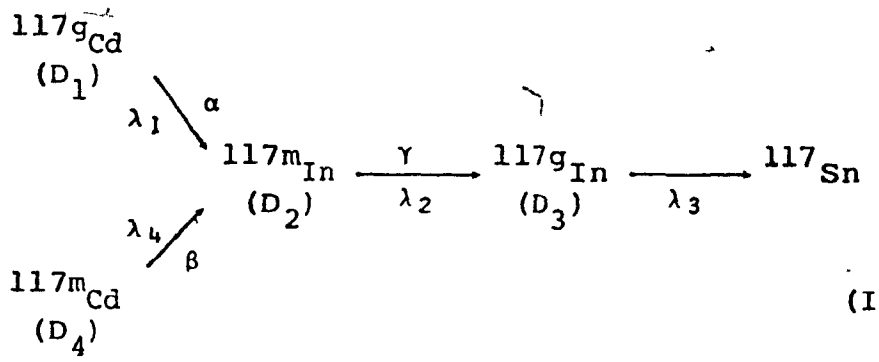

(III.9)

and:

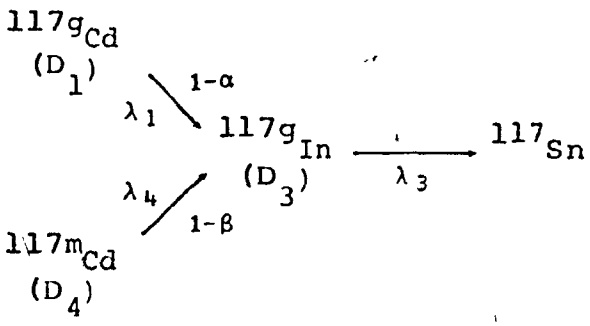

(III.10)

where: α, β and γ = the branching ratios given in Figure (III.1),

λ_{1-4} = the decay constants,

D_{1-4} = the disintegration rates of the nuclides indicated:

The computation of the indium disintegration rates at the end of irradiation required solutions of the differential equations for the successive radioactive transformations indicated by (III.9) and (III.10). Since the indium nuclides were produced through decay of their cadmium precursors as well as directly during irradiation two timed separations of indium from cadmium

Figure III.1

Decay chain A = 117

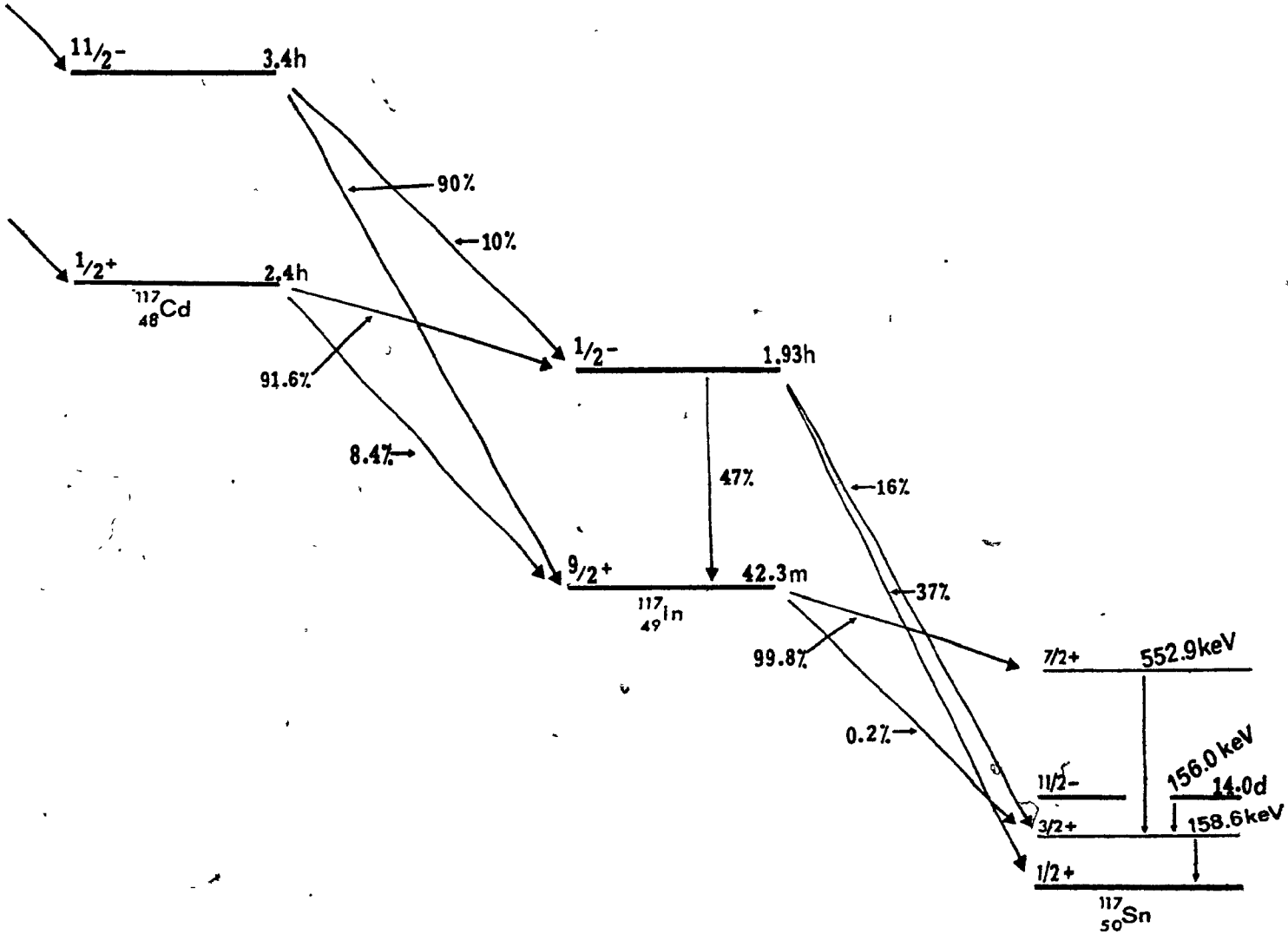
11/2-
3.4h
90%
10%
1/2+
2.4h
117 48Cd
91.6%
8.4%
1/2-
1.93h
47%
16%
9/2+
42.3m
117 49In
37%
99.8%
0.2%
7/2+
552.9keV
11/2-
156.0keV
14.0d
3/2+
158.6keV
1/2+
117 50Sn

were employed to correct for the feeding from the cadmium nuclides. The following times are thus defined:

T = time at the end of irradiation,

t_o = time of the first In/Cd separation,

t_1 = time of the second In/Cd separation,

Δt = duration of the "milking" = $t_1 - t_o$.

The general differential equation to account for the successive radioactive transformations is of the form:

$$\frac{dN_n}{dt} = N_{n-1}\lambda_{n-1} - N_n\lambda_n \qquad \text{(III.11)}$$

where N is the number of atoms of nuclide n. Noting that the disintegration rate $D_n = \lambda_n N_n$, the solution of equation (III.11) is:

$$D_n(t) = \sum_{n=1}^{n} C_n \exp(-\lambda_n t) \qquad \text{(III.12)}$$

where:

$$C_n = \frac{\lambda_1 \lambda_2 \ldots\ldots \lambda_n N_1^o}{(\lambda_1-\lambda_n)(\lambda_2-\lambda_n)\ldots\ldots(\lambda_{n-1}-\lambda_n)} \qquad \text{(III.13)}$$

The following terms are thus defined:

$$a = \frac{\lambda_2}{\lambda_2-\lambda_1} \quad ; \quad b = \frac{\lambda_3}{\lambda_3-\lambda_1} \quad ; \quad c = \frac{\lambda_3}{\lambda_3-\lambda_2} \quad ;$$

$$d = \frac{\lambda_2}{\lambda_2-\lambda_3} \quad f = \frac{\lambda_3}{\lambda_3-\lambda_4} \quad g = \frac{\lambda_2}{\lambda_2-\lambda_4} \quad ;$$

and:

$$C_1 = ab \exp(-\lambda_1\Delta t) - ac \exp(-\lambda_2\Delta t) - bd \exp(-\lambda_3\Delta t),$$

$$C_2 = a[\exp(-\lambda_1\Delta t) - \exp(-\lambda_2\Delta t)],$$

$$C_3 = b[\exp(-\lambda_1\Delta t) - \exp(-\lambda_3\Delta t)],$$

$$C_4 = gf \exp(-\lambda_4\Delta t) - gc \exp(-\lambda_2\Delta t) - fd \exp(-\lambda_3\Delta t),$$

$$C_5 = g[\exp(-\lambda_4\Delta t) - \exp(-\lambda_2\Delta t)] ,$$

$$C_6 = f[\exp(-\lambda_4\Delta t) - \exp(-\lambda_3\Delta t)] .$$

For the path indicated by (III.9) the disintegration rate of ^{117g}In and ^{117m}In at time t_1 is related to the cadmium activities at time t_o by:

$$D_3(t_1) = \gamma[\alpha C_1 D_1(t_o) + \beta C_4 D_4(t_o)] \qquad \text{(III.14)}$$

$$D_2(t_1) = \alpha C_2 D_1(t_o) + \beta C_5 D_4(t_o) \qquad \text{(III.15)}$$

and for the path indicated by (III.10) the disintegration rate of $^{117g}In(D_3')$ will be:

$$D_3'(t_1) = (1-\alpha) C_3 D_1(t_o) + (1-\beta) C_6 D_4(t_o) \qquad \text{(III.16)}$$

After "milking," the observed activity of ^{117g}In, for a given measurement period, t, is given by the following schemes:

i) $^{117m}In \xrightarrow[\lambda_2]{\gamma} {}^{117g}In \xrightarrow[\lambda_3]{} {}^{117}Sn$

ii) $^{117g}In \xrightarrow[\lambda_3]{} {}^{117}Sn$

and the following equations:

i) $D_3(t) = \gamma c D_2(t_1)[\exp(-\lambda_2 t) - \exp(-\lambda_3 t)]$ (III.17)

ii) $D_3(t) = D_3(t_1)\exp(-\lambda_3 t) + D_3'(t_1)\exp(-\lambda_3 t)$ (III.18)

Adding equations (III.17) and (III.18), and substituting for $D_2(t_1)$, $D_3(t_1)$ and $D_3'(t_1)$ gives:

$$D_3(t) = \gamma c[\alpha C_2 D_1(t_o) + \beta C_5 D_4(t_o)]\exp(-\lambda_2 t) + \qquad \text{(III.19)}$$

$$\{[\gamma\alpha C_1 + (1-\alpha)C_3 - \gamma c\alpha C_2]D_1(t_o) + [\gamma\beta C_4 + (1-\beta)C_6 - \gamma c\beta C_5]D_4(t_o)\}\exp(-\lambda_3 t) .$$

The disintegration rates of ^{117m}In and ^{117g}In are amplitudes of

decaying terms in equation (III.9). The disintegration rates of ^{117m}In and ^{117g}In at time t_1 are thus given by:

$$D_2(t_1) = \gamma c[\alpha C_2 D_1(t_o) + \beta C_5 D_4(t_o)] \qquad \text{(III.20)}$$

$$D_3(t_1) = [\gamma\alpha C_1 + (1-\alpha)C_3 - \gamma c\alpha C_2]D_1(t_o) + [\gamma\beta C_4 + (1-\beta)C_6 - \gamma c\beta C_5]D_4(t_o). \qquad \text{(III.21)}$$

A similar set of equations will relate the indium activities at time t_o to the cadmium activities at the end of irradiation. The same notation may be used except for replacing Δt in C_{1-6} by $t_o - T$. The net indium activities will, however, result from beta decay through the chain, in addition to that formed independently. Thus:

$$D_2(t_o) = \gamma c[\alpha C'_2 D_1(T) + \beta C'_5 D_4(T)] + D_2(T)\ \exp[-\lambda_2(t_o - T)] \qquad \text{(III.22)}$$

$$D_3(t_o) = [\gamma\alpha C'_1 + (1-\alpha)C'_3 - \gamma c\alpha C'_2]D_1(T) + [\gamma\beta C'_4 + (1-\beta)C'_6 - \gamma c\beta C'_5]D_4(T) + D_3(T)\ \exp[-\lambda_3(t_o - T)] \qquad \text{(III.23)}$$

where:

$$D_1(T) = D_1(t_o)\ \exp[\lambda_1(t_o - T)],$$

$$D_4(T) = D_4(t_o)\ \exp[\lambda_4(t_o - T)],$$

$$C'_{1-6} = C_{1-6}\ [\Delta t \text{ replaced by } (t_o - T)],$$

$D_{2,3}(T)$ = disintegration rates at end of irradiation.

From equations (III.20) and (III.21) the values $D_1(t_o)$ and $D_4(t_o)$ were obtained. The indium disintegration rates at the end of irradiation were then computed using equations (III.22) and (III.23). These disintegration rates were applied to

equation (III.5) to calculate independent formation cross-sections.

A4. Error analysis

Both systematic and random errors were encountered in the radiochemical experiments. These errors are listed in Table (III.3). The random errors were those arising from imprecisions in the measurements. The errors in the peak area determinations were statistical errors and their variations were due to the yields of the nuclides studied and the backgrounds associated with the measured peaks. The errors in the decay-curves were a result of the photopeak determinations and the agreement between the measured and published half-lives. The error in the sample geometry was due to computing a detector efficiency at a source-to-detector distance less than that at which the actual photopeak efficiency was measured. This error only affected the rubidium measurements where both the branching ratio of the gamma-ray and the formation probability were low. No error was assigned to the chemical-yield measurements as the precision of the analytical balance used was ±0.01mg and the weights of the solid samples ranged from 10 to 20mg. An error has been assigned to the weighing of the target material to account for the procedure employed. The target material was weighed in a closed vial and transferred to a sealed glove-box. The targets were then prepared and each sealed target was weighed. The discrepancy between the

Table III.3: Systematic and Random Errors in the Radiochemical Measurements

TYPE OF ERROR	ERROR
Systematic Errors	
Monitor Cross-sections for $^{65}Cu(p,pn)^{64}Cu$	±5.9%
Efficiency of 40cc Ge(Li) Detector	±2.7%
Random Errors	
Sample Geometry	±7%
Peak Area Determination	±1-6%
Analysis of Decay Curves	±1-6%
Pipetting	±1%
Standardization of Carrier Solutions	±1%
Weighing of Target Material	±3%

initial weight of the target material and that obtained from each sealed target was taken as the error in the weighing of the target material.

The systematic errors were those due to an imprecise knowledge of certain constants used in the cross-section calculations and effect all experimental results equally. The error for the $^{65}Cu(p,pn)^{64}Cu$ cross-sections was the value quoted by Newton et al. (Ne73) in their monitor work. The error in the detector efficiency was that quoted by Chung (Ch76) for his measurements. No error was assigned to the published decay characteristics of the nuclides studied.

The final errors in the determination of the formation cross-sections were calculated as the square root of the sum of the squares of the individual errors cited in Table III.3.

B. Analysis of Mass-Yield Data

B1. Analysis of mass spectra

The data analyses of the mass spectra were carried out using a PDP-15 mini-computer. The mass spectra were first corrected for dead-time losses. Peak areas were then obtained and the background under each peak was subtracted. The background was obtained by averaging the data on each side of a given peak. The mass-peak areas in the background spectra were then subtracted from those in the "beam-on" spectra. Finally, the peak areas in the left- and right-hand spectra were

summed to give relative isotopic yields of the elements under study. The uncertainties due to dead-time losses, peak-area determination and left- and right-peak summation were also computed. The isotopic yields thus obtained required corrections for mass discrimination effects due to distortions in the modulated high voltage, and corrections for beta decay of very short-lived isotopes and added yield due to feeding from precursors.

The mass discrimination effects were obtained by collecting spectra of $^{134-138}$Ba over the entire sweep amplitude. By comparing the relative yields of these isotopes to their natural abundances correction factors for each peak position in a data group were obtained.

The corrections for beta decay of short-lived isotopes and added yield due to feeding from precursors were computed using a code devised by Clara (Cl78) that accounted for successive radioactive transformations. As described in the experimental section diffusion curves were measured before and after each experiment and fitted to two decaying exponentials. Knowing the relative weights, $W_i(t)$, and decay constants, λ_i, of each diffusion mode, the relative production of an isotope in a particular mode was obtained using the following relation:

$$R_i = \frac{1}{m}\frac{\lambda_i+\lambda^*}{\lambda_i} \cdot \frac{W_i(t)}{1-\exp[-(\lambda_i+\lambda^*)t]} \qquad \text{(III.24)}$$

where m is a normalization constant and λ^* is the decay

constant of the isotope. Since the diffusion characteristics are of a chemical nature correction factors were obtained for all the isotopes of a particular element by measuring the diffusion curve of only one isotope.

To account for feeding by precursors the rate of isotope production due to beta decay of the precursors was required. The relative contributions were calculated by applying equations of the type (III.11-III.13). The solution of these equations has been given by Clara (C178). These corrections required the ratio of production of the precursor to that of the isotope being studied. This was approximated assuming equal precursor production to isotope production for equal N/Z ratios. The correction factors change the shapes of the isotopic distributions which in turn change the ratio of precursor production to isotope production. An iterative process was thus employed to obtain more precise correction factors. A judicious choice of the timing sequence and irradiation pulse, together with the speed of the on-line mass spectrometric technique, prevented substantial decay of the isotopes under study and also excessive interference due to feeding from precursors. Thus, corrections to the data never exceeded ±1% in the peak regions of the distributions and ±3% at the edges of the distributions. Therefore, although the assumption of a constant N/Z ratio for neighbouring products may not be true throughout the mass range studied, deviations from this assumption will only have a minimal effect. The activities of the Ga isotopes were too low for diffusion

curves to be measured. Beta decay and precursor feeding corrections were therefore not applied to the Ga measurements. However, although the Ga data are only considered tentative, the magnitude of the corrections for the other isotopes measured warrants the inclusion of these data in the present study.

B2. Normalization of the relative isotopic yields to independent formation cross-sections

The corrected relative isotopic yields were converted to independent formation cross-sections by normalizing the relative yields of the appropriate isotopes to absolute cross-sections measured radiochemically. The isotopes used for the normalization were ^{72}Ga, $^{84,86}Rb$, $^{116,117}In$ and $^{132,134,136}Cs$. The normalization to ^{116}In was only computed for the $^{233}U(p,f)$ reactions as there was very good correlation between the ^{116}In yields interpolated from the normalization to ^{117}In and the ^{116}In yields computed assuming the isomer ratios of ^{116}In and ^{117}In to be the same. Although the correlation still existed for the $^{235}U(p,f)In$ results it was not as good. The normalization was thus only made to ^{117}In. Whenever the normalizations were made to more than one isotope, the final isotopic yields were computed as the mean of the separate normalizations. The normalization errors given in the section on experimental results reflect the accuracy of the radiochemical measurement or measurements used for the normalization. The errors given for each isotope, however, reflect the accuracy of the mass

spectrometric measurements.

In the case of the $^{235}U(p,f)$ results the isotopic distributions were first normalized to the total cross-sections uncorrected for the 6% ^{238}U impurity. This was because the target material used for the mass spectrometric measurements was also isotopically enriched. The cross-section for each isotope was then corrected using equation III.8. The isotopic yields from the $^{238}U(p,f)$ reactions were taken from Lee et al. (Le75) for rubidium and cesium at 80 and 100 MeV, Tracy et al. (Tr72) for rubidium and cesium at 40 and 60 MeV and Chan et al. (Ch77) for indium.

B3. Analysis of isotopic distributions

Certain properties of the isotopic distributions are important in relating the experimental results to the fission process. These properties include the centroids, full-width at half-maximum (FWHM), and shapes of the distribution. In order to characterize the distributions a statistical moments analysis was carried out.

The first moment of the distribution gives the mean or centroid of the distribution and is defined as:

$$M_1 = \bar{A} \equiv \langle A \rangle = \frac{\sum A_i Y_i}{\sum Y_i} \qquad \text{(III.25)}$$

where A_i is the mass number of the i^{th} isotope in the distribution and Y_i is the corresponding yield. The second moment, M_2, is a measure of the variance σ^2 and is given by:

$$M_2 = \sigma^2 = \frac{\sum(A_i - \bar{A})^2 Y_i}{\sum Y_i} \qquad \text{(III.26)}$$

The square root of the variance is the standard deviation of the distribution. Higher moments have the form:

$$M_n = \frac{\sum(A_i - \bar{A})^n Y_i}{\sum Y_i} \qquad \text{(III.27)}$$

and sample towards the edges of the distribution. Odd moments reflect the degree of asymmetry of a distribution about the mean value, and even moments reflect the degree of "peakedness" of the distribution. These characteristics are defined in terms of the second, third and fourth moments as follows:

$$\text{Skewness} = \frac{M_3}{M_2^{3/2}} \qquad \text{(III.28)}$$

$$\text{Excess} = \frac{M_4}{M_2^2} - 3 \qquad \text{(III.29)}$$

Gaussian distributions have a skewness and excess of zero. Asymmetric distributions that have a larger area on the left have a positive skewness and those that have a larger area on the right have a negative skewness. Peaked distributions with respect to a Gaussian shape have a positive excess and flat distributions have a negative excess.

IV. EXPERIMENTAL RESULTS

A. Excitation Functions

The independent formation cross-sections of nuclides studied radiochemically for the proton-induced fission of ^{233}U are given in Tables IV.1 to IV.3, and their excitation functions are shown in Figures IV.1 to IV.5. The independent formation cross-sections of the same nuclides formed from the proton-induced fission of ^{235}U are given in Tables IV.4 and IV.5, and their excitation functions are shown in Figures IV.6 to IV.9. All cross-sections, together with their associated errors, were calculated as described in the section on data analysis. As shown in the excitation functions, an energy spread of ±2 MeV has been assigned to each measurement to allow for the energy resolution of the internal beam of the McGill synchrocyclotron.

The excitation functions of $^{132,134,136}Cs$ have been measured previously by Tomita and Yaffe (To69) for $^{233}U(p,f)$ and Saha et al. (Sa71) for $^{235}U(p,f)$. Their data, renormalized to the monitor cross-sections used in this work, are compared to the present measurements. For most of the data there is good agreement between the various studies.

The measurements of the independent formation cross-sections of ^{117m}In, ^{117g}In, ^{134m}Cs and $^{134m+g}Cs$ allowed isomer ratios of these nuclides to be computed. The results for ^{117}In are given in Table IV.6 and shown in Figure IV.10. The data from Hagebø (Ha65) and Sarkar (Sa74) for $^{238}U(p,f)^{117}In$ are

also shown in this figure. Each isomer ratio has been computed as the cross-section of the high-spin state divided by that of the low-spin state, as this is the form most commonly reported in the literature for ^{117}In. The results show that the isomeric yield ratio is independent of the target. This supports the findings of Hagebø (Ha65) that the isomeric-yield ratios of ^{117}In are the same for bismuth, thorium and uranium targets. The increase in the isomer ratio of ^{117}In with an increase in the bombarding energy is quite different from the isomer-ratio trend observed for ^{134}Cs. The results for this nuclide are given in Table IV.7 and shown in Figure IV.11. Each isomer ratio has been computed as the cross-section of the high-spin state divided by the total cross-section, as this is the form most commonly reported in the literature for ^{134}Cs. The results from Saha et al. (Sa69) are also shown in Figure IV.11, and in general there appears to be no dependence of the ratios on the targets. A slight increase in the ratio with an increase in the bombarding energy seems evident although the large error bars may indicate a constant ratio throughout the energy range. In general, it can be seen from both Figures IV.10 and IV.11 that the formation of the high-spin state of an isomeric pair is favoured. Several studies on isomer ratios (Wa64, Ha65, Sa69) have concluded that angular momentum is generated in fission. This appears predominantly as intrinsic spin of the primary fragments, which results in an enhancement of the production of the higher-spin isomer. As the energy of the bombarding

particle is increased more angular momentum is deposited in the target nucleus and this manifests itself as an increase in the isomer ratio. Such an explanation may account for the ^{117}In results but does not explain the ^{134}Cs data. Khan (Kh69) has suggested that constant isomer ratios with an increase in energy may be the result of several factors such as: the increasing importance of direct reactions at higher energies resulting in less angular momentum transfer; an increase in the orbital angular momentum of the primary fragments resulting in less intrinsic spin. However, such explanations are at variance with the interpretation for the ^{117}In data and a complete understanding of isomer ratios in fission is still in order.

B. Isotopic Distributions

The isotopic yields of Ga,Rb,In and Cs from ^{233}U(p,f) are given in Table IV.8 to IV.11, and the isotopic distributions are shown in Figures IV.12 to IV.15. The isotopic yields of Rb,In, and Cs from ^{235}U(p,f) are given in Tables IV.12 to IV.14 and the corresponding distributions are shown in Figures IV.16 to IV.18.

The full energy of the external proton beam of the McGill synchrocyclotron was taken as 102 MeV in accordance with the range-energy measurements of Newton et al. (Ne73), and lower energies were obtained by degrading the beam as explained in the section on experimental procedures. The proton-beam energy

associated with each distribution was computed as the mean value between the energy entering and leaving the target stack. Thus the energy spread for each mean value is as follows: ±1.9 MeV at 100 MeV; ±2.4 MeV at 80 MeV; ±2.8 MeV at 60 MeV; ±3.6 MeV at 40 MeV. All mean values are given to the nearest MeV.

The normalization of the relative isotopic yields to independent formation cross-sections has been explained in the section on data analysis. For all nuclides studied radiochemically the formation cross-sections at 100 MeV were extrapolated from the excitation functions and the associated errors were computed relative to those at 90 MeV.

For each element the isotopic distributions have been displaced along the ordinate by the scaling factor given in the figures. This was done for clarity and to make more readily visible the shift of the isotopic distributions to lower mass numbers with increasing bombarding energy.

Table IV.1: Independent formation cross-sections of ^{72}Ga, $^{84,86}Rb$ from $^{233}U(p,f)$

E_p (MeV)	FORMATION CROSS-SECTIONS (mb)		
	^{72}Ga	^{84}Rb	^{86}Rb
40	--	--	3.5±0.5
45	0.5±0.1	--	--
55	1.0±0.1	--	4.7±0.8
60	--	0.21±0.05	5.2±0.8
65	1.2±0.1	--	--
70	--	--	5.2±0.7
75	--	0.4±0.1	5.6±0.9
80	1.8±0.2	0.5±0.1	6.7±0.7
90	2.1±0.2	0.7±0.2	7.8±1.5

Table IV.2: Independent formation cross-sections of $^{116m,117g,117m+g}In$ from $^{233}U(p,f)$

E_p (MeV)	FORMATION CROSS-SECTIONS (mb)		
	^{116m}In	^{117g}In	$^{117m+g}In$
35	2.4±0.4	7.8±0.8	10.0±0.9
40	3.4±0.3	9.6±1.0	12.0±1.0
45	5.9±0.6	14.1±1.2	16.4±1.3
60	6.2±0.6	16.2±1.4	18.8±1.4
65	9.8±1.0	20.8±1.8	23.3±1.8
80	12.8±1.2	23.7±1.9	26.3±2.0
90	15.5±2.4	26.2±4.4	28.5±4.5

Table IV.3: Independent formation cross-sections of $^{132,134m,134m+g,136}Cs$ from $^{233}U(p,f)$

E_p (MeV)	FORMATION CROSS-SECTIONS (mb)			
	^{132}Cs	^{134m}Cs	$^{134m+g}Cs$	^{136}Cs
40	7.5±0.8	16.4±1.2	22.3±1.7	24.2±1.4
55	10.8±1.0	18.7±1.4	21.9±2.3	22.4±1.4
60	11.8±1.0	17.3±1.3	20.5±1.6	19.2±1.0
70	--	13.8±1.2	18.6±1.6	19.2±1.0
75	13.3±1.4	15.7±1.2	20.5±1.7	18.8±1.1
80	14.3±1.5	15.1±1.3	21.6±1.5	19.0±1.0
90	14.1±1.5	15.2±1.3	20.6±2.1	18.3±1.2

Figure IV.1

Excitation function for the independent formation of ^{72}Ga from $^{233}U(p',f)$

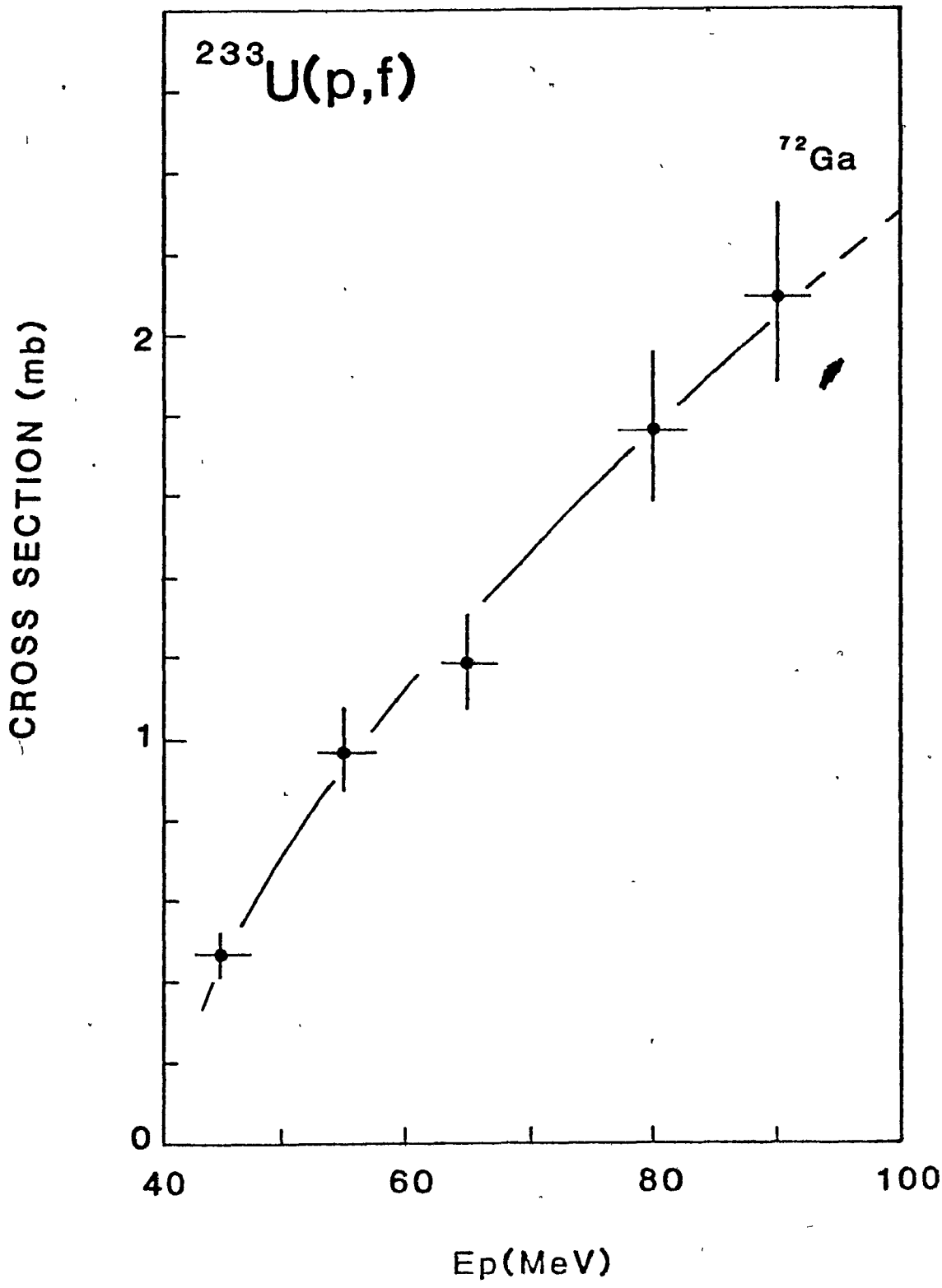
^{233}U(p,f)
^{72}Ga
CROSS SECTION (mb)
0
1
2
40
60
80
100
Ep(MeV)

Figure IV.2

Excitation functions for the independent formation of ^{84}Rb and ^{86}Rb from $^{233}U(p,f)$

■: ^{84}Rb

●: ^{86}Rb

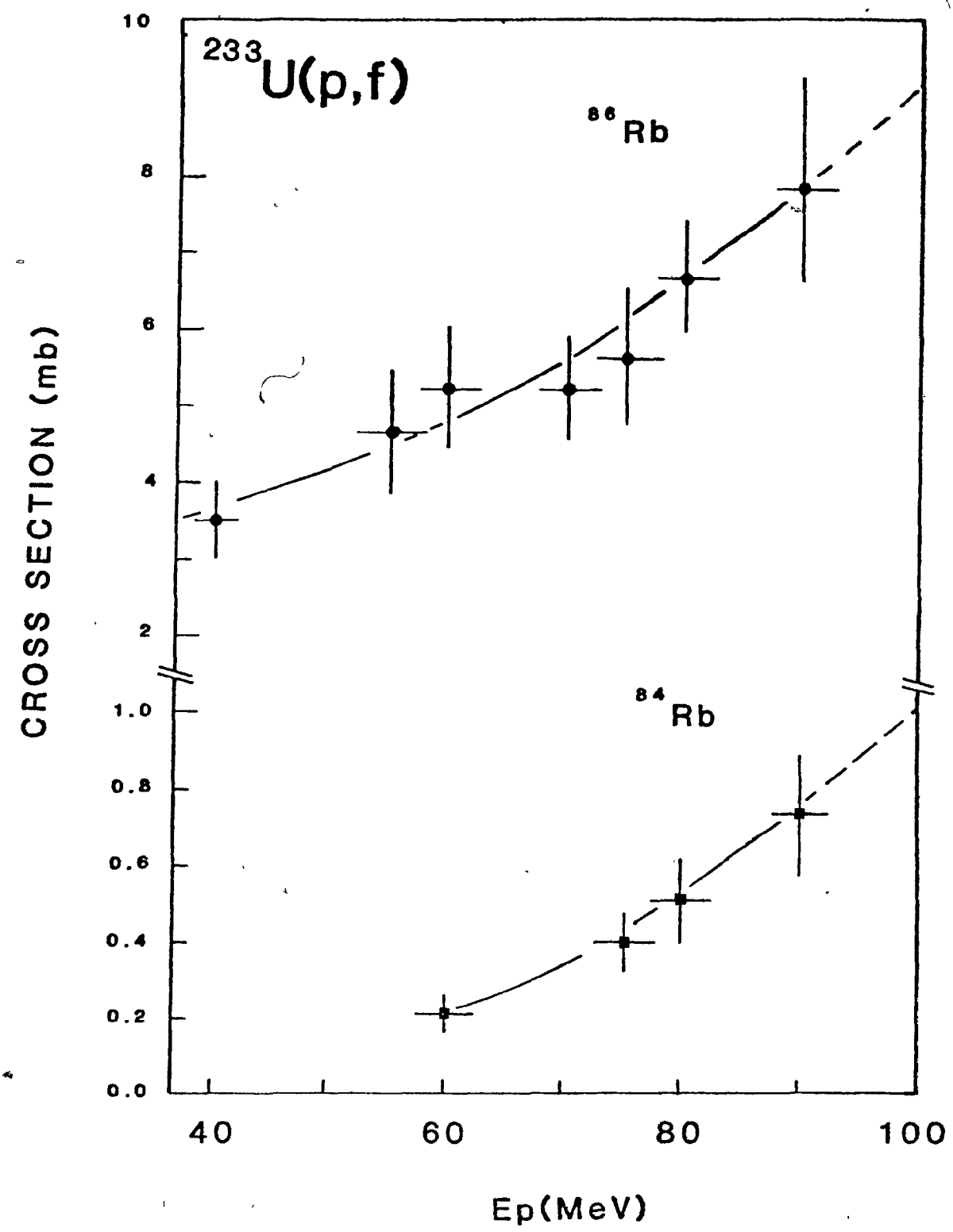
^{233}U(p,f)
^{86}Rb
^{84}Rb
CROSS SECTION (mb)
10
8
6
4
2
1.0
0.8
0.6
0.4
0.2
0.0
40
60
80
100
Ep(MeV)

Figure IV.3

Excitation functions for the independent formation of ^{116m}In and $^{117m+g}In$ from $^{233}U(p,f)$

■: ^{116m}In

●: $^{117m+g}In$

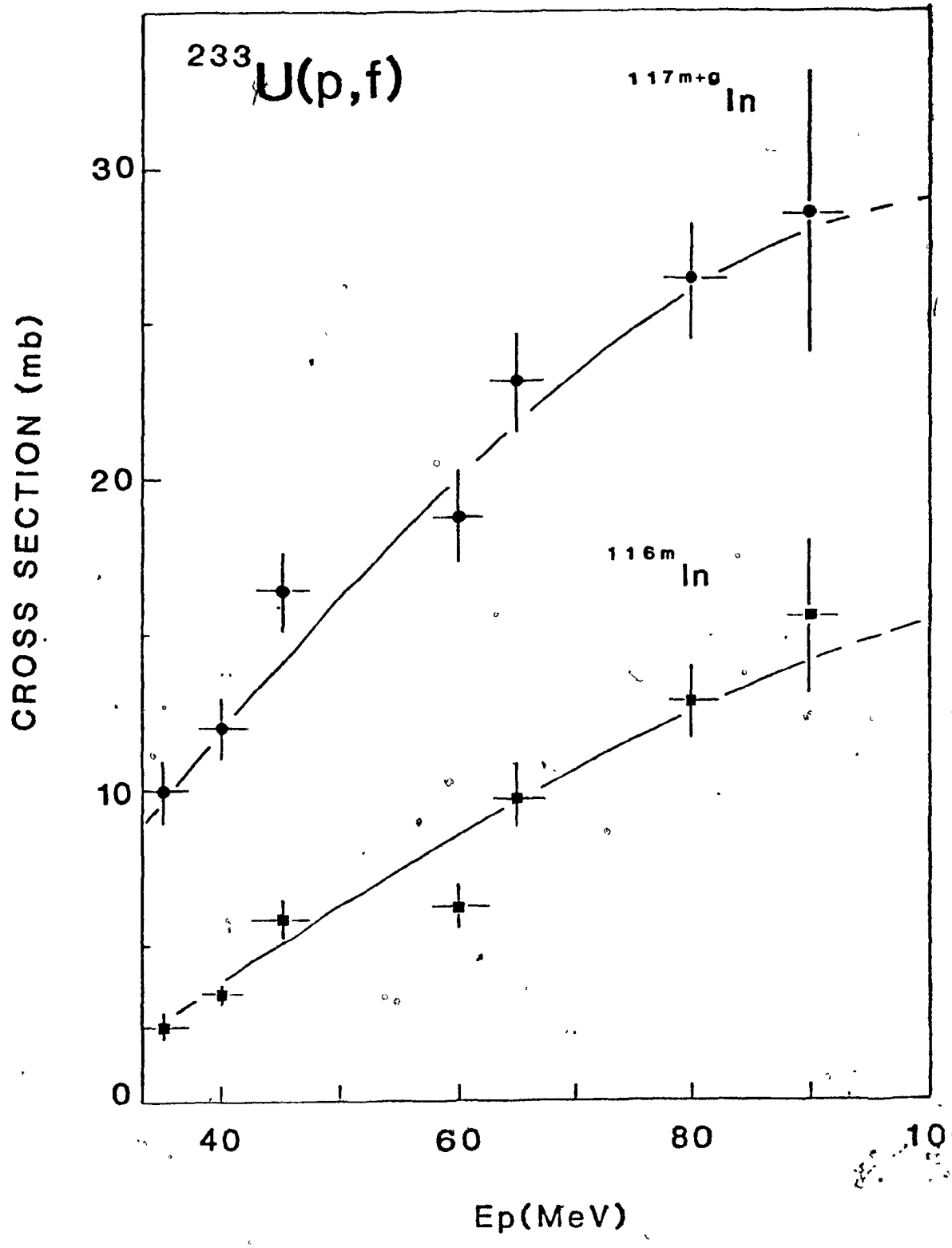
^{233}U(p,f)
$^{117m+g}$In
^{116m}In
CROSS SECTION (mb)
0
10
20
30
40
60
80
100
Ep(MeV)

Figure IV.4

Excitation functions for the independent formation of ^{134m}Cs and $^{134m+g}Cs$ from $^{233}U(p,f)$

○: ^{134m}Cs This work

●: $^{134m+g}Cs$ This work

□: ^{134m}Cs Renormalized data from

■: $^{134m+g}Cs$ Tomita and Yaffe (To69)

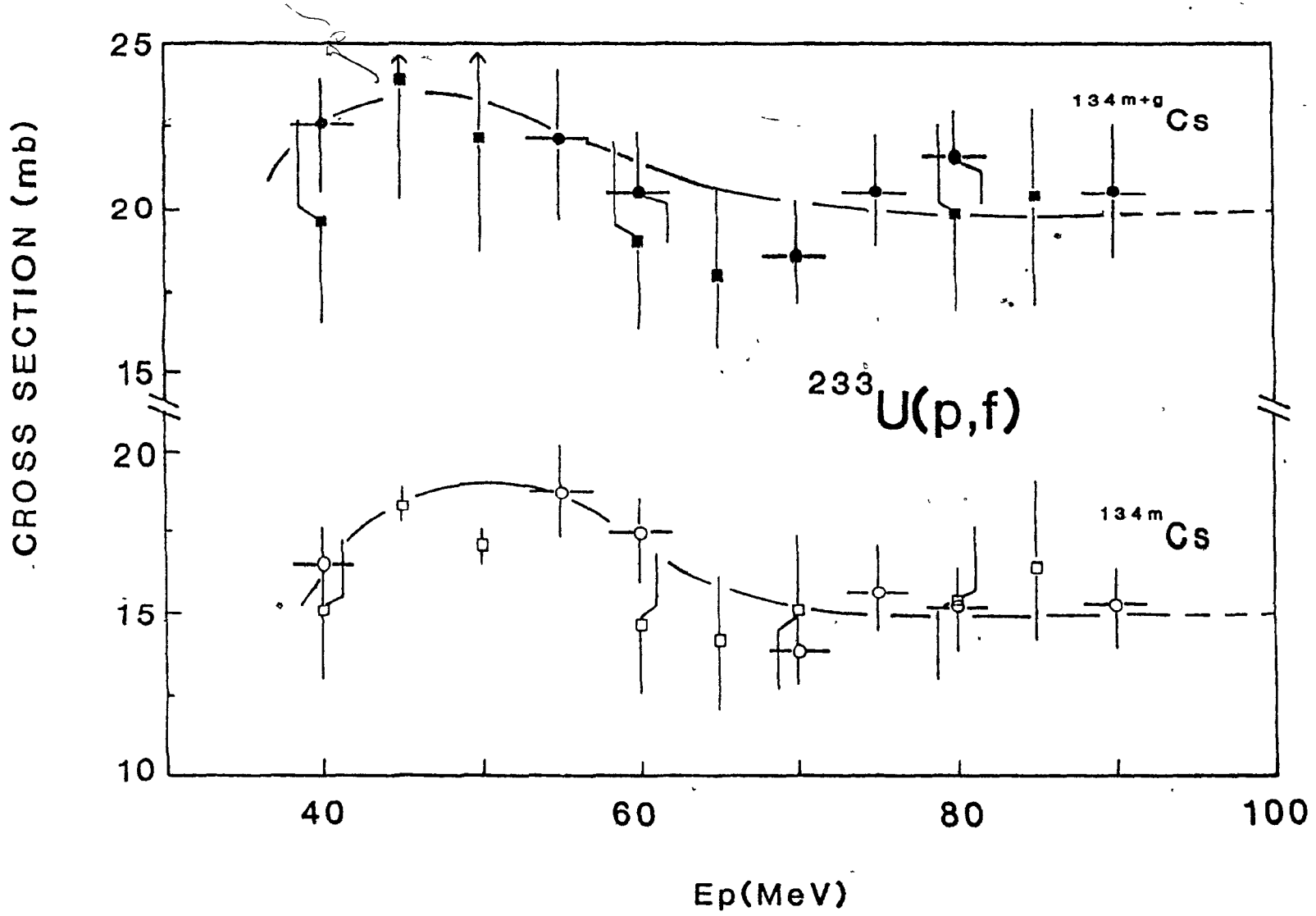
CROSS SECTION (mb)
25
20
15
20
15
10
40
60
80
100
Ep(MeV)
134m+g Cs
233 U(p,f)
134m Cs

Figure IV.5

Excitation functions for the independent formation of ^{132}Cs and ^{136}Cs from $^{233}U(p,f)$

o: ^{132}Cs This work

●: ^{136}Cs This work

□: ^{132}Cs Renormalized data from

■: ^{136}Cs Tomita and Yaffe (To69)

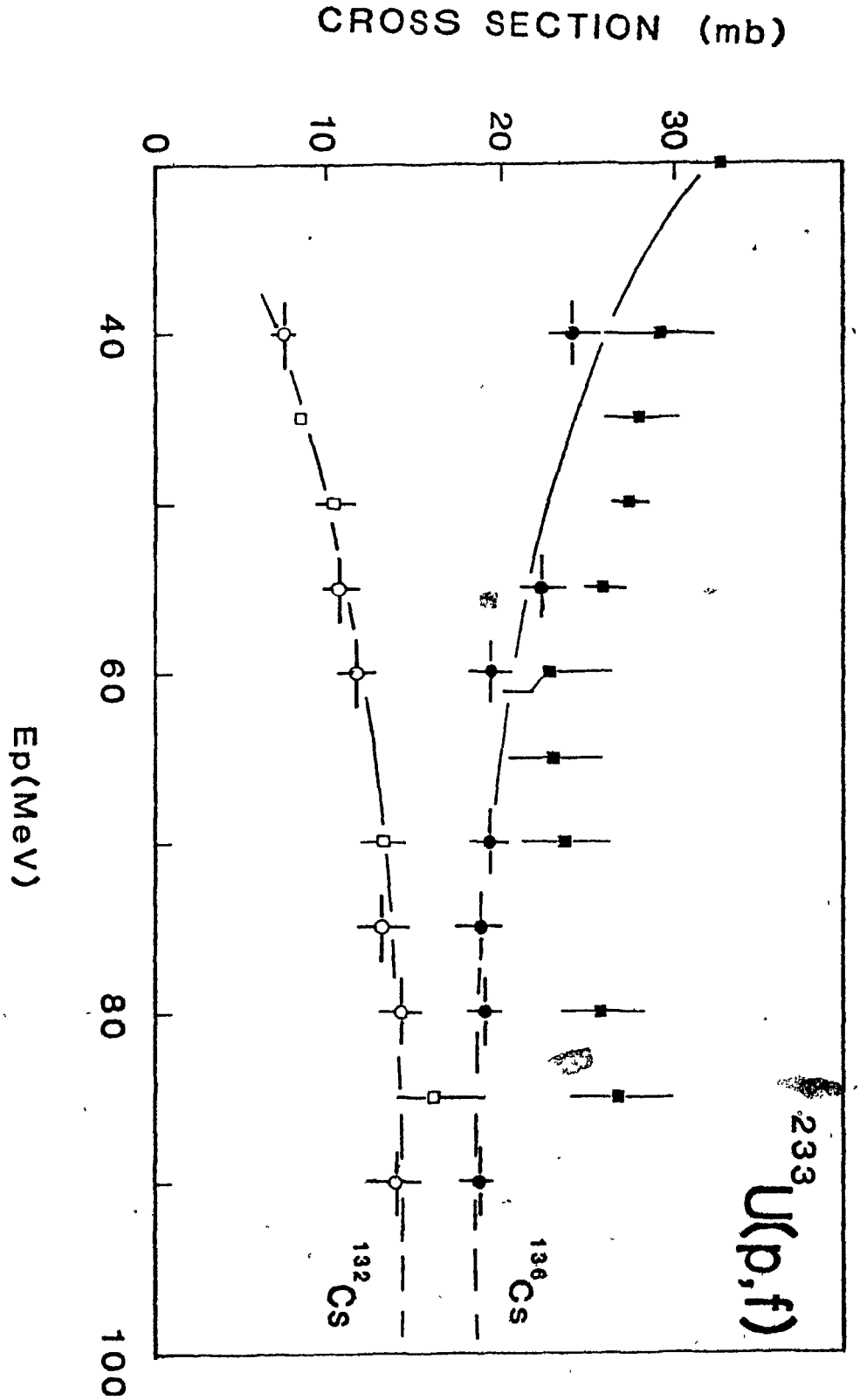
CROSS SECTION (mb)
0
10
20
30
40
60
80
100
Ep(MeV)
^{233}U(p,f)
^{136}Cs
^{132}Cs

Table IV.4: Independent formation cross-sections of $^{84,86}Rb$ and $^{116m,117g,117m+g}In$ from $^{235}U(p,f)$

E_p (MeV)	FORMATION CROSS-SECTIONS (mb)				
	^{84}Rb	^{86}Rb	^{116m}In	^{117g}In	$^{117m+g}In$
40	--	1.00±0.18	0.41±0.07	2.8±0.6	3.5±0.6
50	--	0.93±0.15	1.0±0.1	5.8±0.8	6.9±0.7
60	--	1.12±0.14	3.7±0.4	6.7±1.0	7.8±0.9
70	0.06±0.01	1.34±0.16	5.4±0.4	9.1±0.9	10.2±0.9
80	0.10±0.03	1.85±0.30	5.8±0.5	9.4±1.1	10.4±1.0
90	0.17±0.03	2.06±0.27	6.2±0.5	9.3±1.0	11.2±0.9

Table IV.5: Independent formation cross-sections of $^{132,134m,134m+g,136}Cs$ from $^{235}U(p,f)$

E_p (MeV)	FORMATION CROSS-SECTIONS (mb)			
	^{132}Cs	^{134m}Cs	$^{134m+g}Cs$	^{136}Cs
40	1.8±0.2	6.5±0.5	9.4±0.9	17.2±0.9
50	3.3±0.3	9.7±0.8	12.1±1.7	16.0±1.0
60	4.0±0.3	9.2±0.7	12.4±1.3	12.9±0.9
70	4.2±0.3	8.2±0.6	10.3±1.1	10.0±0.7
80	5.0±0.4	8.0±0.6	9.6±1.0	10.1±0.6
90	5.0±0.5	7.8±0.5	8.6±1.3	8.7±0.7

Figure IV.6

Excitation functions for the independent formation of ^{84}Rb and ^{86}Rb from $^{235}U(p,f)$

■: ^{84}Rb

●: ^{86}Rb

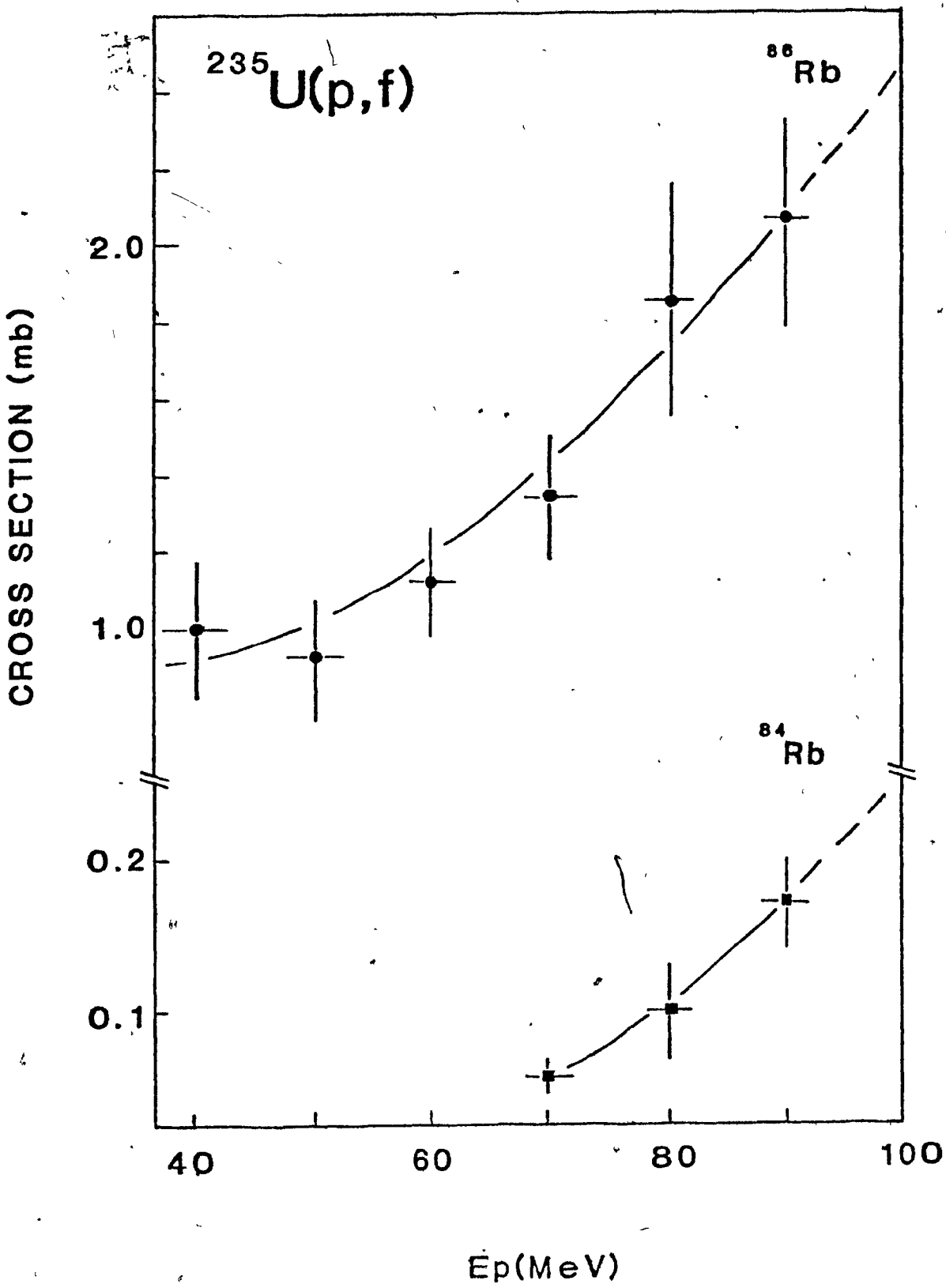
^{235}U(p,f)
^{86}Rb
^{84}Rb
CROSS SECTION (mb)
2.0
1.0
0.2
0.1
40
60
80
100
Ep(MeV)

Figure IV.7

Excitation functions for the independent formation of ^{116m}In and $^{117m+g}In$ from $^{235}U(p,f)$

o: ^{116m}In

●: $^{117m+g}In$

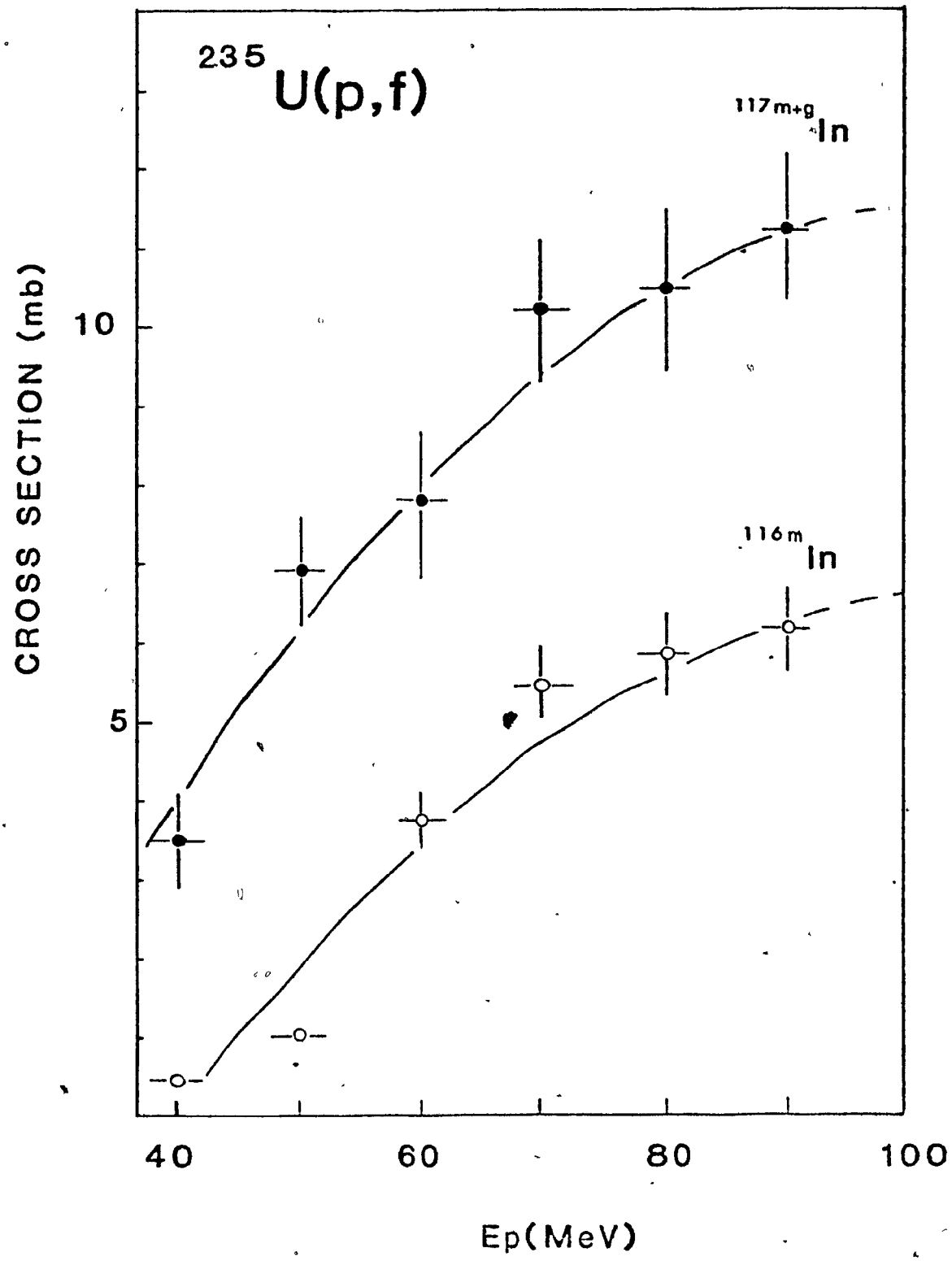
235 U(p,f)
117m+g In
116m In
CROSS SECTION (mb)
10
5
40
60
80
100
Ep(MeV)

Figure IV.8

Excitation functions for the independent formation of ^{134m}Cs and $^{134m+g}Cs$ from $^{235}U(p,f)$

○: ^{134m}Cs This work

●: $^{134m+g}Cs$ This work

□: ^{134m}Cs Renormalized data from

■: $^{134m+g}Cs$ Saha et al. (Sa71)

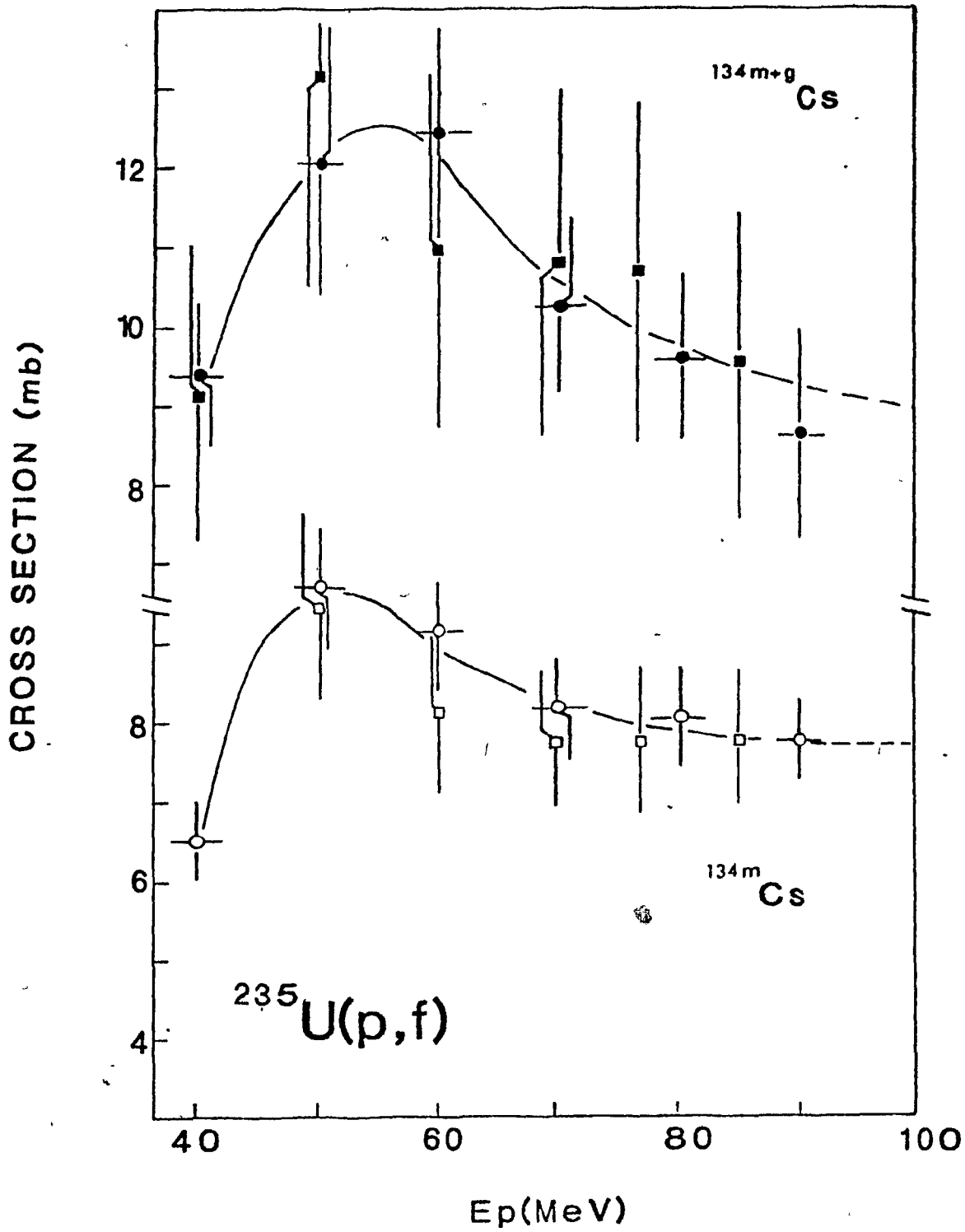
134m+g Cs
134m Cs
235U(p,f)
CROSS SECTION (mb)
Ep(MeV)
12
10
8
8
6
4
40
60
80
100

Figure IV.9

Excitation functions for the independent formation of ^{132}Cs and ^{136}Cs from $^{235}U(p,f)$

o: ^{132}Cs
●: ^{136}Cs This work

□: ^{132}Cs
■: ^{136}Cs Renormalized data from Saha et al. (Sa71)

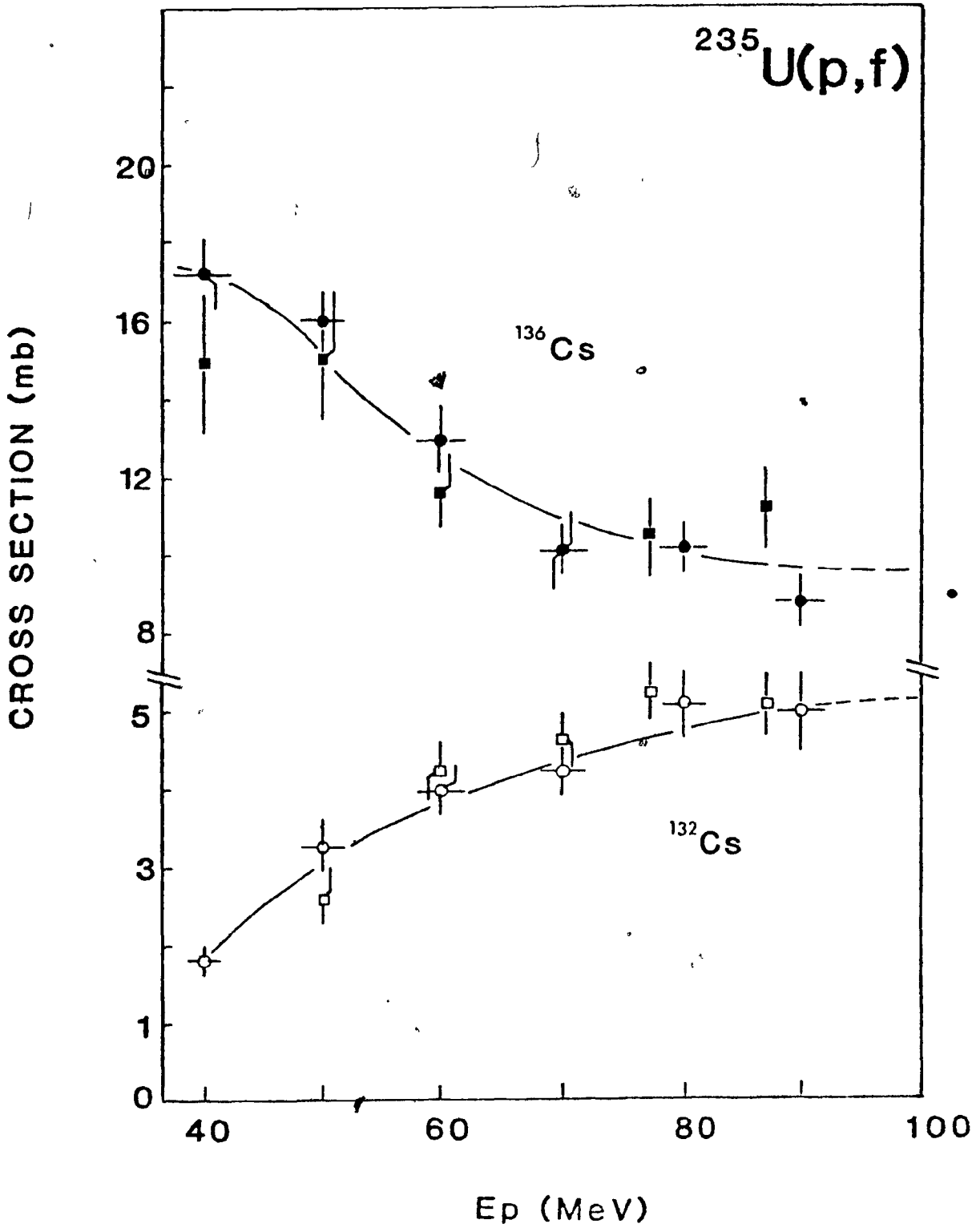
^{235}U(p,f)
^{136}Cs
^{132}Cs
CROSS SECTION (mb)
Ep (MeV)
0
1
3
5
8
12
16
20
40
60
80
100

Table IV.6: Isomer Ratios of ^{117}In from $^{233,235}U(p,f)$

E_p (MeV)	$(^{117g}In/^{117m}In)$	
	$^{233}U(p,f)$	$^{235}U(p,f)$
35	3.5±0.8	--
40	3.7±0.8	3.6±0.9
45	6.1±0.8	--
50	--	5.0±0.8
60	6.4±0.8	6.3±1.0
65	8.2±1.0	--
70	--	8.2±1.0
80	9.2±1.2	9.2±1.0
90	11.5±3.0	10.8±1.4

Figure IV.10

Isomer ratios of ^{117}In,
$\sigma(^{117g}In)/\sigma(^{117m}In)$

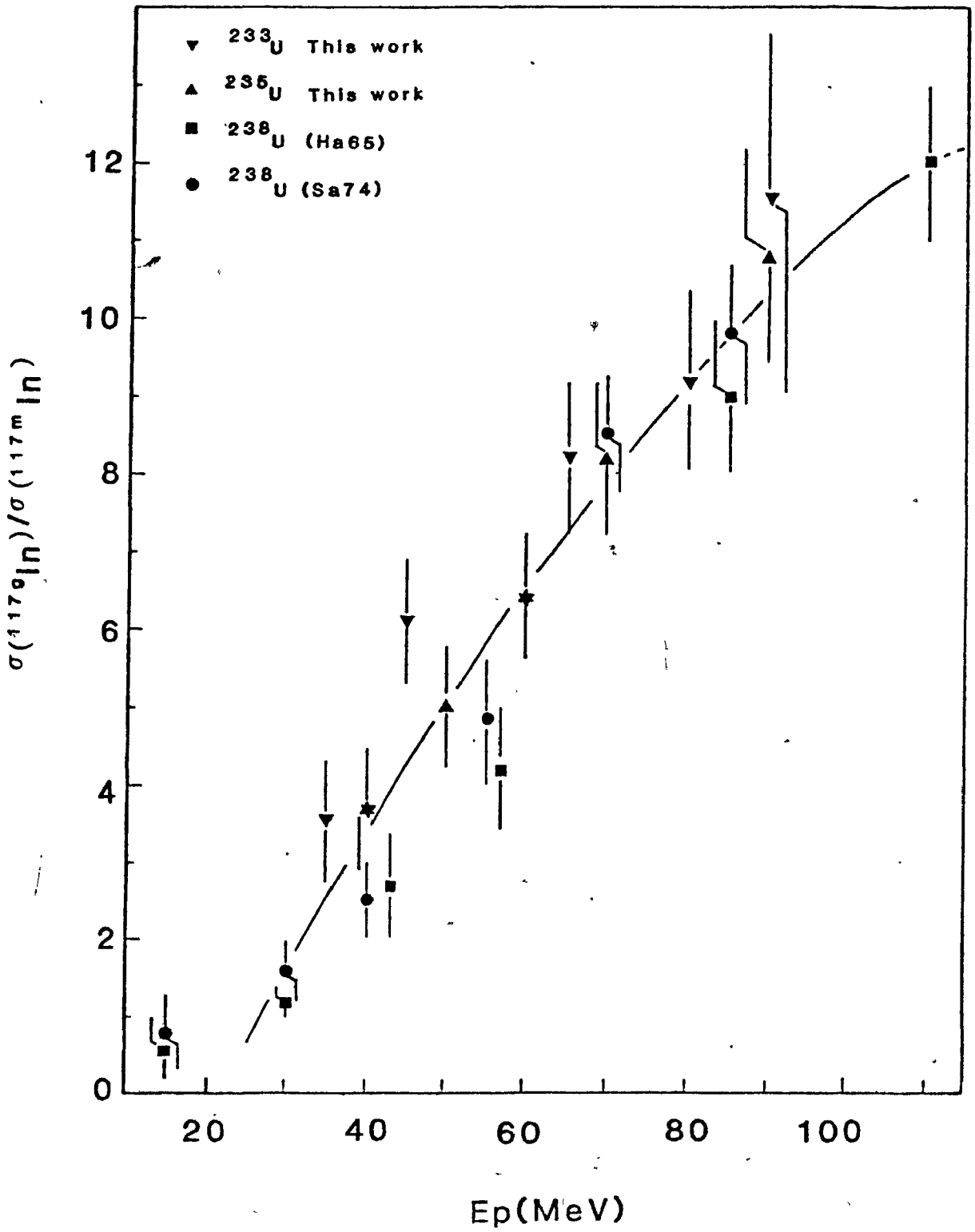
^{233}U This work
^{235}U This work
^{238}U (Ha65)
^{238}U (Sa74)
$\sigma(^{117g}In)/\sigma(^{117m}In)$
Ep(MeV)
0
2
4
6
8
10
12
20
40
60
80
100

Table IV.7: Isomer Ratios of ^{134}Cs from $^{233,235}U(p,f)$

E_p (MeV)	σ_m/σ_{m+g}	
	$^{233}U(p,f)$	$^{235}U(p,f)$
40	0.73±0.08	0.69±0.08
50	--	0.80±0.13
55	0.85±0.11	--
60	0.84±0.09	0.74±0.09
70	0.74±0.09	0.80±0.10
75	0.76±0.08	--
80	0.70±0.08	0.83±0.10
90	0.74±0.10	0.90±0.15

Figure IV.11

Isomer ratios of ^{134}Cs,
$\sigma(^{134m}Cs)/\sigma(^{134m+g}Cs)$

●: from $^{233}U(p,f)$ This work

■: from $^{235}U(p,f)$ This work

o: from $^{233}U(p,f)$ Saha et al.(Sa69)

□: from $^{235}U(p,f)$ Saha et al.(Sa69)

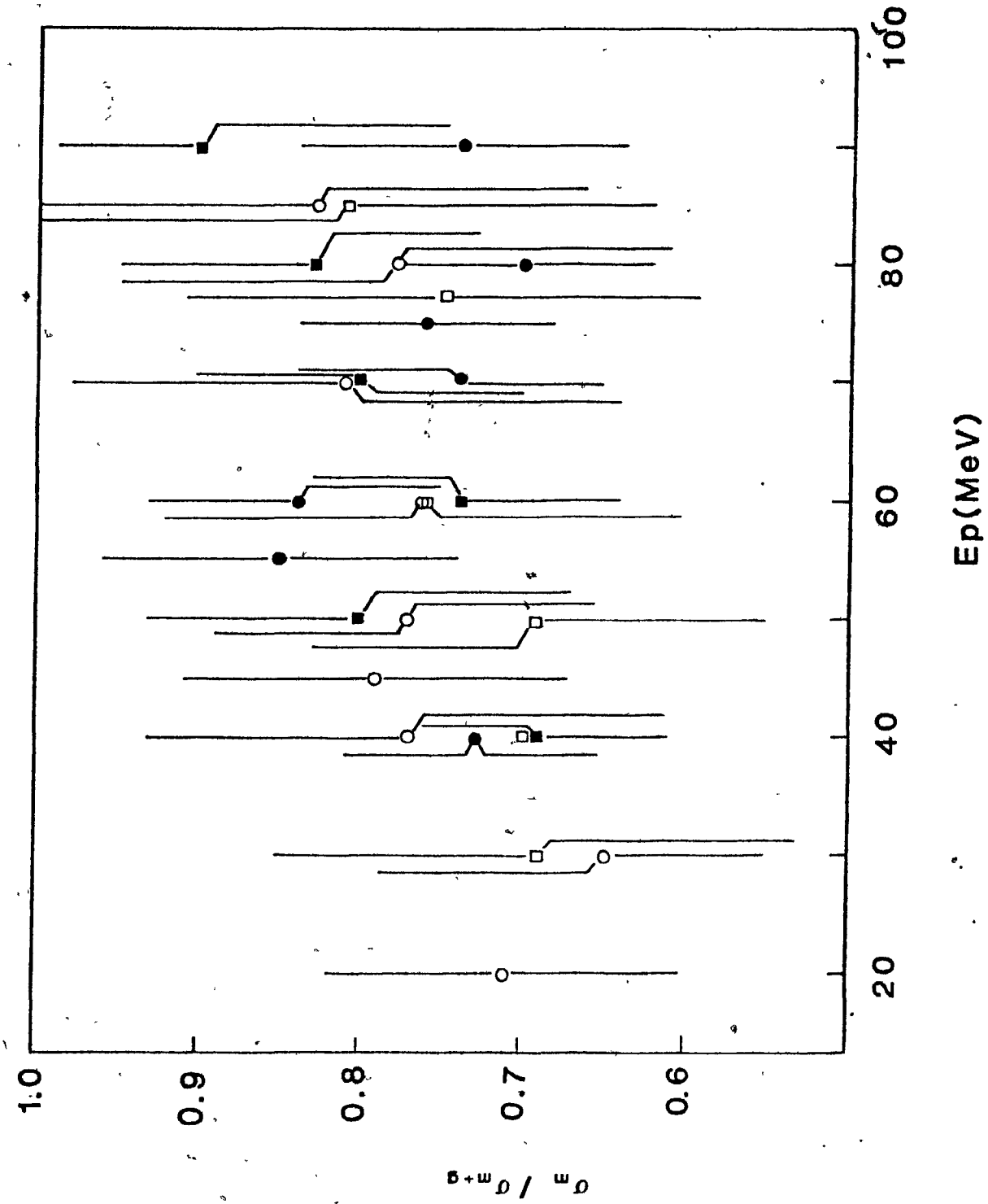
1.0
0.9
0.8
0.7
0.6
$\sigma_{\pi^-} / \sigma_{\pi^+ g}$
20
40
60
80
100
Ep(MeV)

Table IV.8: Isotopic Yields of Ga from $^{233}U(p,f)$

MASS NUMBER	CROSS-SECTIONS (mb)	
	E_p= 80MeV	100MeV
71	2.1±1.0	0.7±0.6
72	1.8±0.2	(2.3)*
73	3.0±1.1	3.7±1.1
74	6.5±0.8	7.3±0.7
75	6.7±0.7	8.2±0.7
76	4.5±0.5	6.0±0.6
77	2.2±0.6	4.9±0.7
78	--	1.8±0.5
Total Cross-section	31.3±2.0	34.9±1.9
Normalization Error	±11.1%	±9.5%

*Extrapolated from excitation function.

Table IV.9: Isotopic Yields of Rb from $^{233}U(p,f)$

MASS NUMBER	CROSS-SECTIONS (mb)			
	E_p= 40MeV	60MeV	80MeV	100MeV
83	--	--	--	0.26±0.04
84	--	0.21±0.05	0.54±0.05	1.00±0.04
85	--	1.9*	3.6±0.2	6.2±0.2
86	3.5±0.8	4.7±0.5	6.3±0.5	9.2±0.5
87	8.9±0.8	11.6±0.6	14.2±0.5	18.4±0.5
88	18.8±0.9	20.3±0.7	20.5±0.6	26.4±0.6
89	26.7±0.7	26.8±0.7	25.9±0.6	30.1±0.6
90	29.4±0.7	27.5±0.6	26.2±0.5	29.0±0.5
91	24.8±0.7	23.7±0.5	21.8±0.5	24.4±0.5
92	14.6±0.5	13.3±0.4	12.3±0.3	14.1±0.4
93	7.2±0.4	6.1±0.3	5.8±0.3	6.1±0.3
94	1.7±0.4	2.0±0.2	1.6±0.2	1.7±0.2
Total Cross-section	135.6±2.0	138.1±1.6	138.7±1.4	166.9±1.4
Normalization Error	±16.6%	±15.4%	±10.6%	±17.2%

*Interpolated value.

Table IV.10: Isotopic Yields of In from $^{233}U(p,f)$

MASS NUMBER	CROSS-SECTIONS (mb)			
	E_p = 40MeV	60MeV	80MeV	100MeV
113	--	--	0.3±0.4	1.1±0.2
114	--	1.3±1.2	1.7±0.5	3.4±0.2
115	0.3±0.6	2.9±1.0	5.5±0.4	9.5±0.2
116	4.3±0.6	8.3±1.0	14.7±0.5	18.7±0.2
117	11.2±0.6	16.6±1.0	25.3±0.5	28.0±0.3
118	22.3±0.7	26.9±1.1	35.1±0.7	34.8±0.3
119	33.6±0.9	33.0±1.3	37.7±0.7	37.3±0.3
120	35.4±0.9	29.0±1.3	32.6±0.6	31.1±0.3
121	28.7±0.7	21.1±1.1	23.7±0.5	23.0±0.2
122	17.5±0.7	12.4±1.1	14.2±0.5	14.1±0.2
123	9.3±0.6	6.3±0.9	7.0±0.4	6.7±0.1
124	2.5±0.5	2.1±1.0	2.9±0.4	2.7±0.1
125	0.6±0.5	0.6±0.9	--	--
126	0.4±0.6	--	--	--
Total Cross-section	166.6±2.3	160.5±3.8	200.7±1.8	210.8±0.8
Normalization Error	±6.4%	±6.5%	±6.1%	±11.5%

Table IV.11: Isotopic Yields of Cs from $^{233}U(p,f)$

MASS NUMBER	CROSS-SECTIONS (mb)			
	E_p = 40MeV	60MeV	80MeV	100MeV
129	--	0.6±0.2	1.6±0.2	2.8±0.1
130	1.0±0.2	1.9±0.2	3.9±0.2	6.2±0.2
131	2.3±0.2	5.7±0.3	8.5±0.3	11.5±0.2
132	6.9±0.3	11.2±0.4	14.5±0.4	16.1±0.3
133	15.3±0.7	16.9±0.7	21.1±0.6	21.3±0.3
134	22.2±0.7	21.1±0.6	21.1±0.5	20.5±0.4
135	26.4±0.6	21.5±0.5	21.1±0.4	20.4±0.4
136	24.3±0.7	19.6±0.6	19.2±0.5	18.9±0.4
137	21.0±0.8	17.3±0.6	18.3±0.5	17.8±0.4
138	13.9±1.4	9.2±1.0	13.1±0.8	10.8±0.5
139	8.5±0.4	8.1±0.4	9.2±0.3	9.1±0.2
140	4.4±0.3	4.2±0.2	4.8±0.2	4.9±0.1
141	2.7±0.2	2.3±0.2	2.6±0.2	2.3±0.1
142	1.0±0.3	--	0.8±0.2	0.9±0.1
Total Cross-section	149.9±2.2	139.6±2.0	159.8±1.6	163.5±1.1
Normalization Error	±4.9%	±4.2%	±4.8%	±13.2%

Figure IV.12

Isotopic distributions of Ga

from $^{233}U(p,f)$

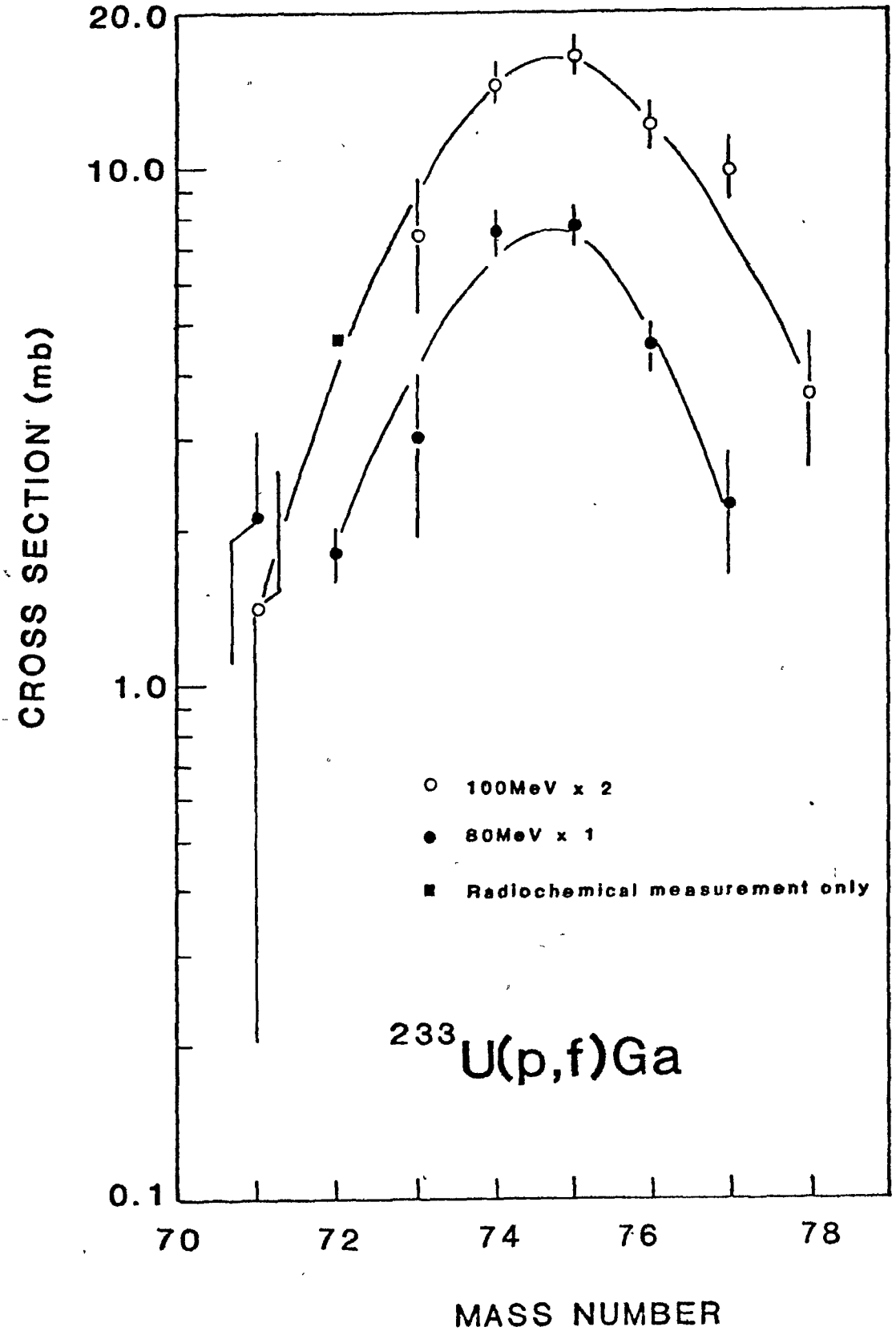
20.0
10.0
1.0
0.1
CROSS SECTION (mb)
100MeV x 2
80MeV x 1
Radiochemical measurement only
^{233}U(p,f)Ga
70
72
74
76
78
MASS NUMBER

Figure IV.13

Isotopic distributions of Rb
from $^{233}U(p,f)$

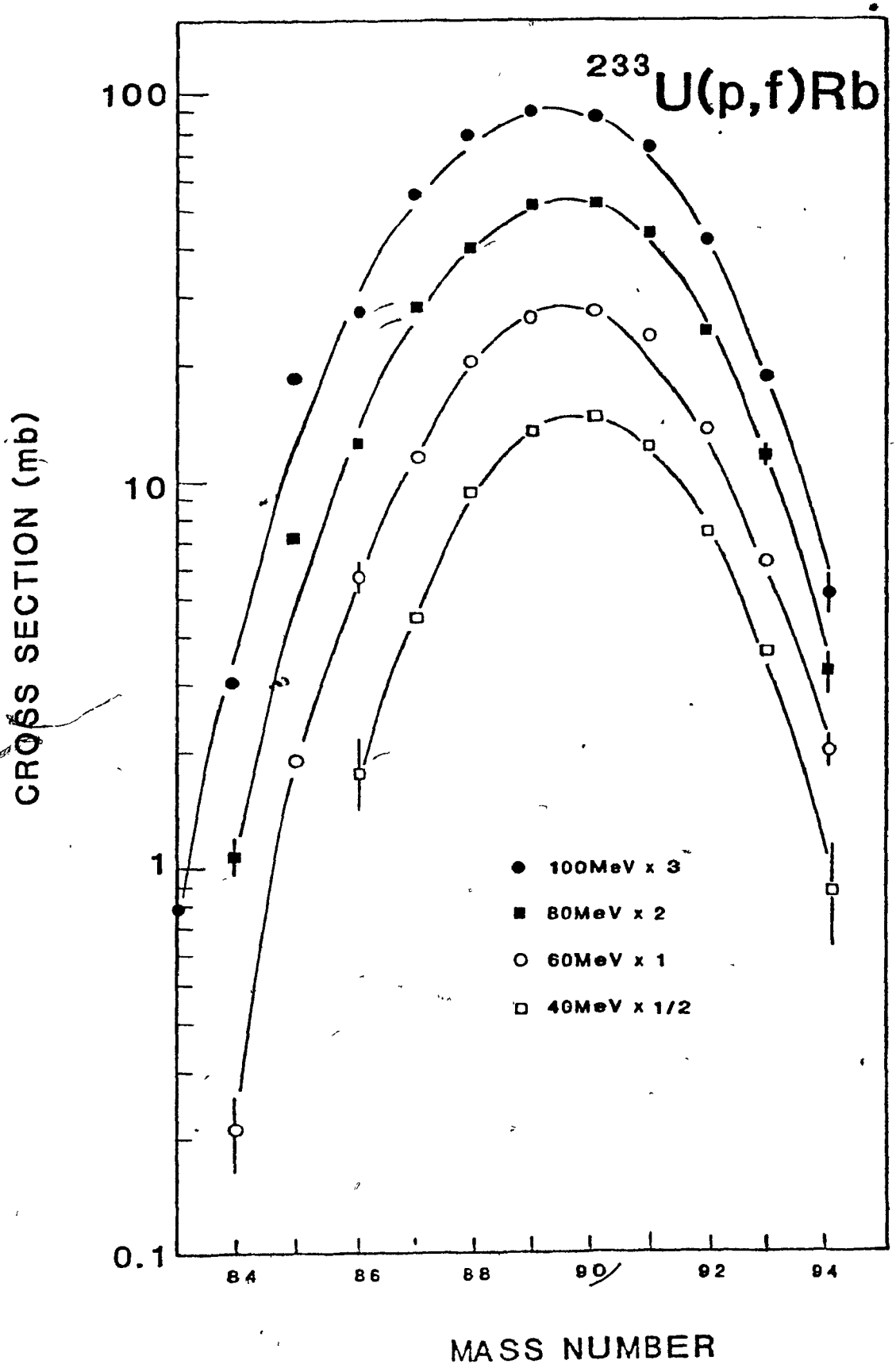
^{233}U(p,f)Rb
100
10
1
0.1
CROSS SECTION (mb)
84
86
88
90
92
94
MASS NUMBER
100MeV x 3
80MeV x 2
60MeV x 1
40MeV x 1/2

Figure IV.14

Isotopic distributions of In from $^{233}U(p,f)$

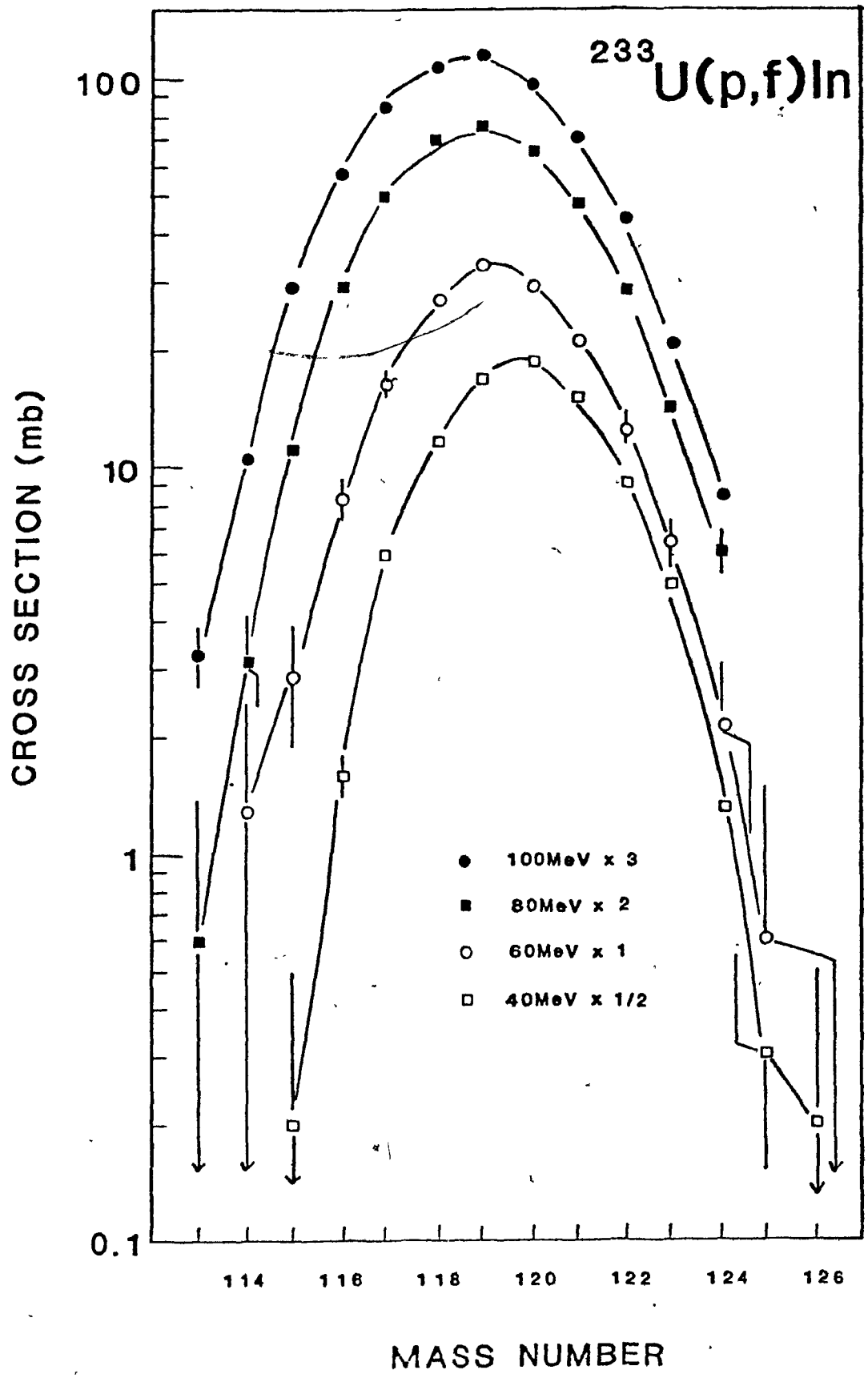
^{233}U(p,f)In
100
10
1
0.1
CROSS SECTION (mb)
100MeV x 3
80MeV x 2
60MeV x 1
40MeV x 1/2
114
116
118
120
122
124
126
MASS NUMBER

Figure IV.15

Isotopic distributions of Cs

from $^{233}U(p,f)$

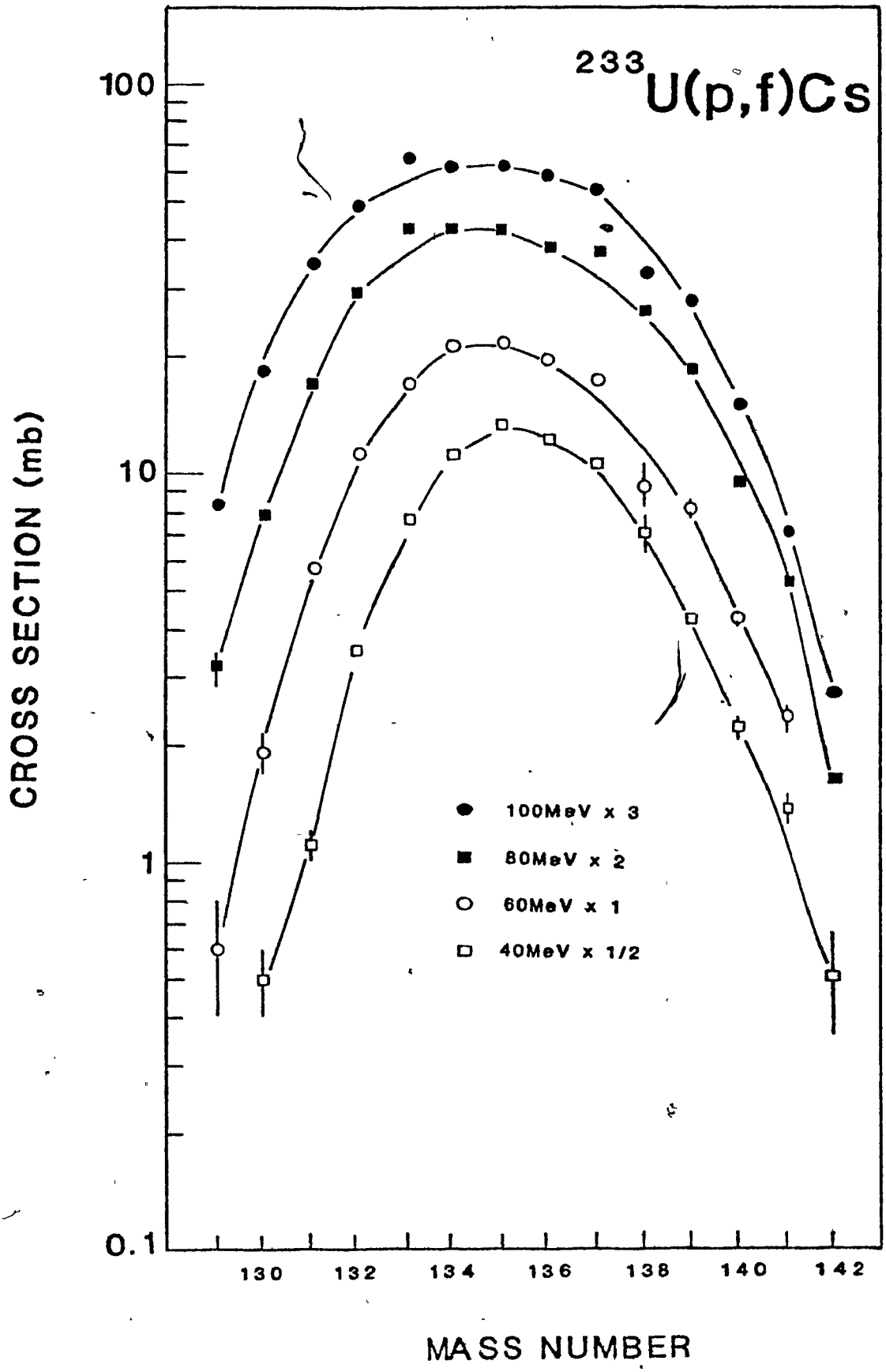
^{233}U(p,f)Cs
100
10
1
0.1
CROSS SECTION (mb)
100MeV x 3
80MeV x 2
60MeV x 1
40MeV x 1/2
130
132
134
136
138
140
142
MASS NUMBER

Table IV.12: Isotopic Yields of Rb from $^{235}U(p,f)$

MASS NUMBER	CROSS-SECTIONS (mb)			
E_p =	40MeV	60MeV	80MeV	100MeV
86	1.0±0.2	1.1±0.2	1.8±0.1	2.5±0.1
87	3.9±0.4	4.6±0.3	4.8±0.2	6.1±0.1
88	8.9±0.4	9.4±0.2	8.4±0.2	9.6±0.1
89	17.1±0.5	15.8±0.3	12.7±0.3	13.3±0.2
90	24.1±0.5	20.1±0.4	14.7±0.3	15.2±0.2
91	26.3±0.5	20.3±0.3	15.2±0.3	15.2±0.2
92	20.1±0.4	14.8±0.3	10.9±0.2	10.9±0.1
93	11.5±0.3	8.8±0.2	6.3±0.1	6.2±0.1
94	4.3±0.1	3.2±0.2	2.5±0.1	2.4±0.1
Total Cross-section	117.2±1.2	98.3±0.8	77.3±0.6	81.5±0.4
Normalization Error	±18.0%	±12.5%	±16.2%	±13.1%

Table IV.13: Isotopic Yields of In from $^{235}U(p,f)$

MASS NUMBER	CROSS-SECTIONS (mb)			
E_p =	40MeV	60MeV	80MeV	100MeV
114	0.2±0.3	--	0.6±0.2	0.9±0.2
115	0.3±0.3	1.1±0.3	1.7±0.2	2.6±0.2
116	0.5±0.3	3.2±0.3	4.9±0.3	6.1±0.2
117	3.5±0.3	7.8±0.3	10.4±0.3	11.5±0.2
118	10.4±0.3	16.4±0.4	17.1±0.3	16.4±0.3
119	20.4±0.5	26.2±0.5	23.1±0.4	19.6±0.3
120	27.6±0.6	28.9±0.6	23.1±0.4	19.2±0.3
121	30.2±0.6	26.7±0.5	20.0±0.4	16.1±0.3
122	23.8±0.6	18.1±0.6	13.7±0.3	11.2±0.2
123	14.2±0.5	9.7±0.4	7.4±0.3	6.2±0.2
124	5.2±0.4	4.7±0.3	3.2±0.2	2.8±0.2
125	2.2±0.3	1.8±0.3	1.1±0.2	1.5±0.2
126	0.6±0.4	0.2±0.2	0.2±0.2	--
Total Cross-section	139.3±1.6	144.6±1.4	126.7±1.1	114.2±0.8
Normalization Error	±16.1%	±11.7%	±9.9%	±8.3%

Table IV.14: Isotopic Yields of Cs from $^{235}U(p,f)$

MASS NUMBER	CROSS-SECTIONS (mb)			
	E_p = 40MeV	60MeV	80MeV	100MeV
130	--	--	0.7±0.2	1.3±0.1
131	--	0.5±0.4	1.7±0.2	2.9±0.1
132	1.5±0.5	3.2±0.4	4.3±0.3	5.0±0.2
133	5.6±0.9	8.8±0.7	7.3±0.4	7.5±0.2
134	9.8±0.8	12.5±0.7	10.6±0.4	9.2±0.2
135	16.7±1.1	16.6±0.9	10.9±0.5	9.7±0.3
136	20.5±1.2	16.6±0.9	10.9±0.5	9.3±0.2
137	21.7±1.3	16.8±0.9	10.6±0.5	9.8±0.3
138	14.4±1.2	10.7±0.8	6.9±0.8	7.0±0.2
139	11.3±0.8	8.5±0.6	6.6±0.3	6.0±0.2
140	7.1±0.6	5.3±0.4	4.8±0.3	4.1±0.1
141	3.6±0.6	3.2±0.4	2.6±0.2	2.7±0.1
142	0.1±0.6	0.9±0.4	1.0±0.5	1.0±0.3
143	--	--	--	0.3±0.1
Total Cross-section	112.4±3.0	113.6±2.7	94.8±1.9	76.0±0.7
Normalization Error	±4.6%	±5.1%	±4.8%	±6.6%

Figure IV.16

Isotopic distributions of Rb

from $^{235}U(p,f)$

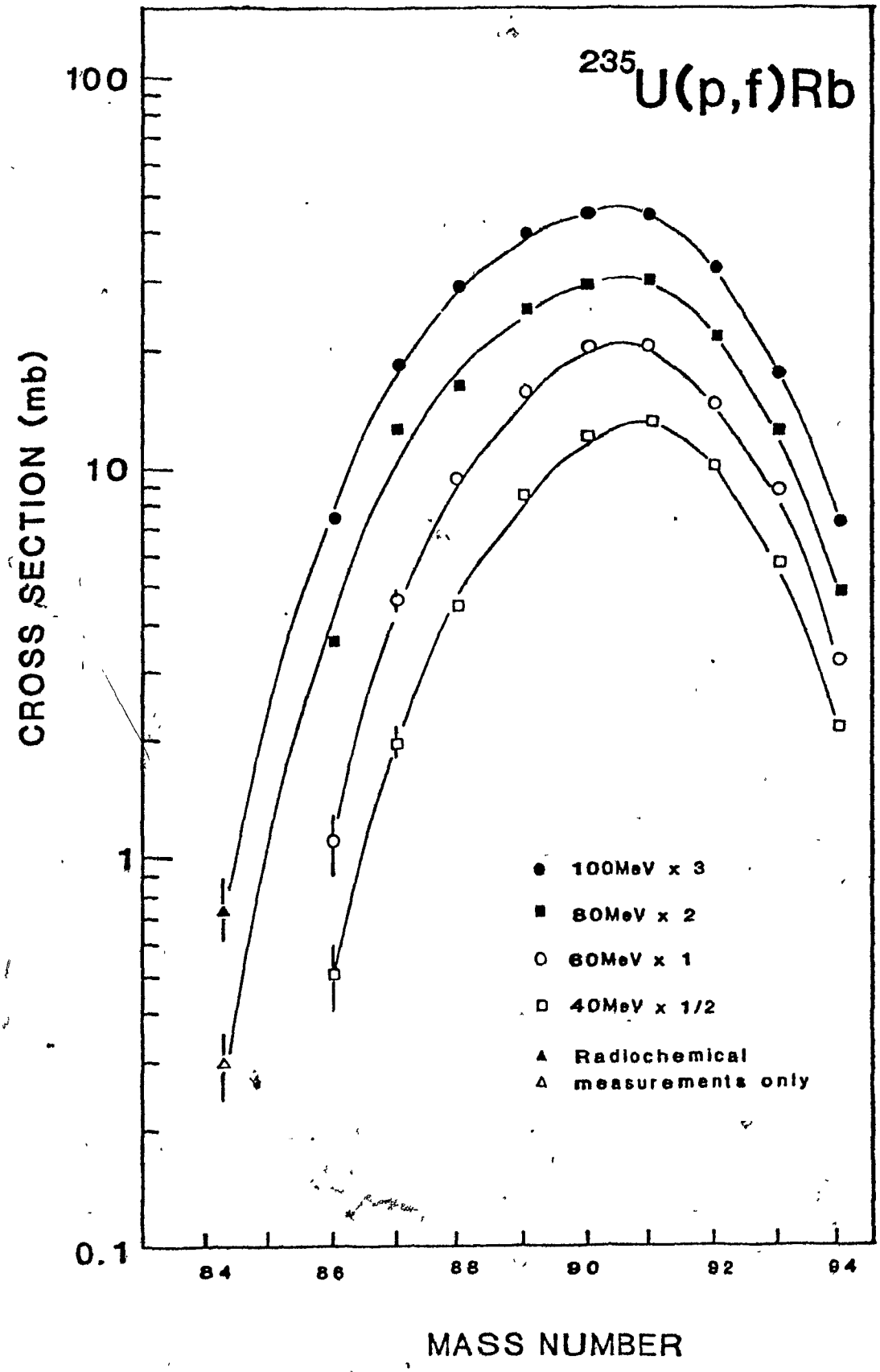
^{235}U(p,f)Rb
100
10
1
0.1
CROSS SECTION (mb)
84
86
88
90
92
94
MASS NUMBER
100MeV x 3
80MeV x 2
60MeV x 1
40MeV x 1/2
Radiochemical
measurements only

Figure IV.17

Isotopic distributions of In

from $^{235}U(p,f)$

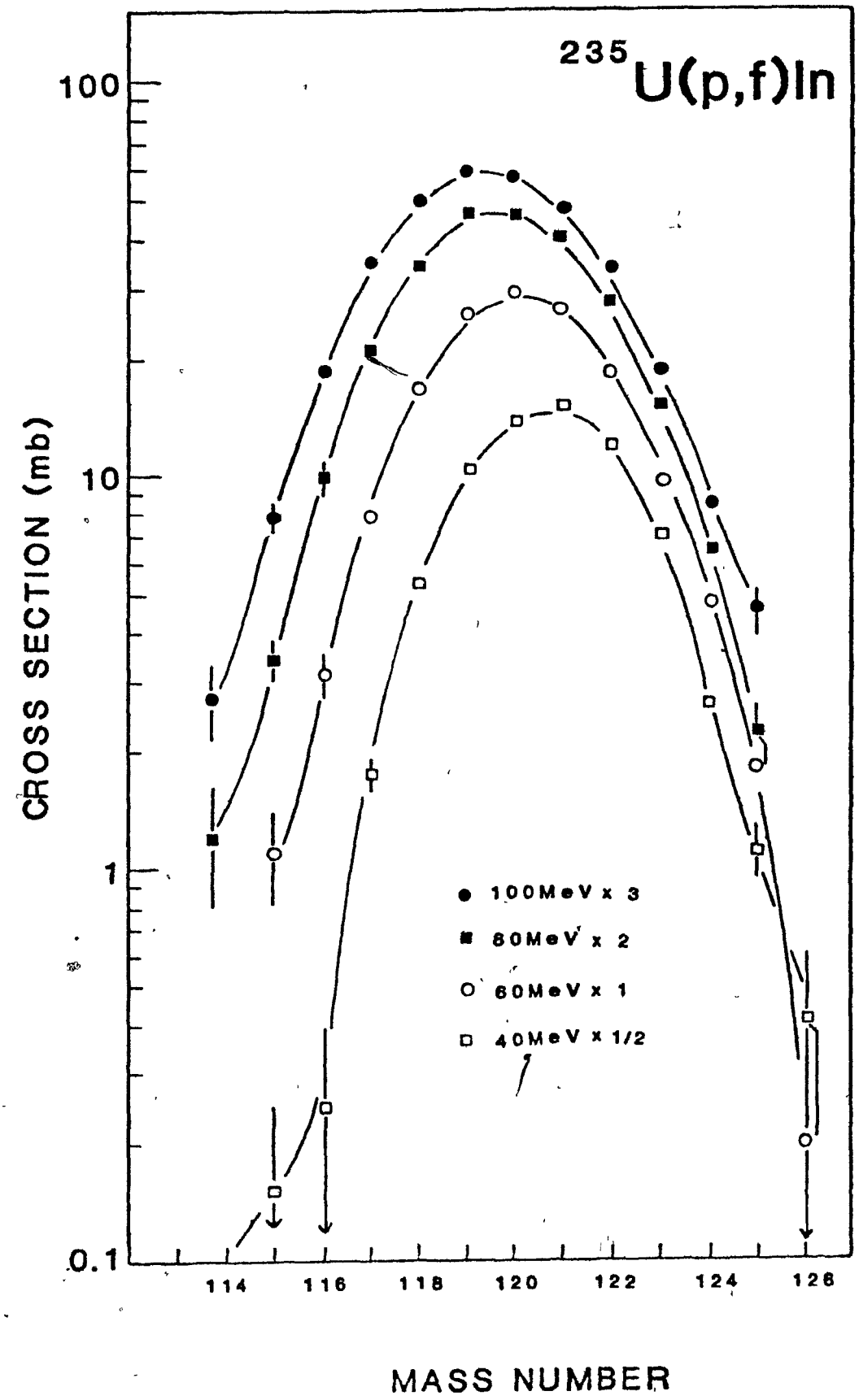
^{235}U(p,f)In
100
10
1
0.1
CROSS SECTION (mb)
100MeV x 3
80MeV x 2
60MeV x 1
40MeV x 1/2
114
116
118
120
122
124
126
MASS NUMBER

Figure IV.18

Isotopic distributions of Cs

from $^{235}U(p,f)$

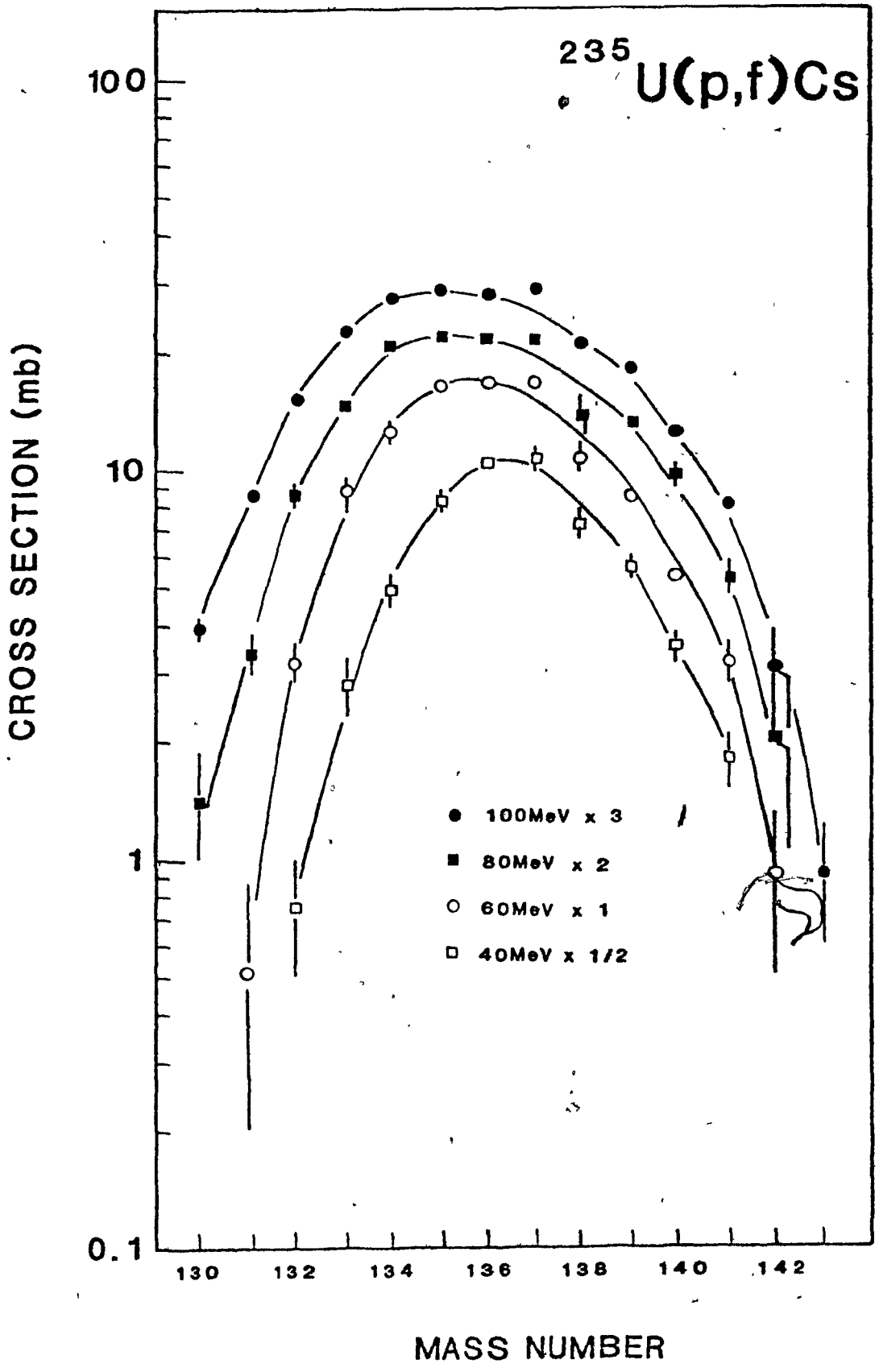
^{235}U(p,f)Cs
100
10
1
0.1
CROSS SECTION (mb)
100MeV x 3
80MeV x 2
60MeV x 1
40MeV x 1/2
130
132
134
136
138
140
142
MASS NUMBER

V. DISCUSSION

A. Excitation Functions

The excitation functions of independently-formed nuclides exhibit trends that are characteristic of their neutron-to-proton ratios: the higher the value of N/Z, the lower the energy at which the excitation function will peak. Thus the independent cross-sections of ^{72}Ga, $^{84,86}Rb$, ^{116m}In, $^{117m+g}In$ are observed to increase monotonically in the energy range 40 to 90 MeV, the cross-sections of ^{132}Cs initially increase and level off between 70 to 80 MeV, the cross-sections of $^{134m+g}Cs$ peak near 50 MeV, and the cross-sections of ^{136}Cs peak below 40 MeV and then decrease. Friedlander et al.(Fr63) were the first to correlate the peaks of the excitation functions to the neutron-to-proton ratios of the fission products. Since then a number of measurements have confirmed this correlation as shown by the compilation of Galinier and Yaffe (Ga77a) for $^{238}U(p,f)$ in the energy range 0.03 to 2 GeV. The formation cross-sections of $^{132-137}Cs$ from the proton-induced fission of ^{233}U (To69) and ^{235}U (Sa71) also show an energy dependence of the peaks of the excitation functions. The results from these studies, together with the present measurements, are shown in Figure V.1. In general, the peaks of the excitation functions exhibit the expected variation with N/Z of the fission product. However, the trend indicated by Tomita and Yaffe's (To69) original data from $^{233}U(p,f)$ is at variance with the trends observed from other fissioning systems.

Figure V.1

Energies at which the excitation functions reach their peak

■: ^{233}U data from Tomita and Yaffe (To69)

●: ^{235}U data from Saha et al. (Sa71)

□: ^{233}U data - This work

o: ^{235}U data - This work

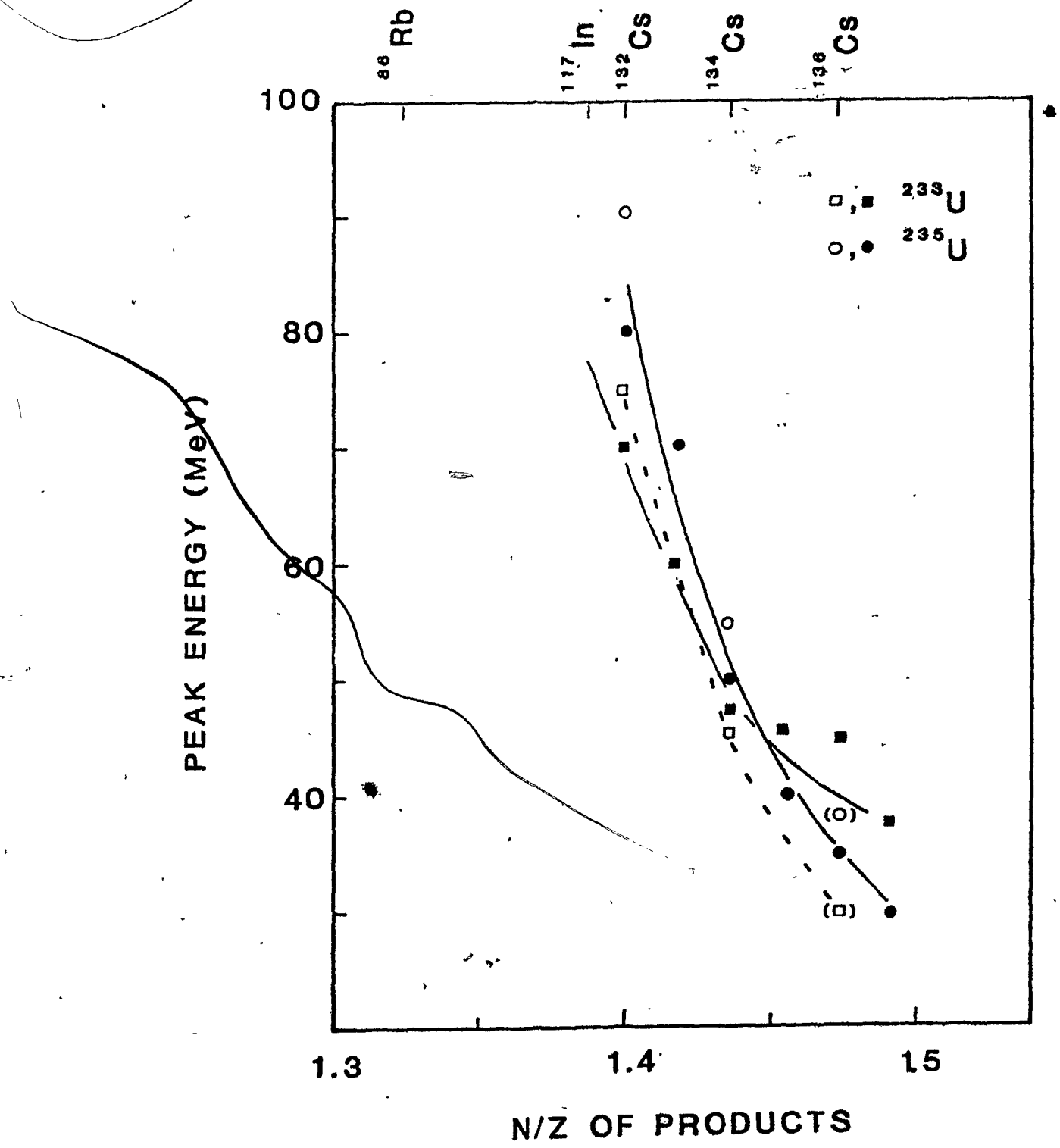
^{86}Rb
^{117}In
^{132}Cs
^{134}Cs
^{136}Cs
100
80
60
40
□,■ ^{233}U
○,● ^{235}U
(○)
(□)
PEAK ENERGY (MeV)
1.3
1.4
1.5
N/Z OF PRODUCTS

For example, the compilation made by Saha et al.(Sa71), for the proton-induced fission of ^{232}Th, $^{235,238}U$, and ^{239}Pu, indicates that the peak of the excitation function of a given product occurs at a relatively lower energy in the fission of a target of lower N/Z. As can be seen from Figure V.1 the major discrepancy is due to the measured excitation function of ^{136}Cs from $^{233}U(p,f)$. Although Tomita and Yaffe's original data showed a distinct peak at 45 MeV in the ^{136}Cs excitation function no peak existed when their data were normalized to the monitor cross-sections used in this work as shown in Figure IV.5. Furthermore, the present measurements show that the $^{233}U(p,f)^{136}Cs$ excitation function peaks below 35 MeV. The $^{132,134,136}Cs$ excitation functions measured in this work thus support the target dependent trend shown by Saha et al. (Sa71). It should be noted that the $^{135,137}Cs$ results given by Tomita and Yaffe were interpolated from the charge dispersion curves which are peaked near ^{136}Cs. Consequently, any error in the ^{136}Cs excitation function will manifest itself in the interpolated results for ^{135}Cs and ^{137}Cs. Although the isotopic yield distributions measured in this work could be used to show the general trend of the excitation functions for other nuclides, four points were insufficient to define the shapes of the curves, and supplement the measured excitation functions. However, the systematics observed for the cesium data do not contradict the trends observed for the other data measured in this work. For example, the curve for the $^{235}U(p,f)$ data in

Figure V.1 indicates that the ^{117}In excitation function should peak near 100 MeV, and the data shown in Figure IV.7 indicate that the excitation function is levelling off at this energy. For the ^{233}U(p,f) measurements, Figure V.1 indicates that the ^{117}In excitation function should peak near 80 MeV. Although the data in Figure IV.3 show that the excitation function is still increasing above 80 MeV, measurements at energies greater than 90 MeV are needed to define the shape of this curve clearly. The cross-sections of all other nuclides measured in this work appear to still be increasing above 90 MeV, which is consistent with the predictions of the cesium systematics.

The general shapes of the excitation functions of independently-formed fission products can be explained qualitatively by considering the mode of de-excitation of the primary fragments. As mentioned in the introduction, the primary mode of de-excitation is by neutron emission and this requires sufficient energy to overcome the neutron binding energy. The fission process results predominantly in neutron-rich fragments so that fission products with considerably lower neutron-to-proton ratios are formed with low probabilities at low excitation energies. As the incident energy is increased the formation cross-sections of these products increase until the production of products with even lower neutron-to-proton ratios becomes energetically possible, causing a levelling off and/or decrease in the formation cross-sections of the now relatively neutron-rich products. The observation that the excitation functions of fission products

do not decrease monotonically after they peak is a result of the increasing influence of direct reactions with increasing bombarding energy. Direct reactions in which charged particles and neutrons are emitted prior to fission will result in fissioning nuclei with lowered excitation energies. Thus the persisting influence of fission events with relatively lower excitation energies, when compared to the incident energies, will manifest itself in the fission product excitation functions.

B. Energy and Mass Correlations of the Isotopic Distributions

The statistical moments analysis of the isotopic distributions from the proton-induced fission of ^{233}U and ^{235}U are given in Tables V.1 and V.2 respectively. Except for the gallium data no errors have been assigned to the neutron-to-proton ratios ($\langle N/Z \rangle$) of the centroids of the distributions as the errors are less than the least significant number of the values given. The skewness and excess reflect the asymmetry and "peakedness" of the distributions and were defined in section III on data analysis.

The negative excess for all the data from both targets indicates that the distributions are flat with respect to a Gaussian shape. This was also observed by Mobed et al. (Mo81) for isotopic distributions from $^{233}U(d,f)$ in the energy range 18 to 44 MeV, and in both cases the isotopic distributions are quite different from those measured by Amiel et al. (Am73) for

Table V.1: Statistical Moments Analysis of Isotopic Distributions from $^{233}U(p,f)$

E_p (MeV)	CENTROID ⟨A⟩	⟨N/Z⟩	FWHM	SKEWNESS	EXCESS
		- GALLIUM -			
80	74.64±0.10	1.408±0.002	3.17±0.10	-0.11	-0.60
100	74.78±0.12	1.412±0.002	3.85±0.18	-0.46	-0.48
		- RUBIDIUM -			
40	89.83±0.04	1.428	4.06±0.03	0.012	-0.44
60	89.61±0.02	1.422	4.09±0.06	-0.047	-0.64
80	89.44±0.02	1.417	4.21±0.03	-0.004	-0.72
100	89.36±0.02	1.415	4.27±0.02	-0.027	-0.77
		- INDIUM -			
40	119.84±0.03	1.446	4.22±0.07	0.077	-0.30
60	119.30±0.07	1.435	4.62±0.14	-0.011	-0.21
80	118.96±0.02	1.428	4.82±0.04	0.092	-0.36
100	118.80±0.02	1.424	5.07±0.02	0.073	-0.46
		- CESIUM -			
40	135.62±0.03	1.466	5.20±0.04	0.15	-0.28
60	135.21±0.03	1.458	5.70±0.04	0.20	-0.46
80	134.91±0.03	1.453	6.19±0.03	0.09	-0.59
100	134.73±0.02	1.450	6.44±0.02	0.12	-0.63

Table V.2: Statistical Moments Analysis of Isotopic Distributions from $^{235}U(p,f)$

E_p (MeV)	CENTROID ⟨A⟩	⟨N/Z⟩	FWHM	SKEWNESS	EXCESS
		- RUBIDIUM -			
40	90.62±0.02	1.449	3.92±0.04	-0.08	0.53
60	90.37±0.02	1.442	4.19±0.03	-0.10	0.50
80	90.19±0.02	1.437	4.41±0.02	-0.10	-0.56
100	90.06±0.03	1.434	4.51±0.01	-0.07	-0.63
		- INDIUM -			
40	120.74±0.03	1.464	4.19±0.06	0.11	-0.18
60	120.15±0.03	1.452	4.57±0.05	0.03	-0.18
80	119.76±0.03	1.444	4.87±0.04	-0.01	-0.24
100	119.49±0.01	1.438	4.90±0.03	0.02	-0.57
		- CESIUM -			
40	136.65±0.06	1.484	4.83±0.11	0.09	-0.49
60	136.19±0.05	1.476	5.57±0.07	0.20	-0.61
80	135.97±0.04	1.472	6.11±0.07	0.14	-0.57
100	135.79±0.03	1.469	6.50±0.03	0.10	-0.66

$^{235}U(n_{th},f)$. For the thermal-neutron-induced fission measurements a positive or only slightly negative excess was obtained when the distributions were analysed by the statistical moments procedure used in this work. The notion of an "elementary" distribution arising from the fission of only one nucleus at a given excitation energy therefore seems conceivable. The flat distributions observed in this work may then be due to multi-chance fission at these energies resulting in a variety of fissioning nuclei at different excitation energies. The concept of an "elementary" distribution was also suggested by Holub and Yaffe (Ho73) for their charge dispersion studies on ^{232}Th.

The positive skewness most apparent in the cesium data indicates that there are shoulders on the heavier-mass side of the distributions and the negative skewness most apparent for the rubidium data from $^{235}U(p,f)$ indicates that the shoulders are on the lighter-mass side of the distributions. The positive skewness of the cesium distributions has been attributed to a deformed stable region near N = 86-88 (Un73, Wi76) and its competition with N = 82 spherical shell closure (Mo81). This explanation is further supported by the negative skewness of the rubidium distributions that may be attributed to the influence of N = 50 spherical shell closure. The observation that the skewness of Rb distributions are more noticeable for the measurements from $^{235}U(p,f)$ may be due to the experimental procedures employed. The amplitude of the triangular modulation on the 5 kV bias applied to the mass spectrometer extraction system was such

that only nine masses could be observed in the rubidium region during one measurement period. In order to extend the mass region being studied two such measurements with overlapping mass regions were carried out for $^{233}U(p,f)Rb$ reactions at 60, 80, and 100 MeV. The relative yields in the overlapping mass regions were then normalized. Inherent in this procedure was the uncertainty introduced by the mass discrimination correction which may have masked a possible small skewness. However, only one measurement was carried out at each energy for $^{235}U(p,f)Rb$ reactions. The skewness observed for each indium distribution is small. This is consistent with the observation that the indium isotopes observed in this work do not cross any major shell closure.

The variation of the FWHM of all the distributions is a function of both bombarding energy and target mass, as shown in Figures V.2 and V.3 respectively. Included in these figures are the data from $^{238}U(p,f)$ (Tr72, Le75, Ch77). Error bars have not been included in these figures for clarity. The curves show that the FWHM of all the isotopic distributions increase with increasing bombarding energy. Yaffe and his co-workers (Ya69) have observed analogous broadening of the charge dispersion curves in the heavy mass region. Although a number of charge dispersion studies in the light-mass regions (Kh70, Ma73) have indicated a constant width in the energy range 20 to 85 MeV, Galinier et al. (Ga77b) observed an increase in the widths of the charge dispersion curves centered near mass 80. The

Figure V.2

Full-Width at Half-Maximum (FWHM)

as a function of bombarding energy (E_p)

$^{235}U(p,f)$Cs data at 50MeV from Tracy et al. (Tr72)

$^{238}U(p,f)$Rb,Cs data at 80 and 100MeV from Lee et al. (Le75)

$^{238}U(p,f)$Rb,Cs data at 40 to 60MeV from Tracy et al. (Tr72)

$^{238}U(p,f)$In data from Chan et al.(Ch77)

All other data - This work

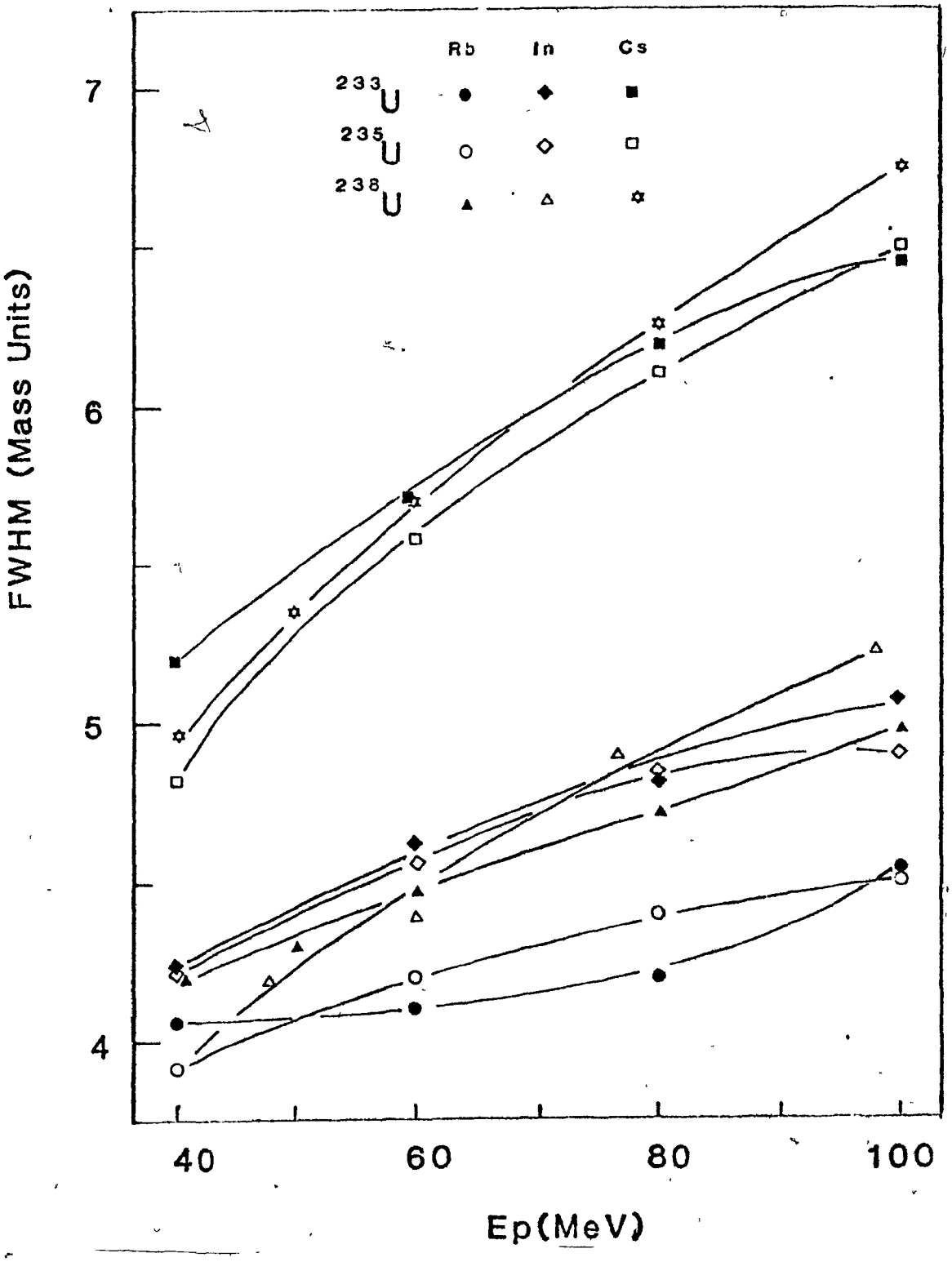
Rb
In
Cs
^{233}U
^{235}U
^{238}U
FWHM (Mass Units)
7
6
5
4
40
60
80
100
Ep(MeV)

Figure V.3

Full-Width at Half-Maximum (FWHM)

as a function of mean mass number

^{238}U(p,f)Ga,In data from
Chan et al.(Ch77)

^{238}U(p,f)Rb,Cs data at 100MeV
from Lee et al.(Le75)

^{238}U(p,f)Rb,Cs data at 40MeV
from Tracy et al.(Tr72)

^{235}U(p,f)Ga data from
Sutherland (Su77)

All other data - This work

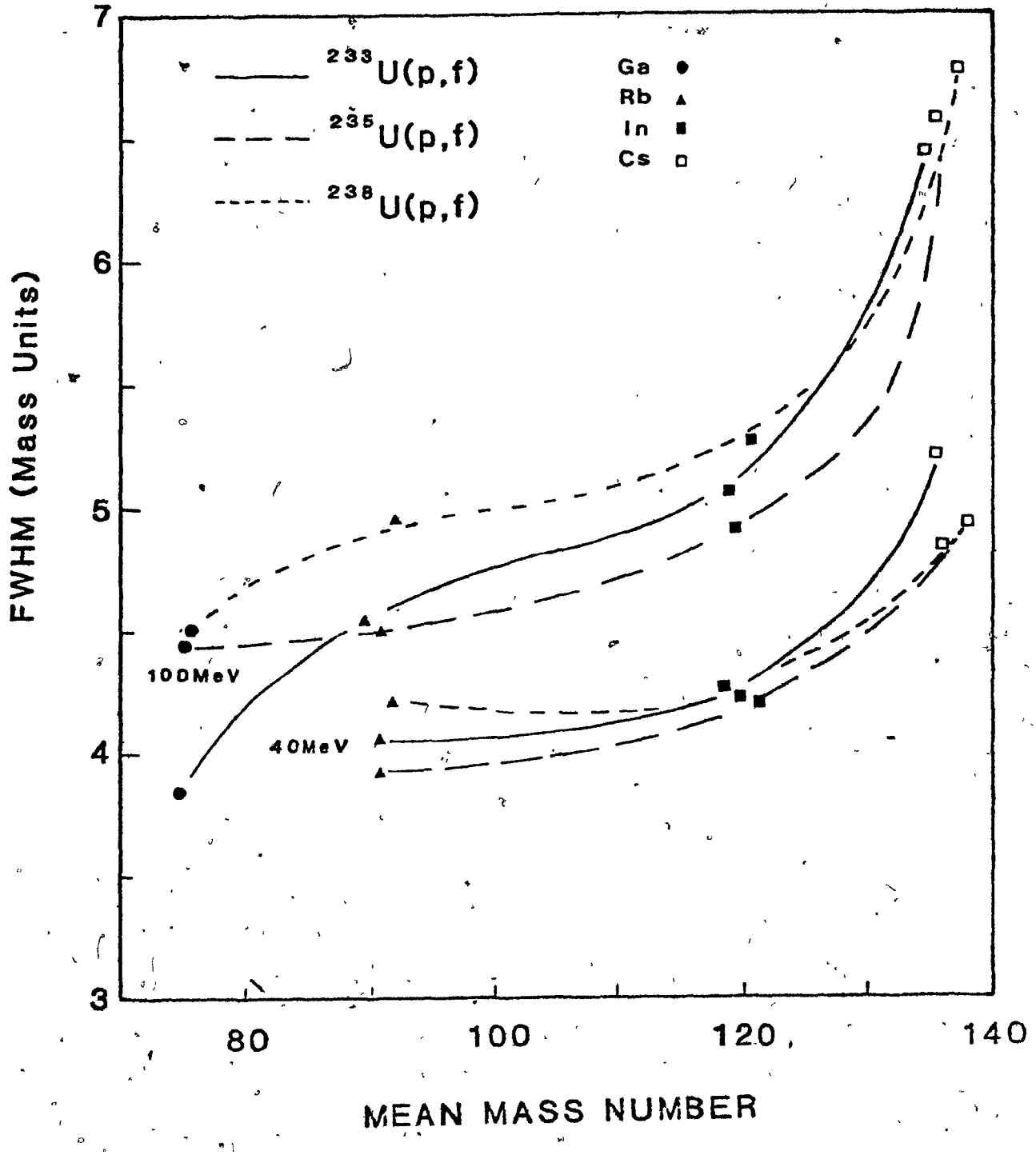
^{233}U(p,f)
^{235}U(p,f)
^{238}U(p,f)
Ga
Rb
In
Cs
100MeV
40MeV
FWHM (Mass Units)
MEAN MASS NUMBER
7
6
5
4
3
80
100
120
140

increase in the widths of the isotopic distributions may be attributed to the increase in multi-chance fission events in the energy range 40 to 100 MeV. The variation of the FWHM with mean mass number of the isotopic distributions shows a steady increase with mass and a sharp rise in the cesium region. This sharp rise in the cesium region was also shown in the compilation of charge-dispersion data made by Galinier and Yaffe(Ga77a), and for both cases may be attributed to neutron shell effects in this region. The charge-dispersion data, however, show a decrease in the FWHM between mass 100 and 130, whereas in general the isotopic distribution data show a slight increase in the FWHM over this mass range. This apparent contradiction may not be a discrepancy of the data, but rather a possible effect due to Z = 50 proton spherical shell closure. Such a shell effect would not be apparent in the isotopic distributions as the measurements are over a constant Z, however, the charge dispersions in the mass region 115 to 125 may be affected. The general increase in the FWHM of the isotopic mass distributions with increasing mass number may be attributed to the partitioning of the excitation energy between the primary fragments. Thus, if it is accepted that the excitation energy is shared between complementary fragments in accordance with their mass ratios, then more neutrons will be emitted from the possible heavier fragments, resulting in broader distributions of the heavier products.

It has recently been suggested by Nikkinen et al. (Ni80)

that the broad widths of the Cs distributions may be the result of multi-chance fissions at bombarding energies pertinent to this work. These authors therefore decomposed their Cs distributions from ^{232}Th(p,f) into two Gaussian curves and attributed the curves peaked at the lower mass numbers to high excitation energy events and the curves peaked at the higher mass numbers to low excitation energy events. However, no discernible structure was observed in the Rb distributions as might be expected, since for the 1 GeV proton-induced fission of ^{238}U Belyaev et al. (Be80) observed comparable broadening of both Rb and Cs distributions. It is therefore felt in this work that although a two-Gaussian distribution due to different excitation energies may be valid in the GeV energy range it is probably not the cause for the broadening of the Cs distributions at bombarding energies up to 100 MeV.

The variation of the mean neutron-to-proton ratios (<N/Z>) of the isotopic distributions with bombarding energy is shown in Figure V.4. The published measurements from ^{238}U(p,f) (Tr72, Le75, Ch77) are also shown in this figure. The decrease in <N/Z>of the products with an increase in the bombarding energy indicates that the centroids of the isotopic distributions are moving to lower mass numbers. This may be attributed to higher neutron yields from the primary fragments with an increase in their excitation energies, resulting in more relatively neutron-deficient products. Figure V.4 also indicates that a more neutron-rich target results in more neutron-rich products and

Figure V.4

Mean neutron-to-proton ratio (<N/Z>)

as a function of bombarding energy (E_p)

$^{235}U(p,f)$Cs data at 50MeV from Tracy et al. (Tr72)

$^{238}U(p,f)$Rb,Cs data at 80 and 100MeV from Lee et al. (Le75)

$^{238}U(p,f)$Rb,Cs data at 40 to 60MeV from Tracy et al.(Tr72)

$^{238}U(p,f)$In data from Chan et al.(Ch77)

All other data - This work

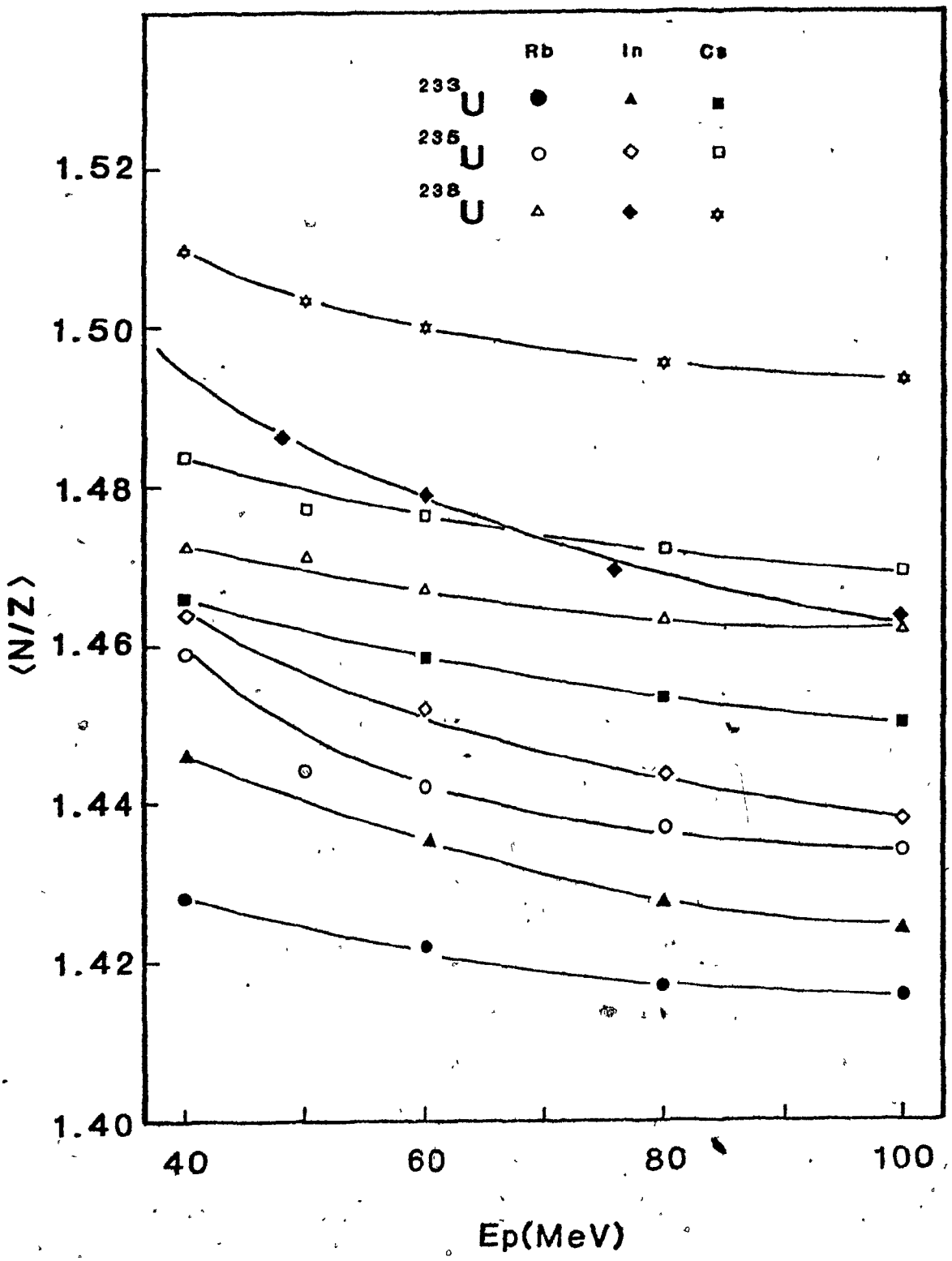
Rb
In
Cs
^{233}U
^{235}U
^{238}U
1.52
1.50
1.48
1.46
1.44
1.42
1.40
⟨N/Z⟩
40
60
80
100
Ep(MeV)

the correlation between N/Z of the target and <N/Z> of the products is linear as shown in Figure V.5. It is apparent from this compilation that the data from ^{232}Th(p,f) (Ni80) do not follow the systematics observed for the data from the uranium nuclei. This observation was also made by Tracy et al. (Tr72) for the 50 MeV proton-induced fission of ^{232}Th and ^{235,238}U, and in both cases indicates the importance of the identities of the fissioning nuclei when correlating fission product data.

The variation of <N/Z> with mean mass number of the fission products, or as it more frequently appears in the literature, N/Z_p versus mass number (A), is of importance when isotopic mass distributions are used to test the charge distribution postulates or isotopic charge-dispersion curves are constructed. In order to construct accurate variation of N/Z as a function of A, a large number of data points are required, and this has been restricted to the data from ^{238}U(p,f) in the energy range pertinent to this work. Galinier et al. (Ga77b) have compiled these data from the McGill group and shown that N/Z rises steeply in the mass region 80 to 90, levels off but still increases slightly over the mass range 90 to 120, increases steeply to mass 135, and then levels off over the energy range 50 to 85 MeV. Dikšić et al. (Di74) have also shown that the variation of the most probable charge (Z_p) with mass number is linear over the mass range 130 to 135, indicating that N/Z_p is a function of A in this mass region. The scarcity of data from ^{233}U(p,f) and ^{235}U(p,f) reactions in the energy range pertinent to this work

Figure V.5

Mean neutron-to-proton ratio (<N/Z>) of the fission products as a function of neutron-to-proton ratio (N/Z) of the targets*

$^{238}U(p,f)$Rb,Cs data from Lee et al. (Le75)

$^{238}U(p,f)$Ga,In data from Chan et al. (Ch77)

□: from Sutherland (Su77)

$^{232}Th(p,f)$ data from Nikkinen et al. (Ni80)

All other data - This work

*E_p = 100 MeV

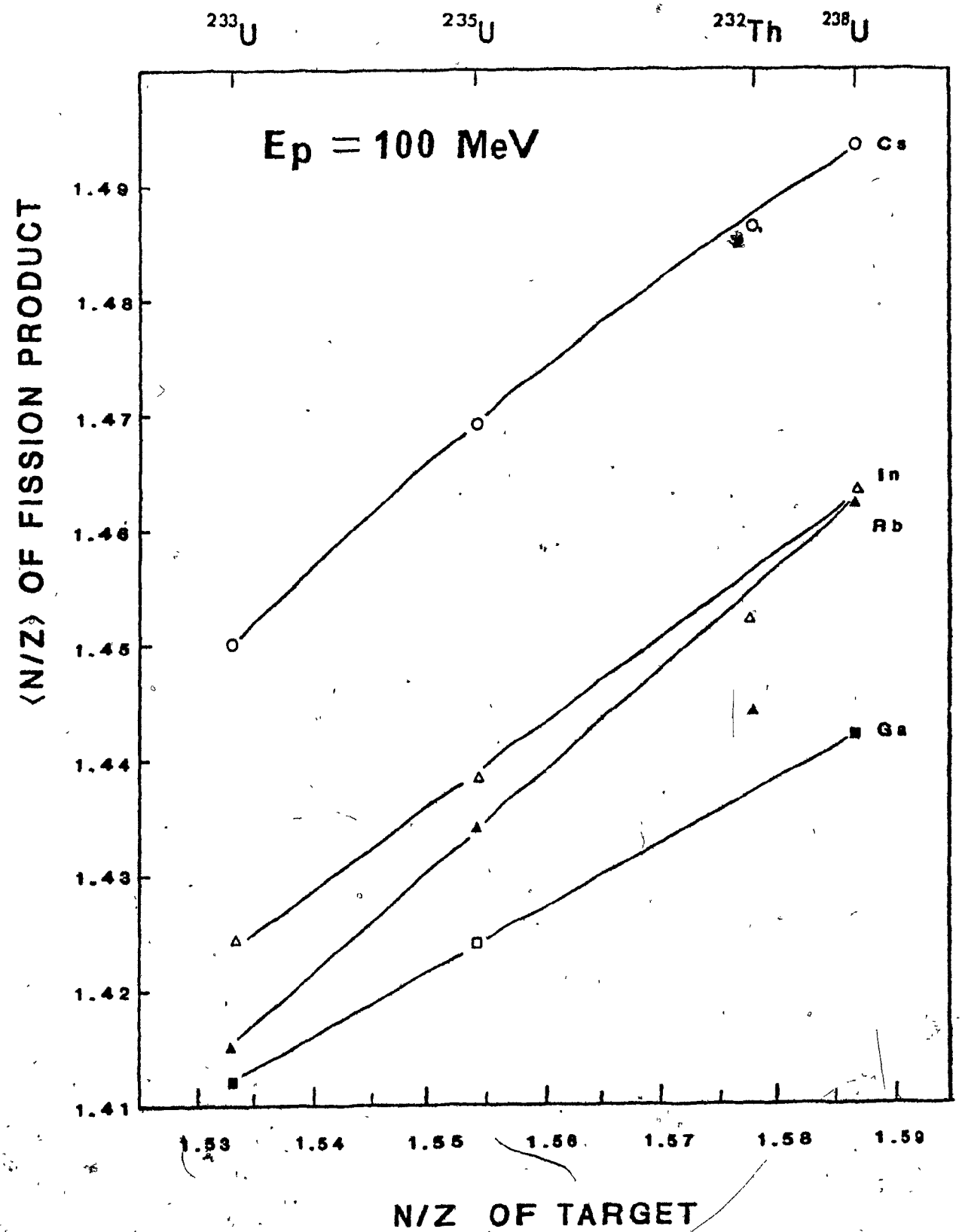
^{233}U
^{235}U
^{232}Th
^{238}U
Ep = 100 MeV
Cs
In
Rb
Ga
⟨N/Z⟩ OF FISSION PRODUCT
1.49
1.48
1.47
1.46
1.45
1.44
1.43
1.42
1.41
1.53
1.54
1.55
1.56
1.57
1.58
1.59
N/Z OF TARGET

makes it difficult to contruct accurate variations of <N/Z> with A. However, the data obtained in this work together with the measurements of Marshall and Yaffe (Ma73) and Khan et al. (Kh70) indicate that the atomic numbers of the fission products vary linearly with respect to their mean mass numbers over the mass range 90 to 135. This correlation is shown for the data from $^{233}U(p,f)$ and $^{235}U(p,f)$ in Figures V.6 and V.7 respectively. Although the gallium data have not been included in these figures the systematics indicate that this linear relation can be extended to mass 74. For example, the centroid of the gallium distribution from $^{233}U(p,f)$ at 80 MeV is 74.64 ±0.10 and the systematics indicate that the centroid should be at 74.57. Furthermore, this trend is supported by the data collected by Yaffe's group for $^{238}U(p,f)$ over the mass range 80 to 152 and is illustrated for a bombarding energy of 50 MeV in Figure V.8. Included in this figure are the mass spectrometric data from Tracy et al. (Tr72) and Chan et al. (Ch77). This linear variation of the atomic number with mean mass number indicates that N/Z is a function of the mass of the fission products. For all three uranium targets $(\partial Z/\partial A)_E \approx 0.38 \pm 0.02$, in agreement with the findings of Dikšić et al. (Di74) and McHugh and Michel (Mc68).

C. Fission Information from the Pre-equilibrium/Exciton Model

The fission option of the pre-equilibrium/exciton model

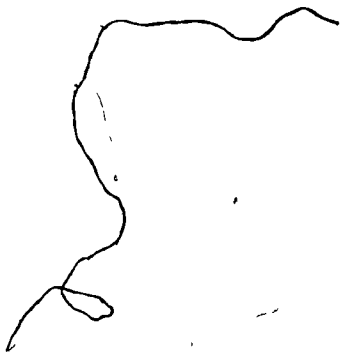

Figure V.6

Variation of the atomic number (Z) with the mean mass number of the fission products from ^{233}U(p,f)

▲: Marshall and Yaffe (Ma73)

●: This work

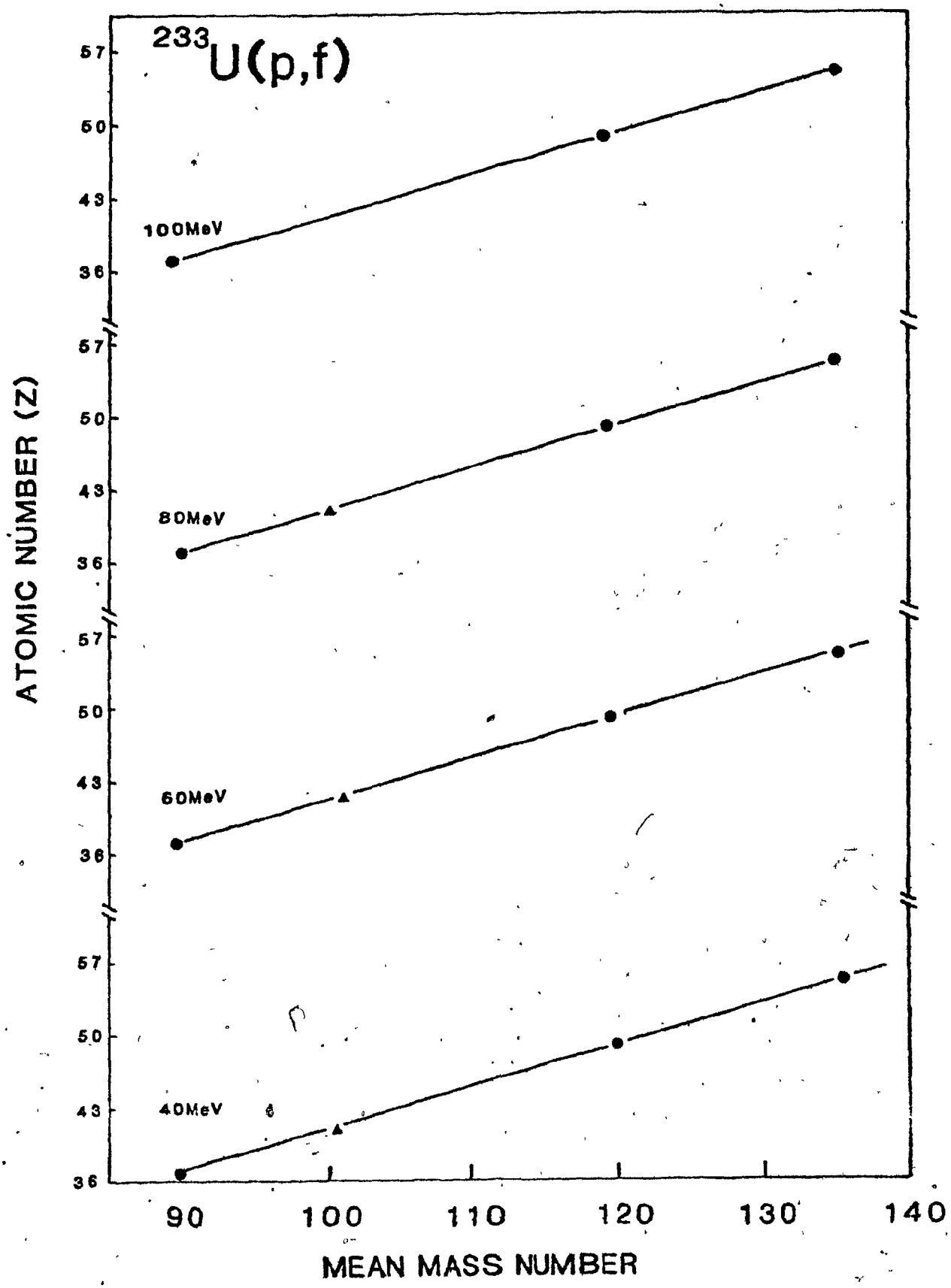
^{233}U(p,f)
100MeV
80MeV
60MeV
40MeV
ATOMIC NUMBER (Z)
MEAN MASS NUMBER
57
50
43
36
90
100
110
120
130
140

Figure V.7

Variation of the atomic number (Z) with the mean mass number of the fission products from $^{235}U(p,f)$

▲: Khan et al. (Kh70)

■: Tracy et al. (Tr72)

●: This work

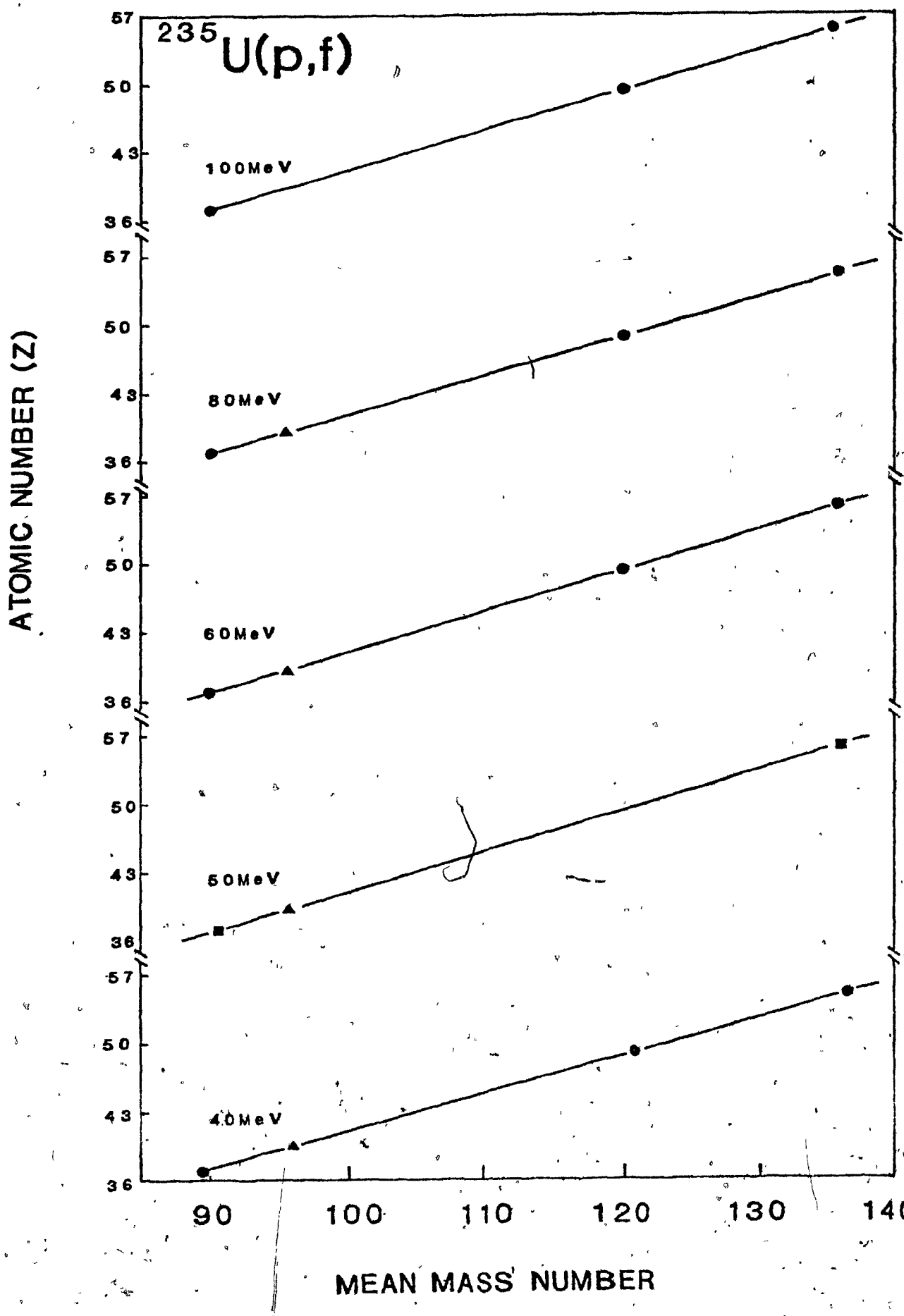
^{235}U(p,f)
100MeV
80MeV
60MeV
50MeV
40MeV
ATOMIC NUMBER (Z)
MEAN MASS NUMBER
57
50
43
36
90
100
110
120
130
140

Figure V.8

Variation of atomic number (Z) with mean mass number of the fission products for $^{238}U(p,f)$ at 50MeV

From charge dispersion measurements:

■: Davies and Yaffe (Da63)
▲: Parikh et al. (Pa67)
●: Khan et al. (Kh70)
□: Miller and Yaffe (Mi73)
◆: Dikšić et al. (Di74)
○: Sarkar (Sa74)
Δ: Galinier and Yaffe (Ga77a)
✱: Galinier et al. (Ga77b)

From isotopic yield measurements:

◇: Tracy et al. (Tr72)
¤: Chan et al. (Ch77)

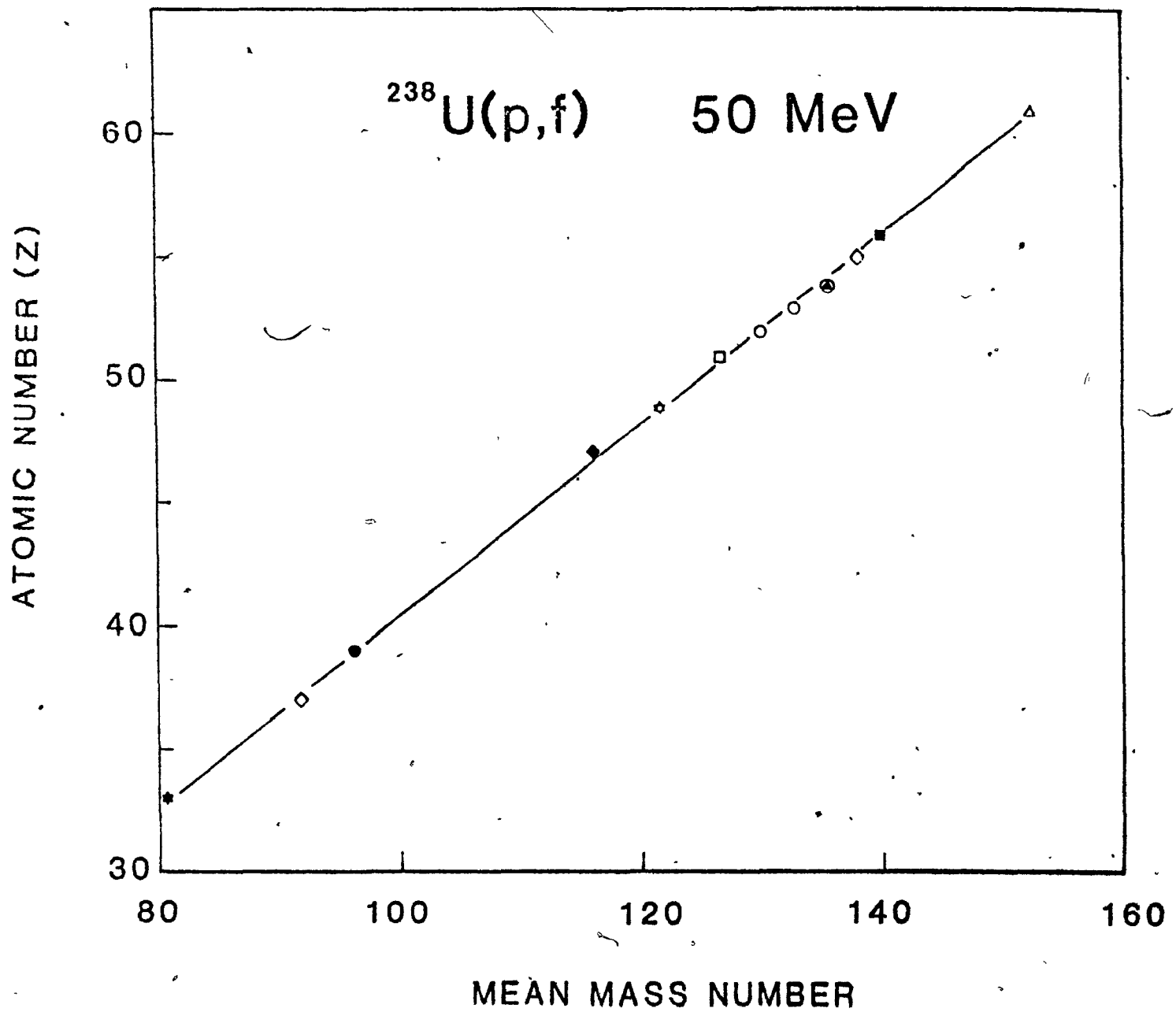
^{238}U(p,f) 50 MeV
ATOMIC NUMBER (Z)
60
50
40
30
80
100
120
140
160
MEAN MASS NUMBER

summarized in the introduction was used to predict the identities and specific probabilities of fissioning nuclides from all $^{233}U(p,f)$ and $^{235}U(p,f)$ reactions at bombarding energies up to 100 MeV. This information was required in order to estimate pre-fission nucleon emissions and, in conjunction with the fission product data measured in this work, to estimate average total neutron yields. These estimates were then used to test the charge distribution postulates which will be discussed in due course.

This model was chosen because of the recent success it has had in fitting the spallation data from $^{232}Th(p,XnYp)$ reactions to 100 MeV (Ho79) and the conclusion by the authors that their treatment of fissionability is valid. Furthermore, no spallation data exist for proton-induced reactions in ^{233}U and ^{235}U because the nuclear properties of the possible spallation products do not allow for easy measurement; and the formation cross-sections of these products should be low considering the high fissility of the targets. A rigorous test of the model for the uranium targets used in this work is therefore not appropriate. However, Boyce (Bo72) has measured total fission cross-sections from $^{233}U(p,f)$ and $^{235}U(p,f)$ reactions in the energy range 4 to 30 MeV and these data are compared to the theoretical results from the pre-equilibrium/exciton model in Figure V.9.

The only free variable in the model is the level-density parameter, a_f/a_n, for which a value of 1.05 was chosen. This

Figure V.9

Total fission cross-sections as a function of bombarding energy (E_p) for $^{233,235}U(p,f)$

●,○ : Boyce (Bo72)

■ : McCormick and Cohen (Mc54)

□ : Fulmer (Fu59)

—— : From the pre-equilibrium/exciton model (a_f/a_n= 1.05, 2000 cascades)

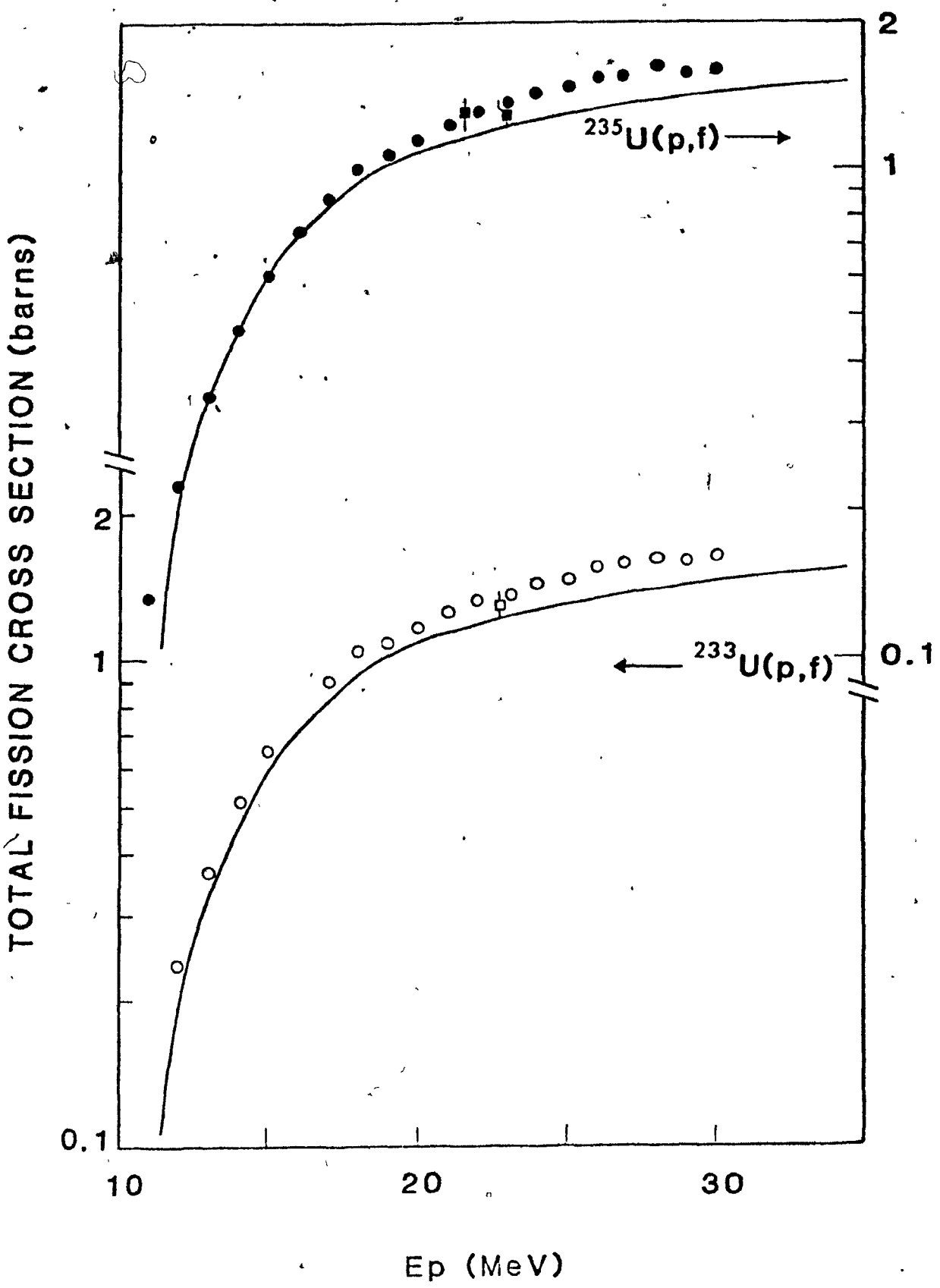
TOTAL FISSION CROSS SECTION (barns)
2
1
0.1
$^{235}U(p,f)$
$^{233}U(p,f)$
2
1
0.1
10
20
30
Ep (MeV)

choice was based on the findings of Chung (Ch80), that a value of 1.05 could best reproduce the broad range of their data up to 100 MeV, and the work of Mobed et al. (Mo81). The latter authors found that for ^{233}U(d,f) reactions a value of 1.05 in the pre-equilibrium/hybrid code (ALICE) derived by Blann (Bl78) reproduced the average fissionabilities (Γ_f/Γ_n) given by Vandenbosch and Huizenga (Va73). As can be seen in Figure V.9, the calculations based on a_f/a_n = 1.05 never underestimate the data by more than 15%. This is certainly better than the 20 to 60% discrepancy shown by Hogan et al. (Ho79) for ^{232}Th(p,f) in the energy range 15 to 32 MeV. However, Chung (Ch80) has shown that at energies above 40 MeV the calculations based on a_f/a_n = 1.05 for ^{232}Th(p,f) give better fits to the experimental data. No fission cross-section data exist for ^{233}U(p,f) and ^{235}U(p,f) reactions in the energy range 40 to 100 MeV, thus the same value of 1.05 for a_f/a_n was chosen for this energy range.

The computed fission information for ^{233}U(p,f) and ^{235}U(p,f) reactions is given in Tables V.3 and V.4 respectively. For the purpose of the present study the grouping of this information according to the charges of the fissioning nuclei was considered quite adequate. Thus the average fissioning mass from all (p,Xnf) reactions was computed as the weighted sum of all fissioning nuclei of neptunium. The same procedure was applied to all (p,pXnf), (p,2pXnf), and (p,αXnf) reactions. The average fissilities, calculated as the total fission cross-sections divided by the total reaction cross-sections, remain

Table V.3: Average Fission Information for $^{233}U(p,f)$ (a_f/a_n = 1.05, 2000 cascades)

FISSION INFORMATION	E_p (MeV) 40	60	80	100
$\Sigma(p,Xnf)\sigma$ (mb)	1423.40	1172.72	907.61	728.77
$\langle A_F \rangle$	233.25	233.05	232.83	232.71
Z_F	93	93	93	93
$\Sigma(p,pXnf)\sigma$ (mb)	159.60	369.98	482.12	602.29
$\langle A_F \rangle$	232.50	232.09	231.93	231.76
Z_F	92	92	92	92
$\Sigma(p,2pXnf)\sigma$ (mb)	--	--	--	14.30
$\langle A_F \rangle$	--	--	--	230.70
Z_F	--	--	--	91
$\Sigma(p,\alpha Xnf)\sigma$ (mb)	6.07	17.82	29.10	35.38
$\langle A_F \rangle$	229.50	229.00	229.05	228.80
Z_F	91	91	91	91
Total Fission Cross-sections (mb)	1589.07	1560.52	1418.83	1380.74
Average Fissioning Mass	233.16	232.78	232.44	232.17
$\langle \nu_{pre} + \chi_{pre} \rangle$	0.84	1.22	1.56	1.83
$\langle \nu_{pre} \rangle$	0.72	0.94	1.13	1.27
Average Fissility	91.7%	91.9%	90.4%	91.7%
Average Excitation Energy (MeV)	31.85	39.13	45.43	50.77

Table V.4: Average Fission Information for $^{235}U(p,f)$ (a_f/a_n = 1.05, 2000 cascades)

FISSION INFORMATION	E_p (MeV) 40	50	60	80	100
$\Sigma(p,Xnf)\sigma$ (mb)	1442.60	1296.90	1149.34	915.10	748.48
$\langle A_F \rangle$	234.91	234.84	234.77	234.54	234.50
Z_F	93	93	93	93	93
$\Sigma(p,pXnf)\sigma$ (mb)	81.06	193.17	294.57	409.35	489.66
$\langle A_F \rangle$	234.29	233.92	233.71	233.52	233.40
Z_F	92	92	92	92	92
$\Sigma(p,2pXnf)\sigma$ (mb)	--	--	--	--	9.84
$\langle A_F \rangle$	--	--	--	--	231.27
Z_F	--	--	--	--	91
$\Sigma(p,\alpha Xnf)\sigma$ (mb)	1.74	12.29	17.88	32.40	46.17
$\langle A_F \rangle$	230.93	230.83	230.32	229.83	230.17
Z_F	91	91	91	91	91
Total Fission Cross-section (mb)	1525.40	1502.36	1461.79	1356.85	1294.15
Average Fissioning Mass	234.88	234.69	234.50	234.12	233.91
$\langle \nu_{pre} + \chi_{pre} \rangle$	1.12	1.31	1.50	1.88	2.09
$\langle \nu_{pre} \rangle$	1.07	1.15	1.25	1.48	1.56
Average Fissility	87.5%	85.6%	85.9%	86.0%	85.5%
Average Excitation Energy (MeV)	30.84	35.37	38.82	44.49	51.10

fairly constant over the energy range 40 to 100 MeV and indicate that between 90 to 92% of all reactions go to fission for $^{233}U(p,f)$, and 85 to 87% of all reactions go to fission for $^{235}U(p,f)$. The differences in the average fissilities for the two fissioning systems reflect the dependence of the fissilities on Z^2/A of the fissioning nuclides, as shown by Chung (Ch80). The average excitation energy accompanied with fission, for a given incident proton energy, was computed as the weighted sum of the excitation energies of each fissioning nuclide. These average values, when compared to the incident proton energies, reflect the broad energy distribution of the fissioning nuclei, resulting from multi-chance fission. The fission cross-sections, when grouped according to the charges of the fissioning nuclei, show the increasing probabilities of charge particle emission with increasing bombarding energies. For example, at 40 MeV the total (p,Xnf) cross-section for the ^{233}U target is 1423.4 mb corresponding to 89.6% of the total fission cross-section. Ten per cent of the remaining cross-section may be attributed to (p,pXnf) reactions and 0.4% goes to (p,αXnf) reactions. At an incident proton energy of 100 MeV, however, only 52.8% of all fissions are attributed to (p,Xnf) reactions, 43.6% are attributed to (p,pXnf) reactions, and the remaining 4.6% go to (p,2pXnf) and (p,αXnf) reactions.

The fission information given in Tables V.3 and V.4 was used directly to calculate average total pre-fission nucleon and neutron yields from all (p,XnYpαf) reactions. The average total nucleon yield at each energy is given by:

$$\langle \nu_{pre} + \chi_{pre} \rangle = (A_T + 1) - \langle A_F \rangle_T \qquad (V.1)$$

where: $\langle \nu_{pre} + \chi_{pre} \rangle$ = the average pre-fission nucleon yield,

A_T = the mass number of the target,

$\langle A_F \rangle_T$ = the average fissioning nucleus from all possible fission reaction channels.

The average number of pre-fission neutrons emitted was calculated in a similar manner, allowing for pre-fission charged particle emission. Thus:

$$\langle \nu_{pre} \rangle_{Z_F} = (A_T + 1) - \chi_{pre} - \langle A_F \rangle_{Z_F} \qquad (V.2)$$

where: $\langle \nu_{pre} \rangle_{Z_F}$ = the average pre-fission neutron yield for a given fissioning charge (Z_F),

χ_{pre} = the total mass number of all charge particles emitted for a given fissioning charge (Z_F),

$\langle A_F \rangle_{Z_F}$ = the average fissioning mass for a given fissioning charge (Z_F).

The average total pre-fission neutron yield was then calculated as the weighted sum of values obtained from all (p,Xnf), (p,pXnf), (p,2pXnf), and (p,αXnf) reactions using equation (V.2).

D. Computations of Average Total Neutron Yields

In a number of on-line mass spectrometric studies of charged particle induced fissions (Tr72, Le75, Ch77, Ni80, Mo81) average total neutron yields have been deduced for mass splits

resulting in Rb,Cs, and In products. In order to estimate these yields the following assumptions were made:

1. The probabilities of charged particle emission in the entire fission process are small and may be neglected in the energy range covered.

2. The centroids of the complementary products of Rb,Cs, and In may be estimated by assuming a constant N/Z ratio for neighbouring products.

The reliability of these neutron yield estimates is dependent on the validity of these assumptions. Since the results from this investigation indicate that the centroids of the isotopic distributions are a linear function of the fission-product charge, and the pre-equilibrium/exciton model calculations indicate that the probability of pre-fission charged particle emission is not small enough to be neglected, the effects of the assumptions given above must be examined.

Before these assumptions are examined the following correlations between the identities of the fissioning nucleus, primary fragments, and fission products must be made. The sum of complementary primary fission fragment charges ($Z_L' + Z_H'$) and masses ($A_L' + A_H'$) are equal to the fissioning charge (Z_F) and mass (A_F) respectively. The relationship between the primary fission fragment and fission product charges is dependent on the probability of charged particle emission from the primary fragments. Since these fragments are usually neutron rich, the binding energies for charged particles are large and the coulomb

barriers are high, so that the probability of charged particle emissions should be small and their emission may be neglected. Thus:

$$Z'_L = Z_L; \quad Z'_H = Z_H$$

$$A'_L = A_L + \nu_L; \quad A'_H = A_H + \nu_H$$

where the primed and unprimed Z's and A's refer to the primary fission fragments and products respectively; subscripts L and H refer to the light and heavy fragments or products respectively; and ν_L and ν_H denote the numbers of neutrons emitted from the light and heavy fragments respectively.

It is evident from the correlations given above that the charges of complementary fission products is dependent on the charge of the fissioning nucleus (Z_F). Since Z_F is determined by pre-fission charged particle emission and the pre-equilibrium/exciton model calculations indicate that these emissions are not negligible, the predicted charges of the fissioning nuclei must be taken into account when determining the identities of complementary fission products. The assumption that the centroids of the complementary products, of at least Rb and Cs, can be estimated by assuming a constant N/Z for neighbouring products seems justified, since the isotopic distributions of the measured products are centred where the mass yield curve is expected to be reasonably flat. However, the linear variation of the centroids of fission product distributions with atomic number, shown in Figures V.6 and V.7, allows the centroids of

complementary products to be interpolated directly from the experimental systematics. Although this latter method of estimating complementary centroids may be more reliable, as it is based directly on experimental evidence, the extent to which the estimates deviate from those obtained assuming a constant N/Z is small. For example, for the proton-induced fission of uranium nuclei the complementary product of Rb(Z=37) is Ba(Z=56) if charged particle emission is neglected. For $^{233}U(p,f)$ at 40 MeV the systematics shown in Figure V.6 indicate that $\langle A_{Ba} \rangle = 138.14$. The measured centroid of Cs at this energy is 135.62, and the predicted centroid of Ba, assuming a constant N/Z, will be 56x135.62/55=138.09. The 0.05 discrepancy between the predictions thus indicates that the assumption of a constant N/Z for neighbouring products will not seriously effect the neutron yield estimates for fissions resulting in Rb,Cs, and their complementary products. However, both methods of estimating the complementary centroids were used in this work in order to illustrate the small difference between the estimated neutron yields.

The assumption that the centroids of the complementary products of In(Z=49) can be estimated by assuming a constant N/Z ratio is, however, questionable since if charged particle emission is neglected the complementary Ru(Z=44) product is five charge units displaced from In. However, the systematics shown in Figures V.6 and V.7 indicate, somewhat surprisingly, that the assumption of a constant N/Z over this charge region

is valid. For example, for $^{233}U(p,f)$ at 40MeV the In centroid is 119.84, and assuming a constant N/Z ratio, $\langle A_{Ru} \rangle = 44 \times 119.84/49 = 107.61$, which is 0.04 mass units displaced from the interpolated value of 107.65 from Figure V.6. It is, however, felt that, since (p,2pXnf) and (p,αXnf) reactions will result in the complementary product of In being Mo(Z=42), which is seven charge units displaced from the measured product, the interpolated centroids of the complementary products are more reliable than those obtained assuming a constant N/Z ratio. Thus, in computing average total neutron yields from near-symmetric fissions, the centroids of indium's complementary products were interpolated from Figures V.6 and V.7 for $^{233}U(p,f)$ and $^{235}U(p,f)$ respectively.

Thus far it has been assumed that the measured centroids of the isotopic distributions may be used in average total neutron yield computations. Although this assumption is valid if there is no pre-fission charged-particle emission, its validity for the present studies requires further examination. It is conceivable that for fissioning nuclei of a given charge there exists an isotopic distribution of a given fission product. Thus in the case of the Rb product from the proton-induced fission of uranium nuclei there may exist centroids attributable to (p,Xnf), (p,pXnf), (p,2pXnf), and (p,αXnf) reactions, together with corresponding centroids for the complementary products. If the centroids for (p,Xnf), (p,pXnf), (p,2pXnf), and (p,αXnf) reactions are denoted by subscripts 0,1,2, and 3 respectively, and the corresponding probabilities for these fission channels

are denoted by ω_o, ω_1, ω_2, and ω_3, then total neutron yields may be computed according to the following equations:

$$\nu_{T_o}(\text{Rb-Ba}) = (A_T+1) - (A_{Rb_o}+A_{Cs_o}+\delta A_{Cs_o}) \qquad (V.3)$$

$$\nu_{T_1}(\text{Rb-Cs}) = A_T-(A_{Rb_1}+A_{Cs_1}) \qquad (V.4)$$

$$\nu_{T_2}(\text{Rb-Xe}) = (A_T-1) - (A_{Rb_2}+A_{Cs_2}-\delta A_{Cs_2}) \qquad (V.5)$$

$$\nu_{T_3}(\text{Rb-Xe}) = (A_T-3) - (A_{Rb_3}+A_{Cs_3}-\delta A_{Cs_3}) \qquad (V.6)$$

where A_T is the mass number of the target and δ corresponds to the amount by which the complementary centroid of Rb deviates from that of Cs. The average total numbers of neutrons emitted may then be computed as the weighted sum of the values obtained using equations V.3 to V.6. Thus:

$$\bar{\nu}_T = \bar{A}-\langle A_{Rb}\rangle-\langle A_{Cs}\rangle-\omega_o\delta A_{Cs_o}+\omega_2\delta A_{Cs_2}+\omega_3\delta A_{Cs_3} \qquad (V.7)$$

where:

$$\bar{A} = \omega_o(A_T+1)+\omega_1 A_T+\omega_2(A_T-1)+\omega_3(A_T-3),$$

$\langle A_{Rb}\rangle$ = the measured mean Rb centroid,

$\langle A_{Cs}\rangle$ = the measured mean Cs centroid,

It should be noted that if a constant N/Z ratio is assumed for neighbouring products then $\delta = 1/55$. If it is further assumed that the measured mean centroids may be substituted for the true centroids in equations V.3 to V.7 then the corresponding average total neutron yield at a given bombarding energy will be given by:

$$\langle\nu_T\rangle = \bar{A}-\langle A_{Rb}\rangle-\langle A_{Cs}\rangle-\omega_o\delta\langle A_{Cs}\rangle+\omega_2\delta\langle A_{Cs}\rangle+\omega_3\delta\langle A_{Cs}\rangle . \qquad (V.8)$$

By subtracting equation V.8 from V.7 the deviation between these neutron yield computations will be:

$$\Delta\nu_T = \omega_o\delta(\langle A_{Cs}\rangle - A_{Cs_o}) + \omega_2\delta(A_{Cs_2} - \langle A_{Cs}\rangle) + \omega_3\delta(A_{Cs_3} - \langle A_{Cs}\rangle) \qquad (V.9)$$

From equation V.9 it can be seen that, if δ=1/55, average total neutron yields estimated by using the measured centroids in the computations will deviate from the true neutron yields by the weighted sum of 1/55th of the differences between the measured centroids and the true centroids.

Although it would be a formidable task to resolve the measured distributions into contributions from the various fission channels given previously, the magnitude of $\Delta\nu_T$ can be estimated by noting the FWHM of the measured distributions and utilizing the calculated probabilities for the various fission channels. Thus at a bombarding energy of 40 MeV the FWHM of the Cs distribution from $^{233}U(p,f)$ is 5.20 mass units, and the pre-equilibrium/exciton model calculations indicate that ω_o, ω_2, and ω_3 equal 0.896, 0, and 0.004 respectively. It is evident from these numbers that, even if the centroid for (p,αXnf) reactions is five mass units displaced from the measured centroid, the last term in equation V.9 will not contribute significantly to $\Delta\nu_T$. The term involving ω_o thus determines the magnitude of $\Delta\nu_T$. Since (p,Xnf) reactions represent 89.6% of all fissions at 40 MeV it is reasonable to assume that $\langle A_{Cs}\rangle - A_{Cs_o}$ will not exceed half the FWHM or 2.60 mass units; thus $\Delta\nu_T$=0.04. At a bombarding energy of 100 MeV the FWHM of the Cs distribution from

$^{233}U(p,f)$ is 6.44 mass units, and the pre-equilibrium/exciton model calculations predict that ω_o, ω_2, and ω_3 equal 0.528, 0.01, and 0.026 respectively. Substituting these probabilities into equation V.9 and assigning an upper limit of 6.44 mass units to the differences between the measured centroids and the possible correct centroids results in a value of 0.07 for $\Delta\nu_T$. It is thus concluded that, providing the identities of complementary products can be obtained, average total neutron yields can be estimated by using the measured mean centroids in the computations.

Average total neutron yields were thus computed for fissions resulting in Rb,Cs,In, and their possible complementary products according to the following equations:

for all (p,Xnf) reactions:

$$\nu_T(\text{Rb-Ba}) = (A_T+1) - (\langle A_{Rb}\rangle+\langle A_{Ba}\rangle) \qquad \text{(V.10)}$$

$$\nu_T(\text{Sr-Cs}) = (A_T+1) - (\langle A_{Sr}\rangle+\langle A_{Cs}\rangle) \qquad \text{(V.11)}$$

$$\nu_T(\text{Ru-In}) = (A_T+1) - (\langle A_{Ru}\rangle+\langle A_{In}\rangle) \qquad \text{(V.12)}$$

for all (p,pXnf) reactions:

$$\nu_T(\text{Rb-Cs}) = A_T - (\langle A_{Rb}\rangle+\langle A_{Cs}\rangle) \qquad \text{(V.13)}$$

$$\nu_T(\text{Tc-In}) = A_T - (\langle A_{Tc}\rangle+\langle A_{In}\rangle) \qquad \text{(V.14)}$$

for all (p,2pXnf) reactions:

$$\nu_T(\text{Rb-Xe}) = (A_T-1) - (\langle A_{Rb}\rangle+\langle A_{Xe}\rangle) \qquad \text{(V.15)}$$

$$\nu_T(\text{Kr-Cs}) = (A_T-1) - (\langle A_{Kr}\rangle+\langle A_{Cs}\rangle) \qquad \text{(V.16)}$$

$$\nu_T(\text{Mo-In}) = (A_T-1) - (\langle A_{Mo}\rangle+\langle A_{In}\rangle) \qquad (V.17)$$

and for all (p,αXnf) reactions by using equations V.15 to V.17 with (A_T-1) replaced by (A_T-3). Finally, average total neutron yields from fissions resulting in Rb-A_H, A_L-Cs, and A_L-In products were computed, using the fission probabilities obtained from the pre-equilibrium/exciton model calculations, as the weighted sum of the values obtained using equations V.10 to V.17. The centroids of the possible complementary products were interpolated from Figures V.6 and V.7 when a linear variation of charge with mean fission product mass number was assumed. When a constant N/Z was assumed for neighbouring products in the Rb and Cs mass regions the complementary centroids were estimated as: $\langle A_{Sr}\rangle=38/37\langle A_{Rb}\rangle$, $\langle A_{Kr}\rangle=36/37\langle A_{Rb}\rangle$, $\langle A_{Ba}\rangle=56/55\langle A_{Cs}\rangle$, and $\langle A_{Xe}\rangle=54/55\langle A_{Cs}\rangle$. In order to illustrate the degree to which pre-fission charged particle emission effects the neutron yield estimates the values obtained using equations V.8 and V.9 only were also computed. The results from all these computations are given in Tables V.5 and V.6, and are shown in Figures V.10 and V.11 for ^{233}U(p,f) and ^{235}U(p,f) reactions respectively. Average pre-fission nucleon and neutron yields obtained from the pre-equilibrium/exciton model calculations are also shown in these figures. The computations of $\langle\nu_T\rangle$ indicate that the values estimated assuming a constant N/Z ratio for neighbouring products do not differ greatly from those obtained by utilizing the experimental systematics. This refinement to the previous assumption is thus small. However, neglecting pre-fission

Table V.5: Average Total Neutron Yields for Asymmetric and Symmetric Mass Splits from $^{233}U(p,f)$

E_p (MeV)		$\langle \nu_{Total} \rangle$		
		Rb-A_H	A_L-Cs	A_L-In
40	a)	6.09±0.05	6.12±0.05	--
	b)	6.23±0.05	6.27±0.05	--
	c)	6.19±0.05	6.18±0.05	6.67±0.04
60	a)	6.72±0.04	6.76±0.04	--
	b)	7.08±0.03	7.10±0.03	--
	c)	7.04±0.03	7.03±0.03	7.94±0.08
80	a)	7.20±0.04	7.23±0.04	--
	b)	7.68±0.03	7.73±0.04	--
	c)	7.67±0.03	7.66±0.03	8.43±0.02
100	a)	7.46±0.03	7.50±0.03	--
	b)	8.14±0.02	8.05±0.02	--
	c)	8.10±0.02	8.11±0.02	9.12±0.09

a) Assuming no charged particle emission prior to fission.

b) Assuming a constant $\langle N/Z \rangle$ for neighbouring products.

c) Allowing for a variation of $\langle N/Z \rangle$ with mass.

Table V.6: Average Total Neutron Yields for Asymmetric and Near-Symmetric Mass Splits from $^{235}U(p,f)$

E_p (MeV)		$\langle \nu_{Total} \rangle$		
		Rb-A_H	A_L-Cs	A_L-In
40	a)	6.25±0.06	6.28±0.06	--
	b)	6.33±0.06	6.36±0.06	--
	c)	6.27±0.06	6.27±0.06	6.85±0.04
50*	a)	6.87±0.06	6.91±0.06	--
	b)	7.20±0.04	7.23±0.04	--
	c)	7.02±0.04	7.03±0.04	--
60	a)	6.96±0.05	7.00±0.05	--
	b)	7.27±0.04	7.30±0.04	--
	c)	7.23±0.04	7.22±0.04	8.10±0.03
80	a)	7.37±0.04	7.40±0.04	--
	b)	7.83±0.03	7.85±0.03	--
	c)	7.79±0.03	7.80±0.03	8.85±0.03
100	a)	7.68±0.04	7.72±0.04	--
	b)	8.29±0.03	8.31±0.03	--
	c)	8.26±0.03	8.26±0.03	9.52±0.01

a) Assuming no charged particle emission.
b) Assuming a constant $\langle N/Z \rangle$ for neighbouring products.
c) Allowing for a variation of $\langle N/Z \rangle$ with mass.
* Computed using data from (Tr72).

Figure V.10

Average nucleon yields as a function of bombarding energy for $^{233}U(p,f)$

$\langle \nu_{pre} + \chi_{pre} \rangle$: Average numbers of pre-fission nucleons emitted

$\langle \nu_{pre} \rangle$: Average numbers of pre-fission neutrons emitted

$\langle \nu_T \rangle$(asym.): Average total numbers of neutrons emitted for asymmetric mass splits

- ◆ Rb-A_H: $\langle N/Z \rangle$ assumed constant
- ◇ A_L-Cs: $\langle N/Z \rangle$ assumed constant
- ▲ Rb-A_H: $\langle N/Z \rangle$ not constant
- △ A_L-Cs: $\langle N/Z \rangle$ not constant
- □ Rb-A_H: pre-fission charged particle emission neglected
- ■ A_L-Cs: pre-fission charged particle emission neglected

$\langle \nu_T \rangle$(sym.): Average total numbers of neutrons emitted for symmetric mass splits: $\langle N/Z \rangle$ not constant.

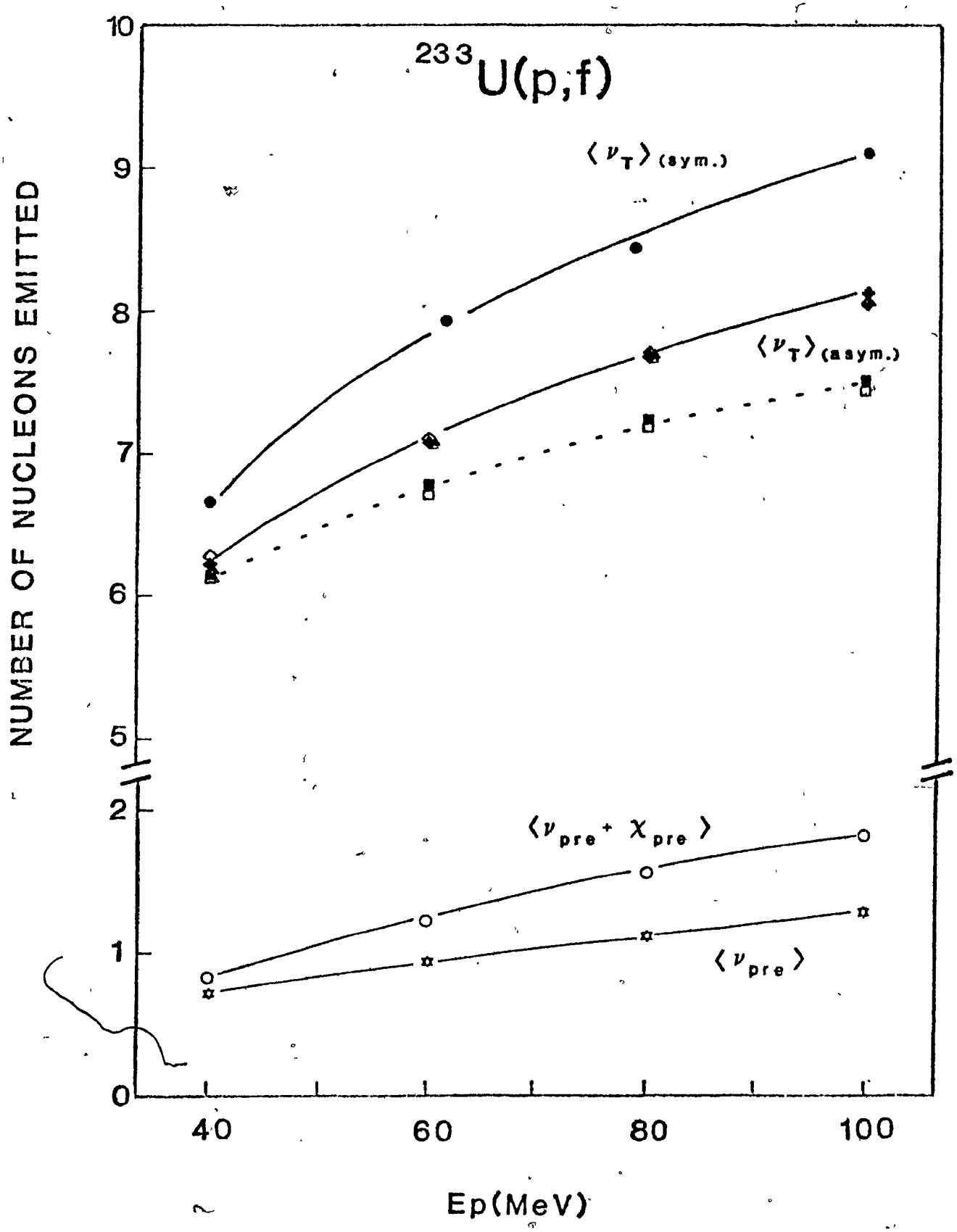
^{233}U(p;f)
NUMBER OF NUCLEONS EMITTED
Ep(MeV)
$\langle \nu_T \rangle$ (sym.)
$\langle \nu_T \rangle$ (asym.)
$\langle \nu_{pre} + \chi_{pre} \rangle$
$\langle \nu_{pre} \rangle$
10
9
8
7
6
5
2
1
0
40
60
80
100

Figure V.11

Average nucleon yields as a function of bombarding energy for $^{235}U(p,f)$

$\langle \nu_{pre} + \chi_{pre} \rangle$: Average numbers of pre-fission nucleons emitted

$\langle \nu_{pre} \rangle$: Average numbers of pre-fission neutrons emitted

$\langle \nu_T \rangle$(asym.): Average total numbers of neutrons emitted for asymmetric mass splits

- ◆ Rb-A_H: $\langle N/Z \rangle$ assumed constant
- ◇ A_L-Cs: $\langle N/Z \rangle$ assumed constant
- ▲ Rb-A_H: $\langle N/Z \rangle$ not constant
- △ A_L-Cs: $\langle N/Z \rangle$ not constant
- □ Rb-A_H: pre-fission charged particle emission neglected
- ■ A_L-Cs: pre-fission charged particle emission neglected

$\langle \nu_T \rangle$(sym.) : Average total numbers of neutrons emitted for symmetric mass splits: $\langle N/Z \rangle$ not constant.

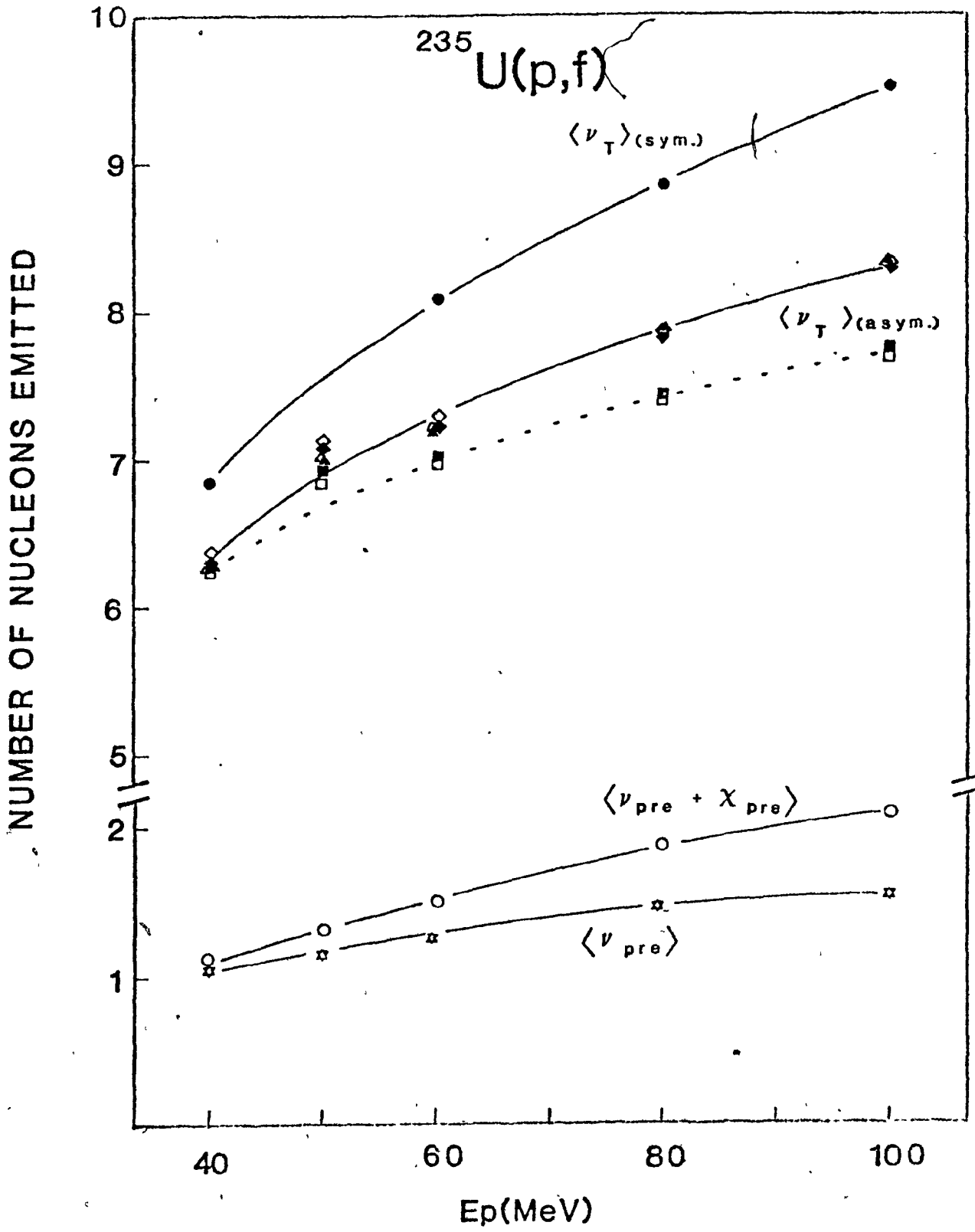
235U(p,f)
⟨ν T⟩(sym.)
⟨ν T⟩(asym.)
⟨ν pre + χ pre⟩
⟨ν pre⟩
NUMBER OF NUCLEONS EMITTED
Ep(MeV)
10
9
8
7
6
5
2
1
40
60
80
100

charged-particle emission in the computations results in neutron yields being underestimated by a substantial amount. Since the magnitude of this discrepancy is dependent on the reliability of the pre-equilibrium/exciton model calculations, it will be interesting to see if possible future experimentation verifies these predictions.

Some interesting features of the neutron yields shown in Figures V.10 and V.11 are as follows:

1. The total numbers of neutrons emitted increases with increasing bombarding energy. This is a result of an increase in the excitation energy of the primary fragments resulting in more prompt neutron emission. The rate of increase of the neutron yields, however, decreases with increasing energy. This is a direct result of the increase in charged-particle emission, resulting in a continuing contribution from lower excitation energy events.

2. There are slightly more neutrons emitted from $^{235}U(p,f)$ than from $^{233}U(p,f)$ reactions. This indicates that the neutron richness of the targets is reflected in the final stages of the fission process.

3. There are more neutrons emitted for near-symmetric fissions (A_L-In) than for asymmetric fissions (Rb-A_H, A_L-Cs). This is a result of the distribution of energy between the excitation and kinetic energy of the fragments. For $^{233}U(p,f)$ at 13 MeV Burnett (Bu68) has shown that the average total kinetic energy of fragments in the near-symmetric mass regions is lower than

in the asymmetric mass regions. Conservation of energy thus implies that for near-symmetric fissions a larger portion of the energy release should be dissipated into excitation energy of the fragment pairs. Since the main mode of de-excitation from the primary fragments is by neutron emission, the net result will be more neutron emission for near-symmetric fissions.

The neutron yields calculated in this work are important to an analysis of the charge distribution postulates as these postulates apply to the primary fragments, whereas the experimental results are of fission products. Although the neutron yield computations carried out thus far can be used to obtain average total prompt neutron yields ($\nu_L+\nu_H^g$), estimates of the numbers of neutrons emitted from complementary light and heavy fragments require the use of energy balance equations for the reactions under study. The purpose of this study is to relate the experimental data to the charge distribution postulates using the minimum amount of ab initio calculations. The charge distribution postulates were thus tested by formulating equations that gave neutron yield ratios (ν_H/ν_L) that could be compared to experimental ratios. The details of the analysis are discussed in the next section.

E. Analysis of the Charge Distribution Postulates

As mentioned in the introduction, charge distribution in fission is usually described in terms of three postulates.

Functional forms of the simple equations previously given for UCD and ECD, and a formulation of MPE were derived as follows:

1. The UCD postulate: This postulate states that the neutron-to-proton ratio of the fissioning nucleus is maintained unchanged in the primary fission fragments. The symbols used to denote the charges and masses of the fissioning nucleus, primary fragments, and fission products, together with the relation between the primary fragments and the products was given in the preceding section. The UCD postulate may thus be formulated as:

$$\frac{(A_L+\nu_L)-Z_L}{Z_L} = \frac{(A_H+\nu_H)-Z_H}{Z_H} = \frac{A_F-Z_F}{Z_F} \qquad (V.18)$$

In order to circumvent the difficulty in obtaining neutron yields from the primary fragments the predictions of the charge distribution postulates are expressed in terms of the following neutron ratios:

$$\alpha = \frac{\nu_H+\nu_L}{\nu_T} \qquad \gamma = \frac{\nu_H}{\nu_L}$$

By substituting for ν_L and ν_H in equation V.18 the following relation between α and γ may be derived for UCD:

$$\alpha = \frac{1+\gamma}{\nu_T}\left[\frac{A_H Z_L - A_L Z_H}{Z_H - \gamma Z_L}\right] \qquad (V.19)$$

2. The ECD postulate: The ECD postulate predicts that the charges of the primary fragments are equally displaced from the beta-stability line. This may be formulated as:

$$\left[Z_{A(L')} - Z_{L'}\right] = \left[Z_{A(H')} - Z_{H'}\right] \qquad (V.20)$$

where Z_A is the charge of the beta-stable isotope of mass A. In this work the beta-stability line was treated as a set of straight lines with different slopes in the major shell regions. Thus $Z_A = cA+d$ where c and d are the slopes and intercepts of the beta-stability lines. These constants were taken from the predictions of Coryell (Co53) for his work on beta-decay energetics, and evaluated from the computations of Z_A, by Chung (Ch81), from the Droplet Model mass equation due to Myers(My77). Both evaluations of Z_A were used in the present calculations and their results will be discussed in due course. By substituting fission fragment masses with product masses, and incorporating the linearity of Z_A, equation V.20 may be expressed as:

$$c_L A_L + c_L \nu_L + d_L - Z_L = c_H A_H + c_H \nu_H + d_H - Z_H,$$

or:

$$Z_{A(L)} - Z_L + c_L\left[\frac{\alpha \nu_T}{1+\gamma}\right] = Z_{A(H)} - Z_H + c_H\left[\frac{\alpha\gamma \nu_T}{1+\gamma}\right]$$

The relation between α and γ for ECD may then be formulated as:

$$\alpha = \frac{1+\gamma}{\nu_T}\left\{\frac{\left[Z_{A(H)} - Z_H\right] - \left[Z_{A(L)} - Z_L\right]}{c_L - \gamma c_H}\right\} \qquad (V.21)$$

For both UCD and ECD, values of γ were computed by setting lower and upper limits to the possible values of α. The value of α chosen for comparing the results was taken as that corresponding to $(\nu_T - \nu_{pre})/\nu_T$, which was evaluated from the neutron-yield calculations and the predictions of the pre-equilibrium/

exciton model. As was the case for the neutron-yield calculations, computations were performed for summed (p,Xnf), (p,pXnf), (p,2pXnf), and (p,αXnf) reactions, and the average values were computed as the weighted sum from all grouped reaction channels.

3. The MPE postulate: As mentioned in the introduction, several formulations of this postulate, which states that the division at scission is such as to minimize the potential energy of the fragments, have been used. In order to present the results in the same form as those from UCD and ECD, this postulate was formulated as:

$$\frac{\partial}{\partial A} PE(A_L', A_H')\Big|_{min} = \frac{\partial}{\partial A}\left[M(Z, A') + M(Z_F - Z, A_F - A')\right] + \frac{\partial}{\partial A}\frac{Z\cdot(Z_F - Z)e^2}{\bar{D}} = 0 \qquad (V.22)$$

where: e^2 = the electrostatic constant = 1.44 MeV-fm,

$\bar{D}$ = the average separation distance of the fragment centres at scission (fm).

The minima in the potential energies corresponding to the most probable primary fragments (A_p') were computed for the pertinent fragment pairs resulting from fission of all neptunium, uranium and protactinium nuclei predicted by the pre-equilibrium/exciton model. The masses of the primary fragments were taken from the Droplet Model calculations of Myers (My77), and the $\bar{D}$ values were estimated from the values derived by Britt et al. (Br63) for ^{232}Th(p,f) and ^{233}U(α,f) reactions. The minima in the curves of potential energy of the fragment pairs versus A_H' or A_L' were obtained using the statistical moments analysis

described previously in this work. It was found that A_p' for a given fragment pair varied linearly with the mass of the fissioning nucleus (A_F) for a given fissioning charge (Z_F). Therefore, average values of A_p' were calculated for the average values of A_F resulting from the summed (p,Xnf), (p,pXnf), (p,2pXnf), and (p,αXnf) reaction channels. The values of ν_L and ν_H were then obtained by subtracting the fission product mean masses from the corresponding values of A_p', and the average values of $\gamma(=\nu_H/\nu_L)$ were computed as the weighted sum from all grouped reaction channels.

The predictions of ν_H/ν_L from the three postulates, for asymmetric mass splits resulting from $^{233}U(p,f)$ and $^{235}U(p,f)$ are given in Tables V.7 and V.8 respectively. The results obtained when the complementary centroids were interpolated from Figures V.6 and V.7 are given in Tables V.9 and V.10 for $^{233}U(p,f)$ and $^{235}U(p,f)$ respectively.

Several neutron yield measurements from primary fragments produced from the charged-particle induced fissions of ^{233}U and ^{238}U have been reported in the literature. All the measurements show that for asymmetric mass splits corresponding to approximately the same mass ratios as those observed in this work, there are more neutrons emitted from the heavy fragments than from the light fragments. For $^{238}U(p,f)$ Cheifitz et al. (Ch70) obtained values of ν_H/ν_L equal to 1.5 and 2.2 at 12 and 155 MeV respectively, and Bishop et al. (Bi70) obtained values of 1.2 and 1.34 at 11.5 and 22 MeV respectively. For $^{233}U(p,f)$

Table V.7: Estimates of v_H/v_L from the Charge Distribution Postulates for Asymmetric Mass Splits from $^{233}U(p,f)$*

E_p (MeV)	FRAGMENT PAIR	$\frac{v_{post}}{v_T}$	v_H/v_L			
			UCD	ECD (Coryell)	ECD (Myers)	MPE
40	A_H-Rb	0.88	0.80	1.92	2.43	1.79
	Cs-A_L		0.78	1.63	1.93	1.75
60	A_H-Rb	0.86	0.88	1.90	2.78	1.81
	Cs-A_L		0.85	1.67	2.16	1.78
80	A_H-Rb	0.85	0.92	1.85	2.90	1.82
	Cs-A_L		0.90	1.70	2.37	1.80
100	A_H-Rb	0.84	0.95	1.82	3.44	1.84
	Cs-A_L		0.93	1.74	2.50	1.82

* <N/Z> assumed constant for neighbouring products.

Table V.8: Estimates of υ_H/υ_L from the Charge Distribution Postulates for Asymmetric Mass Splits from $^{235}U(p,f)$*

E_p (MeV)	FRAGMENT PAIR	$\frac{\upsilon_{post}}{\upsilon_T}$	υ_H/υ_L			
			UCD	ECD (Coryell)	ECD (Myers)	MPE
40	A_H-Rb	0.83	0.82	1.92	2.18	1.68
	Cs-A_L		0.79	1.58	2.03	1.60
50	A_H-Rb	0.84	0.91	1.96	2.17	1.73
	Cs-A_L		0.88	1.63	2.21	1.65
60	A_H-Rb	0.83	0.91	2.01	2.32	1.72
	Cs-A_L		0.88	1.62	2.23	1.65
80	A_H-Rb	0.81	0.92	2.01	2.48	1.69
	Cs-A_L		0.89	1.60	2.45	1.64
100	A_H-Rb	0.81	0.94	1.99	2.92	1.68
	Cs-A_L		0.92	1.59	2.49	1.63

* <N/Z> assumed constant for neighbouring products.

Table V. 9: Estimates of v_H/v_L from the Charge Distribution Postulates for Asymmetric Mass Splits from $^{233}U(p,f)$*

E_p (MeV)	FRAGMENT PAIR	$\frac{v_{post}}{v_T}$	v_H/v_L			
			UCD	ECD (Coryell)	ECD (Myers)	MPE
40	A_H-Rb	0.88	0.79	1.97	2.39	1.75
	Cs-A_L		0.79	1.71	2.01	1.83
60	A_H-Rb	0.87	0.87	1.99	2.76	1.80
	Cs-A_L		0.87	1.74	2.23	1.86
80	A_H-Rb	0.85	0.91	2.00	2.91	1.81
	Cs-A_L		0.91	1.75	2.36	1.86
100	A_H-Rb	0.84	0.93	2.00	3.11	1.84
	Cs-A_L		0.93	1.75	2.54	1.88

*<N/Z> not assumed constant for neighbouring products.

Table V.10: Estimates of υ_H/υ_L from the Charge Distribution Postulates for Asymmetric Mass Splits from $^{235}U(p,f)$*

E_p (MeV)	FRAGMENT PAIR	$\frac{\upsilon_{post}}{\upsilon_T}$	υ_H/υ_L			
			UCD	ECD (Coryell)	ECD (Myers)	MPE
40	A_H-Rb	0.83	0.81	1.88	2.28	1.65
	Cs-A_L		0.81	1.65	1.94	1.66
50	A_H-Rb	0.83	0.89	1.93	2.47	1.69
	Cs-A_L		0.89	1.69	2.09	1.70
60	A_H-Rb	0.82	0.90	1.92	2.55	1.69
	Cs-A_L		0.89	1.67	2.22	1.70
80	A_H-Rb	0.81	0.91	1.95	2.86	1.67
	Cs-A_L		0.90	1.66	2.43	1.68
100	A_H-Rb	0.81	0.93	1.90	3.25	1.66
	Cs-A_L		0.92	1.64	2.57	1.68

* $\langle N/Z \rangle$ not assumed constant for neighbouring products.

Burnett (Bu68) obtained ν_H/ν_L values of 1.50 and 1.52 at 8.5 and 13 MeV respectively, and Britt et al. (Br64) obtained a ratio of 1.7 for $^{233}U(\alpha,f)$ at 30 MeV. This indicates that in general ν_H/ν_L values calculated using the ECD and MPE postulates are in better agreement with the experimental results than those calculated using the UCD postulate. However, if only the ECD calculations, using Myers Droplet Model mass equation, are compared with the other postulates the MPE predictions seem to be in better agreement with the experimental results. Since results from the Droplet Model mass equation were also used for the MPE calculations it may be argued that the latter comparison is more appropriate. Furthermore, the experimental data in this work indicate that the mean masses of the fission products vary linearly with their atomic numbers; thus the calculations based on these experimental systematics may be more reliable. The results given in Table V.9 and V.10 indicate that MPE is in better agreement with the experimental results for asymmetric mass splits resulting from $^{233}U(p,f)$ and $^{235}U(p,f)$.

Since the mean fission product masses were found to be a linear function of their charges, calculations of ν_H/ν_L from the charge distribution postulates were computed for near-symmetric mass splits resulting in In and the possible complementary products. The results from both $^{233}U(p,f)$ and $^{235}U(p,f)$ are given in Table V.11. The ratios of ν_H/ν_L for these near-symmetric mass splits were found to be 1.05 and 1.15 for $^{233}U(p,f)$ at 8.5 and 13 MeV respectively (Bu68). The present

Table V.11: Estimates of v_H/v_L from the Charge Distribution Postulates for Near-Symmetric Mass Splits from $^{233}U(p,f)$ and $^{235}U(p,f)$

E_p (MeV)	FRAGMENT PAIR	$\frac{v_{post}}{v_T}$	v_H/v_L			
			UCD	ECD (Coryell)	ECD (Myers)	MPE
			—$^{233}U(p,f)$—			
40	In-A_L	0.89	1.13	4.77	13.46	0.90
60	In-A_L	0.88	1.12	3.52	6.50	0.92
80	In-A_L	0.86	1.19	3.75	7.15	0.97
100	In-A_L	0.86	1.15	3.17	5.28	0.93
			—$^{235}U(p,f)$—			
40	In-A_L	0.84	1.14	5.10	17.94	0.89
60	In-A_L	0.84	1.18	3.96	8.51	0.94
80	In-A_L	0.83	1.22	3.73	7.16	0.98
100	In-A_L	0.84	1.21	3.34	5.82	0.98

calculations thus indicate that UCD is in better agreement with experimental results for near-symmetric fissions from $^{233}U(p,f)$ and $^{235}U(p,f)$. This supports the findings of Pappas (Pa66) that charge distribution in fission is fragment-mass dependent. The unusually large values of ν_H/ν_L predicted by the ECD postulate for near-symmetric fissions may be due to the complementary primary fragments being located on either side of Z=50 proton shell closure. The lines of beta-stability predicted by Coryell's study (Co53) and Myers' Droplet Model (My77) are shown in Figure V.12. As can be seen when crossing Z=50 the beta-stability line is displaced by nearly five mass units. Thus in order for the complementary primary fragments to be equally displaced from the beta-stability line the heavier fragment must emit considerably more neutrons than the light fragment. Figure V.12 further illustrates why the ECD predictions due to Coryell's study and Myers' Droplet Model are quite different for the asymmetric fissions considered in this work. For fissions resulting in Rb,Cs and their probable complementary products there is a possibility that the primary fragments will be located in the neutron shell regions (N=50, N=82). As can be seen, Coryell's and Myers' predictions are so different in the shell regions that the ECD postulate becomes model dependent. In conclusion, the present study of charge distribution in fission indicates that the MPE postulate should be associated with asymmetric fissions and the UCD postulate should be associated with near-symmetric fissions.

Figure V.12

Predictions of the most stable charge (Z_A)

as a function of mass number (A)

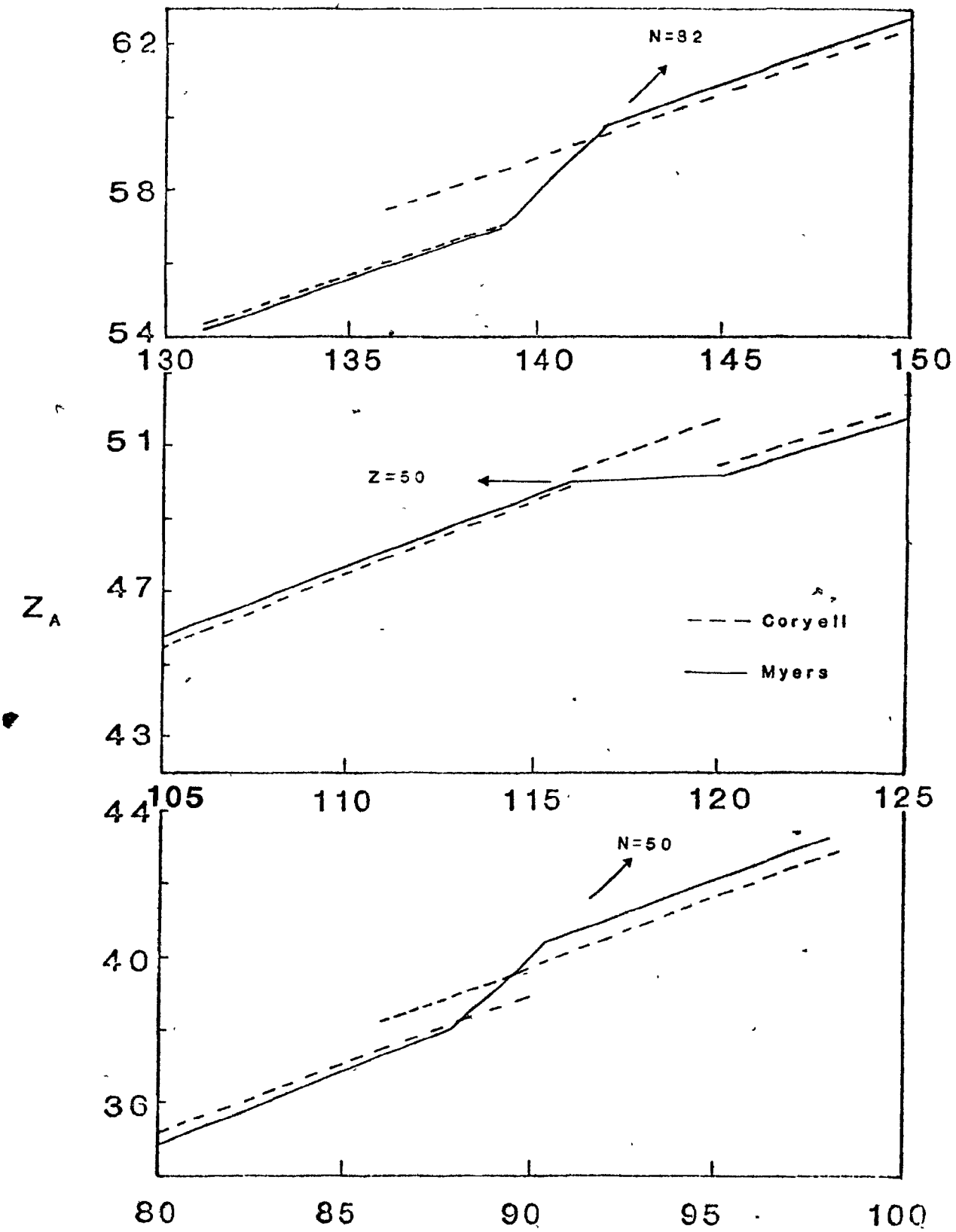
62
58
54
N=82
130
135
140
145
150
51
47
43
Z=50
105
110
115
120
125
Z_A
Coryell
Myers
44
40
36
N=50
80
85
90
95
100
A

VI. SUMMARY AND CONTRIBUTION TO KNOWLEDGE

The independent formation cross-sections of $^{84,86}Rb$, $^{116m,117m,117g}In$, and $^{132,134,134m+g,136}Cs$ produced from $^{233}U(p,f)$ and $^{235}U(p,f)$ reactions, and cross-sections of ^{72}Ga from $^{233}U(p,f)$ have been measured radiochemically at proton energies ranging from 35 to 90 MeV. Excitation functions of these nuclides were constructed and their shapes appeared to be characteristic of their neutron-to-proton ratios.

Isotopic distributions of Rb, In, and Cs from $^{233}U(p,f)$ and $^{235}U(p,f)$ reactions, and Ga distributions from $^{233}U(p,f)$ were measured by the on-line mass spectrometric technique in the energy range 40 to 100 MeV. Their relative yields were normalized to independent formation cross-sections measured radiochemically. The distributions, analysed using a statistical moments procedure, were found to be flat with respect to a Gaussian shape. Both the Rb and Cs distributions were found to have shoulders that may be due to shell effects in the appropriate regions.

Characteristic features of the isotopic distributions such as the FWHM and mean neutron-to-proton ratios of the centroids were found to be a function of bombarding energy, the mean masses of the distributions, and the neutron-to-proton ratios of the targets. Isotopic distributions from $^{238}U(p,f)$ were compared to the present measurements throughout. The increase in the FWHM and the decrease in the mean neutron-to-proton ratios with an increase in the bombarding energy were attributed to the energetics of the fission process. The

increase in the FWHM with an increase in the mean mass number of the fission products was attributed to the distribution of the excitation energy between the fragment pairs, and the discernibly large widths in the cesium region were attributed to shell effects. The linear variation of the neutron-to-proton ratios of the products with the neutron-to-proton ratios of the targets illustrates that the neutron richness of the targets is directly reflected in the neutron richness of the products. The data collected in this work also indicate that the mean masses of the isotopic distributions are directly proportional to their atomic numbers throughout the mass range studied, and $(\partial Z/\partial A)_E = 0.38 \pm 0.02$ is remarkably constant for both $^{233}U(p,f)$ and $^{235}U(p,f)$ data as well as $^{238}U(p,f)$ data compiled from the literature.

The pre-equilibrium/exciton model with the recently developed fission option was used to predict the identities and specific probabilities of fissioning nuclei from $^{233}U(p,XnYp\alpha f)$ and $^{235}U(p,XnYp\alpha f)$ reactions. This information indicated that charged-particle emission prior to fission becomes important at the bombarding energies used in this work. The fission information from this model was used in conjunction with the experimental results to estimate total neutron yields and to aid in the analysis of the charge distribution postulates.

Average total neutron yields were estimated for asymmetric fissions resulting in Rb,Cs, and their complementary products, and near-symmetric fissions resulting in In and its complementary

products. It was found that there are more neutrons emitted for near-symmetric fissions than for asymmetric fissions. This is consistent with the fact that the average total kinetic energy taken away by fragments in the asymmetric mass regions considered in this work is greater than in the near-symmetric mass regions.

An analysis of the charge distribution postulates, ECD, MPE, and UCD was carried out. This analysis indicated that the MPE postulate should be associated with asymmetric fission, although the validity of ECD cannot be ruled out, and the UCD postulate should be associated with near-symmetric fission.

REFERENCES

Am73: S. Amiel and H. Feldstein, Phys. Chem. Fission, Proc. IAEA 3rd Symp., Rochester, N.Y., Vol.II, p.65 (IAEA, Vienna), (1973).

Be80: B. N. Belyaev, V. D. Domkin and YU G. Korobulin, Nucl. Phys., A348, 479 (1980).

Bi70: C. J. Bishop, R. Vandenbosch, R. Aley, R. W. Shaw Jr., and I. Halpen, Nucl. Phys., A150, 129 (1970).

Bl75: M. Blann, Ann. Rev. Nucl. Sci., 25, 123 (1975).

Bl78: M. Blann, Nuclear Structure Research Laboratory Report UR-NSRL-181, University of Rochester, Rochester, N.Y. (1978).

Bo39: N. Bohr and J. A. Wheeler, Phys. Rev., 56, 426 (1939).

Bo72: J. R. Boyce, Ph.D. Thesis, Department of Physics, Duke University (1972) (Unpublished).

Br63: H.C. Britt, H. E. Wegner, and J. Gursky, Phys. Rev., 129, 2239 (1963).

Br64: H.C. Britt and S. L. Whetstone Jr., Phys. Rev., 133, 603 (1964).

Bu68: S. C. Burnett, Ph.D. Thesis, Department of Physics, University of Tennessee (1968) (Unpublished).

Bu71: S. C. Burnett, R. L. Ferguson, F. Plasil, and H. W. Schmitt, Phys. Rev., C3, 2034 (1971).

Bu80: K. I. Burns, Ph.D. Thesis, Department of Chemistry, McGill University (1980) (Unpublished).

Ch77: K. C. Chan, B. P. Pathak, L. Nikkinen, L. Lessard, and I. S. Grant, J. Inorg, Nucl. Chem., 39, 1915 (1977).

Ch70: E. Cheifitz, Z. Frankel, J. Galin, M. Lefort, J. Peter, and X. Tarrago, Phys. Rev., C2, 256 (1970).

Ch78: C. Chung, "Calibration of 40cc Ge(Li) Detector System," Department of Chemistry, McGill University, Internal Report (1978).

Ch80: C. Chung, Ph.D. Thesis, Department of Chemistry, McGill University (1980) (Unpublished). Also Chien Chung and James J. Hogan, Phys. Rev., C24, 180 (1981).

Cl78: A. G. Clara, M.Sc. Thesis, Department of Physics, McGill University (1978) (Unpublished).

Co53: C. D. Coryell, Ann. Rev. Nucl. Sci., 2, 305 (1953).

Co58: G. A. Cowan, "Collected Radiochemical Procedures," Los Alamos Report LA-1721 (1958).

Cu62: J. B. Cummings, National Academy of Science, Nuclear Science Series NAS-NS-3107, 25 (1962).

Da63: J. H. Davies and L. Yaffe, Can. J. Chem., 41, 762 (1963).

Di74: M. Dikšić, D. K. McMillan, and L. Yaffe, J. Inorg. Nucl. Chem., 36, 7 (1974).

Di79: M. Dikšić, J.-L. Galinier, H. Marshall, and L. Yaffe, J. Inorg. Nucl. Chem., 41, 795 (1979).

Do59: I. Dostrovsky, Z. Frankel, and G. Friedlander, Phys. Rev., 116, 683 (1959).

Ev51: H. B. Evans and R. P. Schuman, Paper 235, Nat. Nucl. Energy Ser., Div. IV 9, Book3, 1456, McGraw-Hill (1951).

Ev51a: H. B. Evans, Paper 284, Nat. Nucl. Energy. Ser., Div. IV 9, Book 3, 1646, McGraw-Hill (1951).

Fo56: P. Fong, Bull. Amer. Phys. Soc. Ser. II 1, 303, (1956).

Fo56a: P. Fong, Phys. Rev., 102, 434 (1956).

Fo78: P. Fong, Phys. Rev., C17, 1731 (1978).

Fo72: M. M. Fowler, "Absolute Photopeak Efficiency Calibration of 30cc Ge(Li) Detector," Department of Chemistry, McGill University, Internal Report (1972).

Fr63: G. Friedlander, L. E. Friedman, B. Gordon, and L. Yaffe, Phys. Rev., 129, 1809 (1963).

Fu59: G. B. Fulmer, Phys. Rev., 116, 418 (1959).

Ga73: E. Gadioli and L. Milazzo-Colli, "Lecture Notes in Physics," 1st Ed. (Springer, Berlin), 22, 84 (1973).

Ga77: E. Gadioli, E. Gadioli-Erba, and J. J. Hogan, Phys. Rev., C16, 1404 (1977).

Ga78: E. Gadioli, E. Gadioli-Erba, and A. Moroni, Z. Phys., A288, 39 (1978).

Ga77a: J.-L. Galinier and L. Yaffe, J. Inorg. Nucl. Chem., 36, 7 (1974).

Ga77b: J.-L. Galinier, M. Dikšić, and L. Yaffe, Can. J. Chem., 55, 3609 (1977).

Gl49: L. E. Glendenin, C. D. Coryell, and R. R. Edwards, Phys. Rev., 75, 337 (1949).

Gl51: L. E. Glendenin, Paper 235, Nat. Nucl. Energy Ser., Div. IV 9, Book 3, 1575, McGraw-Hill (1951).

Go48: R. H. Goeckermann and I. Perlman, Phys. Rev., 73, 1127 (1948).

Go49: R. H. Goeckermann and I. Perlman, Phys. Rev., 76, 628 (1949).

Gr76: I. S. Grant, Rep. Prog. Phys., 39, 955 (1976).

Gu72: R. Gunnick and J. B. Niday, Lawrence Livermore Laboratory, University of California, Report UCRL-51061, Vol. 1 (1972)..

Ha65: E. Hagebø, J. Inorg. Nucl. Chem., 27, 927 (1965).

Ho74: D. C. Hoffman and M. M. Hoffman, Ann. Rev. Nucl. Sci., 24, 151 (1974).

Ho74a: Ibid., Ho74, p.169.

Ho69: J. J. Hogan and N. Sugarman, Phys. Rev., 182, 1210 (1969).

Ho77: J. J. Hogan and E. Gadioli, Proc. Int. Conf. on Nucl. Reaction Mechanisms, Varenna, Italy, 198 (1977).

Ho79: J. J. Hogan, E. Gadioli, E. Gadioli-Erba, and C. Chung, Phys. Rev., C20, 1831 (1979).

Ho81: J. J. Hogan (Private communications, 1981).

Ho73: R. Holub and L. Yaffe, J. Inorg. Nucl. Chem., 35, 3991 (1973).

Hy71: E. K. Hyde, "The Nuclear Properties of the Heavy Elements," Vol. III, (Dover Publications Inc., New York) (1971).

Ju79: Phys. Chem. Fission Proc. IAEA 4th Symp. Jülich, (IAEA, Vienna) (1979).

Kh70: A. H. Khan, G. B. Saha, and L. Yaffe, Can. J. Chem., 48, 1924 (1970).

Kl67: R. Klapisch, J. Chaumont, C. Philippe, I. Amarel, R. Fergeau, M. Salome, and R. Burnas, Nucl. Inst. and Methods, 53, 216 (1967).

Ko78: J. C. Kondylakis, M.Sc. Thesis, Department of Physics, McGill University (1978) (Unpublished).

Kr53: K. A. Krauss and G. E. Moore, J. Am. Chem. Soc., 75, 1460 (1953).

Kr54: K. A. Krauss, F. Nelson, and G. W. Smith, J. Phys. Chem., 58, 11 (1954).

La74: A. Latuszyński, K. Zuber, J. Zuber, A. Potempa, and W. Żuk, Nucl. Inst. and Methods, 120, 321 (1974).

Le78: C. M. Lederer and V. S. Shirley, "Table of Isotopes," 7th Ed. (John Wiley and Sons Inc.) (1978).

Le75. J. K. P. Lee, G. Pilar. B. L. Tracy and L. Yaffe, J. Inorg. Nucl. Chem., 37, 2035 (1975).

Le61: J. E. Lewis, "The Radiochemistry of Aluminum and Gallium," Nat. Academy of Sci., National Research Council, Nuclear Seminar Series NAS-NS3032 (1961).

Ma73: H. Marshall and L. Yaffe, J. Inorg. Nucl. Chem., 35, 1797 (1973).

Mc72: T. McGee, C. L. RaO, and L. Yaffe, J. Inorg. Nucl. Chem., 34, 3323 (1972).

Mc54: G. H. McGormick and B. L. Cohen, Phys. Rev., 96, 722 (1954).

Mc68: J. A. McHugh and M. C. Michel, Phys. Rev., 172, 1160 (1968).

Me49: W. W. Meinke, U.S. Atomic Energy Commission Report UCRL 432 (1949).

Mo81: N. Mobed, M.L. Chatterjee, P. Beeley, and J. K. P. Lee, Can. J. Phys., 59, 255 (1981).

Mo74: P. Moller and J. R. Nix, Nucl. Phys., A229, 269 (1974).

Mo75: R. B. Moore, Department of Physics, Foster Radiation Laboratory, McGill University (Internal Report) (1975).

Mu73: M. G. Mustafa, U. Mosel, and H. W. Schmitt, Phys. Rev., C7, 1519 (1973).

My70: W. D. Myers and W. J. Swiatecki, Ann. Phys., 55, 395 (1970).

My77: W. D. Myers, "Droplet Model of Atomic Nuclei," Ist Ed. (IFI/Plenum, New York) (1977).

Na49: N. H. Nachtrieb and R. Fryxell, J. Am. Chem. Soc., 71, 4039 (1949).

Ne73: D. A. Newton, S. Sarkar, L. Yaffe, and R. B. Moore, J. Inorg. Nucl. Chem., 35, 361 (1973).

Ni73: H. Nifenecker, C. Signarbieux, R. Babinet, and J. Poiton, Phys. Chem. Fission, Proc. IAEA 3rd Symp., Rochester, N.Y., Vol. II, p.117 (IAEA, Vienna) (1973).

Ni77: L. M. Nikkinen, M.Sc. Thesis, Department of Physics, McGill University (1977) (Unpublished).

Ni80: L. Nikkinen, B.P. Pathak, L. Lessard, and I. S. Grant,

Phys. Rev., C22, 617 (1980).

Ni80a: L. Nikkinen, B. P. Pathak. L. Lessard, and J. K. P. Lee, Nucl. Inst. and Methods, 175, 425 (1980).

No66: W. Norenburg, Z. Phys., 197, 246 (1966).

Pa67: S. S. Parikh, D. A. Marsden. N. T. Porile, and L. Yaffe, Can. J. Chem., 45, 1863 (1967).

Pa73: H. C. Pauli and T. Ledergerber, Phys. Chem. Fission, Proc. IAEA 3rd Symp, Rochester, N.Y., Vol.I, p.463 (IAEA, Vienna) (1973).

Pi74: G. Pilar, M.Sc. Thesis, Department of Physics, McGill University (1974) (Unpublished).

Re71: W. Reisdorf, J. P. Unik, H. C. Griffin, and L. E. Glendenin, Nucl. Phys., A177, 337 (1971).

Ro73: Phys. Chem. Fission, Proc. IAEA 3rd Symp., Rochester, N.Y. (IAEA, Vienna) (1973).

Sa70: G. B. Saha and L. Yaffe, J. Inorg. Nucl. Chem., 32, 745 (1970).

Sa71: G. B. Saha, I. Tomita, and L. Yaffe, Can. J. Chem., 49, 2205 (1971).

Sa65: Phys. Chem. Fission, Proc. IAEA 1st Symp., Salzburg, Vienna (IAEA, Vienna) (1965).

Sa76: S. Sarkar and L. Yaffe, Can. J. Chem., 54, 2349 (1976).

Sh81: M. Shmid, Y. Nir-El, G. Englar, and S. Amiel, J. Inorg. Nucl. Chem., 43, 867 (1981).

Si51: J. M. Siegel and L. E. Glendenin, Paper 227, Nat. Nucl.

Energy Series, Div. IV 9, Book 3, 1436 (McGraw-Hill) (1951).

St58: P. C. Stevenson, H. G. Hicks, W. E. Nervic, and D. R. Nethaway, Phys. Rev., 111, 886 (1958).

St67: V. M. Strutinsky, Nucl. Phys., A95, 420 (1967).

St68: V. M. Strutinsky, Nucl. Phys., A122, 1 (1968).

Su77: B. H. Sutherland, M.Sc. Thesis, Department of Physics, McGill University (1977) (Unpublished).

Te62: J. Terrell, Phys. Rev., 127, 880 (1962).

To69: I. Tomita and L. Yaffe, Can. J. Chem., 47, 2921 (1969).

Tr72: B. L. Tracy, J. Chaumont, R. Klapisch, J. M. Nitschke, A. M. Poskanzer, E. Roeckl and C. Thibault, Phys. Rev., C5, 222 (1972).

Tu51: A. Turkevich and J. B. Niday, Phys. Rev., 84, 52 (1951).

Un73: J. P. Unik, U. E. Gindler, L. E. Glendenin, K. F. Flynn, A. Gorski, and R. K. Sjoblom, Phys. Chem. Fission, Proc. IAEA 3rd Symp., Rochester, N.Y., Vol.II, p.19 (IAEA, Vienna) (1973).

Va73: R. Vandenbosch and J. R. Huizenga, "Nuclear Fission," (Academic Press, New York) (1973).

Vi69: Phys. Chem. Fission, Proc. IAEA 2nd Symp., Vienna, (IAEA, Vienna) (1969).

Wa62: A. C. Wahl, R. L. Furguson, D. R. Nethaway, D. E. Troutner, and K. Wolfsburg, Phys. Rev., 126, 1112 (1962).

Wa69: A. C. Wahl and A. E. Norris, Phys. Chem. Fission, Proc.

IAEA 2nd Symp., Vienna, Vol.II, p. 813 (IAEA, Vienna) (1969).

Wa48: K. Way and E. P. Wigner, Phys. Rev., 73, 1318 (1948).

Wa51: K. Way and E. P. Wigner, "Radiochemical Studies: The Fission Products," (ed. C. D. Coryell and N. Sugarman), Book 1, Paper 43 (McGraw-Hill, New York) (1951).

Wi76: B. D. Wilkins, E. P. Steinburg and R. R. Chasman, Phys. Rev., C14, 1832 (1976).

Wi62: C. Williamson and J. P. Boujot, "Tables of Range and Rate of Energy Loss of Charged Particles of Energy 0.5 to 150 MeV," Comisariat à l'Energie Atomique, CEA Report No. 2189 (1962).

Ya69: L. Yaffe, Phys. Chem. Fission, Proc. IAEA 2nd Symp., Vienna, Vol.II, p. 701 (IAEA, Vienna) (1969).

Added in proof:

Ch81: C. Chung (Private communication, 1981).